National Research Council Canada
Conseil national de recherches Canada

CONTROLLED AND UNCONTROLLED FLOW SEPARATION IN THREE DIMENSIONS

BY

D.J. PEAKE

NATIONAL AERONAUTICAL ESTABLISHMENT

OTTAWA

JULY 1976

NRC NO. 15471
ISSN 0077-5541

AERONAUTICAL REPORT LR-591

(6)

CONTROLLED AND UNCONTROLLED FLOW SEPARATION IN THREE DIMENSIONS

DECOLLEMENT DE L'ECOULEMENT EN TROIS DIMENSIONS, CONTROLE ET NON-CONTROLE

(11) JOI 76
(12) 71 p.
(14) NAE-LR-591

by/par

(10) D.J. PEAKE

(18) NRC
(19) 15471

L.H. Ohman, Head/Chef
High Speed Aerodynamics Laboratory/
Laboratoire d'aérodynamique à hautes vitesses

F.R. Thurston
Director/Directeur

240 300
bpg

SUMMARY

The advantages of swept, sharp edges that generate controlled (or fixed) three-dimensional flow separations on a vehicle because of the qualitatively unchanging flowfield developed throughout the range of flight conditions are promoted in preference to allowing uncontrolled (or unfixed) separations.

The three-dimensional viscous flowfields and vortical interactions about typical components such as delta wings and bodies at incidence are discussed, in apposition to their use on selected examples of current flight vehicles.

SOMMAIRE

Les avantages des bords aigus à flèche arrière, qui produisent sur un avion les décollements contrôlés (fixés) de l'écoulement en trois dimensions — à cause de l'écoulement non-changé à travers une variété de conditions de vol — sont encouragés de préférence aux décollements non-contrôlés (non-fixés).

Les écoulements avec viscosité en trois dimensions, et les interactions aux tourbillons autour des parties typiques des avions, comme les ailes deltas et les corps à incidence, sont discutés, en apposition à leur usage dans des exemples choisis parmi les avions modernes.

CONTENTS

ILLUSTRATIONS

ILLUSTRATIONS (Cont'd)

ILLUSTRATIONS (Cont'd)

CONTROLLED AND UNCONTROLLED FLOW SEPARATION IN THREE DIMENSIONS

1.0 INTRODUCTION

The earlier studies by Maskell and Küchemann on flow separation in three dimensions[1,2,3,36], drew attention to the constructive role played by lines of separation. They proposed that these three-dimensional (3D) separation lines could be regarded as the skeleton around which the entire flow structure could be assembled.

When the separation lines can be fixed by salient edges (sharply-swept leading-edges, for instance, Fig. 1) we have an example of "controlled flow separation", Figure 2. Throughout the range of flight conditions, the flowfield is virtually invariant in form, being dominated by the viscous shear layers leaving the separation lines, to form well organized and comparatively steady vortex motions. These leading-edge vortices can, in turn, be controlled by additional active means, to induce more lift: first of all, to prevent vortex breakdown, by blowing in a spanwise direction along the axis of the vortex, as discussed by Cornish[4] and others[5,6](Fig. 3); secondly, by blowing normal to the leading-edge, either to enhance the primary vortex[7,8], or to control secondary separations[9]. Clearly, other examples of swept edges, such as strakes (Fig. 4.1) and vortex generators (Fig. 4.2), themselves provide controlled flow separations, but the generated vortex motions are used to promote mixing of high-energy air with recalcitrant viscous flows downstream of the flow separation device.

On the other hand, when the load-carrying, lifting and propulsion components are integrated into an aircraft or missile configuration, the resultant interfering pressure fields produce separations that are often unanticipated, are not fixed in location on the surface for all flight conditions, and so, in this sense, are "uncontrolled". Examples of these separated flows may be catalogued according to their causes[10]:

(a) flows over smooth walls in the presence of slowly varying circumferential and lengthwise adverse pressure gradients. We include here, those flows about bodies whose longitudinal axis in part or in whole is swept with respect to the oncoming stream, such as upswept rear fuselages or pointed and bluff nosed missiles at angles of attack[11,12,13];

(b) flows about protuberances attached to a wall, where adverse pressure gradients are imposed suddenly. Bulbous wheel housings, cockpit canopies, pylons, boundary-layer diverters, and unfaired junctions of the wing and tail surfaces with the body are important examples[11,14];

(c) flows about normal or inclined jets blowing from a wall. Control jets used for thrust vector control cause substantial three-dimensional separation of the local viscous flow in the region where the jet emerges from the vehicle surface[15]. In terms of upstream effect, the "solid blockage" caused by the jet is analogous with that of a protuberance;

(d) flows with shock waves present, sometimes associated with items (a) to (c). We shall pay particular attention to those separations produced in swept shock/boundary-layer interactions[16,17,18], such as on the sidewall of rectangular supersonic inlets or upon swept-wing surfaces.

While the effect of these uncontrolled separations on drag may not always be significant or even apparent, high local heat transfer rates in re-attachment zones[19], and the induced interaction effects of the vortex motions upon downstream control surfaces of a vehicle may be important[20]. In general, the uncontrolled flow separations have not been amenable to prediction, and are not well understood. The symmetry of the vortices and the scale of the separated flow domain, whether large such as in the case of the body vortices, or immersed within the depth of the oncoming boundary layer, as in the protuberance flow, will affect the magnitudes of locally-induced suction pressures, and hence to the non-linear increments in the body forces.

Compressibility alters the quantitative, but not the qualitative features of three-dimensional separated flows. It has been found by experiment that the effect of increasing Mach number is to reduce the scale of the rolled-up shear layers with respect to the oncoming boundary-layer thickness[11,21], and to increase the critical angle for the development of flow asymmetry of the rolled-up shear layers from bodies at high angles of attack[11].

The aerodynamic design of a lifting body, to be successful throughout a range of flight conditions, must ensure that the fluid flow is steady to minimize buffetting; that it should be of the same type throughout the flight envelope; and that there should be no unpleasant changes in force and moment characteristics. The goal to aim for is that flows should be dominated by free viscous vortices (with *no* large bubbles to produce unsteadiness) and that the primary lines of separation should remain fixed on the body throughout the flight range. This much wider that usual view of the aerodynamic design problem[3], incorporating the philosophy of controlled flow separation, should be contrasted with the restricted outlook of allowing separation only at a trailing-edge.

As a base of understanding for these complex flows, we shall attempt a description of the component flow fields about simple shapes, whose geometry may be integrated into the design of an aircraft or missile. The slender delta wing, with subsonic leading-edges, a prime case of controlled or fixed flow separation, will be treated first-of-all. Subsequently, the uncontrolled or unfixed separations upon cone cylinders, prolate spheroids, upswept fuselages and ahead of slender and bluff protuberances will be mentioned. Finally, the case of a swept-shock/turbulent boundary-layer interaction will be discussed, with potential for its control (and, perhaps, removal) by tangential air injection. The combination of some of these constituent flowfields into practical aerodynamic vehicles will be reviewed against examples of current design philosophy.

2.0 ATTACHMENT, SEPARATION AND RE-ATTACHMENT IN THREE-DIMENSIONAL FLOWS

2.1 Modelling

We generally accept that the non-linear Navier-Stokes equations model the motion of a viscous, compressible (laminar or turbulent) heat conducting fluid without chemical reactions, at points in space and time away from discontinuities in the flow such as shock waves. Unfortunately, full time-dependent solutions do not appear attainable in the near future, for to compute the various three-dimensional turbulence structures possessing a substantial range of length and time scales, computional techniques must be further refined. Current finite difference procedures employing numerical artifices such as damping from "artificial viscosity" inputs, for instance, appear inadequate because they introduce errors that may diverge in the development of the instantaneous flow field. Rubesin[22] suggests that to define the three-dimensional turbulent boundary-layer flowfield about an aircraft, the smallest significant scale demands mesh spacing 10^{-5} of the boundary-layer thickness, to require the order of 10^{17} mesh points overall. He discusses that the corresponding allowable time step in any given marching procedure is one microsecond of real time. These requirements demand a computer storage capacity and speed of computation that are in excess of present-day or planned computer facilities. To overcome these difficulties, therefore, we must resort to modelling the turbulence structures in three-dimensional viscous flows with free shear layers springing up from 3D separation lines. An enlightened critique of computer simulation and accuracy limitations of numerical methods with regard to turbulence modelling is given in respective comments by Roache and Bradshaw in Reference 23, in response to the essay of Chapman et al[24]. Hence, for most practical examples under high Reynolds number conditions, we still try to blend an external or inviscid flow solution with an appropriate boundary-layer procedure, rather than attempting to exploit the conceptual simplicity of the more general Navier-Stokes equations. In laminar flow, numerical studies of the viscous/inviscid interactions about pointed[27] and blunt cones[30] have been attempted using approximations to the Navier-Stokes equations, and good comparison with experiment has been obtained, but at the expense of relatively long computation times.

In the classical aircraft example, the art of design has been to eliminate separation ahead of the trailing-edge, usually because increases in drag and flow unsteadiness are introduced with essentially two (2D) separations on wings of high aspect ratio. With increases in speed, range and angle of attack,

over which smaller aspect ratio lifting wings and bodies are required to operate, extensive regions of three-dimensional separated flow are predominant (Figs. 2 and 4.1) and we require new and suitable flow models. On wings or strakes, with sharp, swept leading-edges, 3D separation occurs and is fixed at the salient edges, and is essentially independent of the oncoming boundary-layer properties at the high Reynolds numbers of interest to us. The boundary-layer fluid departs from the surface to form rolled-up viscous shear layers whose scale is usually many times the local boundary-layer thickness. In the limit of infinite Reynolds numbers, or for practical purposes, at high enough Reynolds numbers, the coiled viscous shear layer may be modelled approximately by an inviscid flow vortex sheet. In other words, viscosity causes the separation, the location is determined by the edge geometry, after which the flow many be modelled by inviscid means. The coiled vortex sheet model of Mangler and Smith, and its extensions (see the list of papers in Ref. 10) have provided good qualitative prediction of pressure distributions on slender wings in conical flow with subsonic leading-edges, see Figure 5. A more recent, incompressible, advanced panel-type influence coefficient calculation method of Weber et al[25], is not restricted to conical flow. In this method, the wing, the rolled-up vortex sheets and the wake are represented by "piecewise" continuous quadratic doublet distributions, and the Kutta condition is imposed along both the leading and trailing-edges. Some results of these calculations[25] compare well with the low-speed delta-wing experiments of Marsden et al[26], and are displayed on Figure 6.

On bodies, unfortunately, the separation location is not known *a priori*, and we must attempt to calculate its position via three-dimensional boundary-layer theory, using an initial attached inviscid flow pressure distribution. The inviscid rolled-up vortex sheet model may then be used on simple bodies such as pointed right-circular and elliptic cones, where the separation lines are along generators, and the co-ordinate geometry presents few difficulties[12]. More recently, McRae[27] has attempted to solve the laminar viscous flowfield about a pointed, right-circular cone at high angle of attack, utilizing a simplified set of the Navier-Stokes equations (incorporating the conically symmetric flow approximation) along with MacCormack's finite difference time-dependent scheme[28]. Using a body co-ordinate system, (R, θ, ϕ), a finite difference mesh was set up on the (θ, ϕ) spherical surface at a distance R from the cone apex. The calculation took place on this surface with viscous effects scaled by the Reynolds number based on the radius, R. The finite difference mesh was initialized with freestream values of the flow everywhere, except at the surface, where zero velocities were input. The numerical integration then proceeded in time, to the limit that produced a steady state solution. The outer boundary condition for the integration was the free stream, so that the bow shock wave was captured and allowed for in the use of the conservation form of the governing equations. Figure 7 illustrates the surface pressures and a crossflow velocity vector plot of a computed flowfield about a 10° half-angle cone in a nominally Mach 8 freestream at $\alpha/\theta_c = 2.4$, compared with the experimental data of Tracy with entirely laminar boundary-layer conditions, where a 3D separation was measured using surface flow visualization at $\phi = 150°$. The presence of a three-dimensional separation and rolled-up viscous shear layer is seen in McRae's calculated flowfield.

A new technique for calculating the entire flowfield about a spherically blunted circular cone at high angle of attack with 3D laminar separation has been reported by Lubard and Rakich[30]. The calculations are based on a single layer system of three-dimensional parabolic equations, that are approximations to the full steady Navier-Stokes equations, valid from the body surface to the bow shock wave. This system includes the circumferential shear stress terms and is capable of predicting the flow within the separation zone on the leeward side. The effects of viscous-inviscid interaction and entropy gradients due to both the curved bow shock and angle of attack effects are automatically included. Unseparated initial conditions are assumed at the sphere cone tangency plane and are provided by using an inviscid time dependent solution added to a viscous non-similar boundary-layer solution. The calculated results were compraed with the experimental separated flow data of Cleary[31] for a 15° angle of attack at Mach 10.6 and at a Reynolds number based on the 23-inch slant length of the cone of about 2.3 million. Figure 8 shows the calculated crossflow plane vector velocity distribution in the region close to the leeward generator at 14.8 nose radii downstream from the nose. The three-dimensional separation occurs at 155°—160° in the cross-flow plane at this axial station. The remaining graphs on Figure 8 show the calculated surface pressure and heating distributions on the leeward surface that provide good agreement with experiment. Using the same approximate parabolic system of equations, Lubard and Rakich are now working to solve the flowfields about bodies other than bodies of revolution at angle of attack, to provide design information on vehicles such as the Space Shuttle.

Notwithstanding the potential extensions of these useful laminar cone flow predictions[27,30], our ability to assess the consequences in regions of high heat transfer at three-dimensional attachment points and along re-attachment lines is still unsatisfactory for a general configuration in turbulent flow[19]. For example, on Figure 9, we show the importance of contouring the apex of a 70° swept delta, in a Mach 6 flow, to reduce the leeward centre-line heating in the presence of laminar, transitional and turbulent boundary layers (freestream Stanton number, S_{t_∞}). On the sharp apex wing, the heating is some five times the value predicted on the lee-side meridian by laminar theory[32,33], and that on the hyperbolic planform wing.

In general, then, we are unable yet to model the viscous flow encountered in 3D re-attachment and separation regions that will yield rational design procedures, although some promising avenues are opening in laminar flow. Fortunately, from the pioneering work of Sears[34], Maskell[1,35], Legendre[37,38], Lighthill[39] and others, we do possess some understanding of the physical (mean flow) conditions close to attachment, separation and re-attachment, in three-dimensional flowfields.

2.2 Limiting Streamlines

If we consider the subject of three-dimensional viscous flows in its historical context, Sears in 1948, utilized the very important concept of "limiting streamlines" in a paper discussing the laminar boundary layer on a yawed cylinder[34]. Each streamline near the surface, in the inner collinear part of the boundary layer, is one of a continuous pattern, that originally approached the surface in the attachment region, and which subsequently departs from the surface at separation. No matter how small is the height of the streamline above the surface, the streamline will exist. If this height is allowed to approach a zero value, the streamline will be everywhere tangential to the vanishing fluid velocity as the surface is approached. (In the strictest sense, no streamlines can be drawn on the solid surface of a body, of course, for the no-slip condition at the surface would be violated.) The streamline is then identifiable as a limiting streamline, or, in other words, it possesses the same direction as a skin friction line or surface shear stress trajectory. The pattern of limiting streamlines may be alternatively viewed as a "sheath" surrounding the body, whose projections on to the surface are the skin friction lines. These limiting streamlines at the base of the boundary layer must not be confused with the streamlines of the external inviscid flow over the surface, and they will in general follow paths that are different in direction to the external streamlines. From continuity considerations, and provided the limiting streamline does not form a closed curve on the aforementioned sheath, it must join the sheath at some point of attachment, A, and depart from the sheath again at a subsequent separation point, S. The locus of such points, S, is called a three-dimensional separation line, on either side of which is a distinct set of limiting streamlines.

Sears, moreover, in his early paper, included a sketch[34] that showed apparent convergence of the two sets of limiting streamlines towards the separation line, although he did not call it by name; and later, Wild[40] substantiated Sears' physical interpretation of separation, in his investigation of the laminar boundary layer on yawed "infinite" wings. In subscribing to the Cornell University work, Eichelbrenner and Oudart[41,42] proposed that a three-dimensional separation line was the envelope of the limiting streamlines (conversely, from an attachment line, the limiting streamlines diverge) and this was also supported by Susan Brown[43] in a mathematical treatise. Lighthill[39], on the other hand, disputed the term "envelope", in spite of flow visualization experiments seeming to support the previous authors. Coalescence of the limiting streamlines is an acceptable description, perhaps, to avoid argument.

It remained for Maskell[1], however, to lay the ground rules for interpreting the physical composition of three-dimensional viscous flows — by demonstrating that the limiting streamlines provide a "three-dimensional skeleton structure of the viscous flow". If a flow visualization indicator is very thin on a wind-tunnel model, it has been shown[44] that the direction indicated by the streaks on the surface is very close to the direction of surface shear stress and the limiting direction of the velocity when the indicator is absent. Thus the type of oil-streak flow visualization techniques yield a powerful means of diagnosing and synthesizing the qualitative features of three-dimensional viscous flows.

Two types of separation were conceived by Maskell[1]: a bubble type (Fig. 10(a)) and a free shear layer type (Fig. 10(b)), but the latter appears to be the most common*. In fact, at all but (perhaps) very low Reynolds numbers, the shear layer displayed in Figure 10(a) is of the free shear-layer type rather than the bubble indicated. Fluid accumulating at a three-dimensional separation line, which in general is set obliquely to the direction of the external and essentially inviscid flow field, leaves the separation line usually as a free shear layer (Fig. 10(b)) and rolls-up in the process of passing downstream. It is thought that the fluid departs from the region of the separation line, in a direction tangential to the surface[10]. The shear stress is finite *along* such a three-dimensional separation line on the surface, being locally zero only at a singular point, such as S on Figure 10(a). High local suction pressures are induced on the surface beneath the resulting vortices, Figure 5, close to which are noted inflexion points in the limiting streamline patterns. Examples here are the slender wing flow (the ONERA and RAE work being the most extensive — see the subject list in Ref. 12) and cones, the flows on long pointed and bluff-nosed slender and not-so slender bodies at incidence, those about upswept fuselages, and those about bluff protuberances[12].

2.3 Attachment and Re-attachment

Flow attachment occurs at an upstream stagnation point that is situated upon a forward-facing surface of the vehicle, such as the nose. On a two-dimensional wing, the (singular) stagnation points along the nose of the aerofoil section will also constitute the attachment line. In three-dimensional flows, on the other hand, when a flow field has an inherent plane of symmetry as along the windward generator of a cone at incidence, there will be an "attachment line" in that plane, emanating from the attachment point at the nose. Along this latter attachment line, the pressures will not be equal to the stagnation pressure of the external stream. The mechanism of flow attachment at one point or at many points along an attachment line is still debated[1,39].

Flow re-attachment occurs on the vehicle surface subsequent to a three-dimensional separation, where the attaching streamline may be one from the external flow field, or one from the outer region of the upstream boundary layer. In the latter possibility, the stagnation pressure of the external flow will clearly not be recovered at the attachment point. Lighthill calls the point of attachment a nodal point[39], and sketches a number of possible limiting streamline patterns adjacent to nodal points of attachment, as we see on Figure 11. From each kind of nodal point, an infinite number of limiting streamlines emerges, all having (except one) the same tangent, or otherwise, spirally. Spiral attachment would occur principally when either the surface or the external flow is rotating. However, the most frequent form is the "source flow" shown on the second of the sketches on Figure 11. This would be seen on the nose of an aircraft, for instance.

In Reference 10, Smith cites a potential list of interdependent properties for an attachment line to exist, two of which that are always found being:

1) that the attachment line is a limiting streamline and,

2) that two sets of limiting streamlines (whose origin in Lighthill's picture is the nodal point of attachment) run tangential to the attachment line initially, to eventually diverge from it.

Hence, two "independent" boundary layers develop on either side of the attachment line.

For convenience, we may regard the flow at the leading-edge of a swept wing, to attempt a description of the physics of the flow along an attachment line. There, a limiting streamline more-or-less parallel to the leading-edge divides the limiting streamline flow that passes above the wing from that

---

* We should note that Eichelbrenner[45], in an article somewhat at variance with his previous publications[41,42], considered only the three-dimensional bubble type of flow to be separated, because of its analogy with the corresponding two-dimensional flow case; that is, one that is inaccessible to the viscous flow coming from infinity upstream. Eichelbrenner[45] referred to Maskell's free shear-layer type as a "clash" situation and not a three-dimensional separation!

which passes below the wing, Figure 12. Smith conjectures[10] that somewhere further away in the external flowfield at the edge of the attachment-line boundary-layer flow, there will be another streamline that also runs roughly parallel with the leading-edge, that divides the external flowfield into that which proceeds above the wing and that which passes below.

If we accept Lighthill's interpretation[39], where is the nodal point of attachment situated that is the starting point for the attachment line? For an isolated swept wing, the apex at the intersection of the two swept halves is a stagnation point of the flow and the nodal attachment point.

When the wing is mounted on a fuselage, the effective proturberance pressure field of the wing section at the wing/fuselage junction can cause a horse-shoe shaped separation about the wing root, the separation that is immersed within the depth of the fuselage boundary layer[11] — see Figure 12. We may postulate that a streamline in the outer region of the fuselage boundary layer will pass over the 3-D rolled-up shear layer to form a nodal attachment point on the wing nose. Limiting streamlines emerging from the nodal point of attachment, one of which is the so-called attachment line, proceed along the leading-edge tangential or asymptotic to the attachment line to pass in a more chordwise direction over or beneath the wing. Around the nose and adjacent to the attachment line, the distance apart of these limiting streamlines is infinitesimal, such that they appear on flow visualization oil records as emerging tangentially from the attachment line. In other words, the attachment line appears to be the source or the envelope of the limiting streamlines in close proximity to it.

We note that this view is somewhat at variance with Maskell's interpretation of the conditions along an attachment line. He considered that an attachment line consisted of a number of attachment points such that when two limiting streamlines diverge from a given point on the attachment line, then that point is one at which a single attachment streamline joins the solid surface. Clearly, if there is a boundary-layer development along an attachment line, which measurements have demonstrated to be virtually constant in thickness on a swept wing of large aspect ratio[46], then a large number of external streamlines cannot "attach" themselves to the surface along the attachment line. It would appear that the fluid within the boundary layer diverging or departing from the region of the attachment line is more-or-less balanced by the entrainment of irrotational fluid from outside the boundary layer. Maskell's concept can only be true at the limit of infinite Reynolds number.

2.4 Three-Dimensional Separation

Although there is usually little difficulty in recognizing so-called lines of 3D separation and attachment from the patterns of surface shear stress trajectories on a flight vehicle, there is a continuing debate regarding the fluid mechanics adjacent to them, stemming essentially from the respective postulates of Maskell[1] and Lighthill[39]. The discussion centres around the identification of limiting streamline patterns from surface oil flow visualization.

According to Maskell[1], separation occurs at a point when two distinct limiting streamlines converge and meet there (Fig. 13.1) after which they combine and leave the surface as one separation streamline.

A 3D separation line is then composed of a large number of such "ordinary" points, being an envelope or cusp-locus of these points. Moreover, as we have seen previously, Maskell's view of the attachment line is this same picture but with the flow directions reversed on the limiting streamlines. Lighthill, in a later treatise[39], considered these statements to be approximately valid, but disputed the envelope connotation. He argued that in the topography of the limiting streamlines, they must begin and end at (at least) one nodal point of attachment and one nodal point of separation. When two nodal points of attachment exist, Lighthill proposed that the limiting streamlines from each node must meet somewhere, and there must be a "saddle point". He sketched these as we see on Figure 13.2. Lighthill proceeded to define a separation line as one which issues from both sides of a saddle point of separation, and having embraced the body, disappears into a nodal point.

Let us look at these conceptual limiting streamline patterns about some flow components. The slender wing at incidence, shown on Figure 14, is a convenient first example. Lighthill suggests

that the surface pattern is generated from two nodal points of attachment and a saddle point of separation which are coalesced at a sharp apex, but are distinct if the apex is rounded — see Figure 14.1. The limiting streamlines converging towards the 3D separation line S and diverging from the attachment line A are asymptotes rather than meeting at S or emanating from A.

Maskell's view, on the other hand, is shown on Figure 14.2. Clearly, for a sharp apex, it will not be possible to distinguish from flow visualization patterns which interpretation is philosophically correct, and for most practical purposes, it probably does not matter. The term "envelope" does seem to be a useful word to describe the merging of the limiting streamlines at the 3D separation line, and the mathematical interpretation is bound up with whether we want to look at solutions of the Navier-Stokes equations or boundary-layer equations*; and also whether it is possible for singular behaviour of the limiting flows to occur in practice[10]?

Does the limiting streamline pattern about a blunted slender body at incidence, where lengthwise as well as transverse pressure gradients exist, provide additional help in diagnosing the approach to separation? An investigation of the subcritical flow about a 6:1 ellipsoid at high Reynolds number was reported in References 11 and 47, in which circumferential measurements of surface static pressure, surface impact pressure and oil-dot flow visualization were made, to identify the 3D viscous flow development. In contrast with the near conic viscous flowfield about the slender wing, the more general body flow exhibits substantial lengthwise effects, although the circumferential pressure gradients still dominate.

Figure 15 presents limiting streamlines on the ellipsoid at Mach 0.74, and at a Reynolds number of 44 million based on the 54-inch length of the body. The boundary layers were turbulent. The streamlines were deduced from oil-dot flow visualization records at angles of incidence from 10° to 25°, with only a few of them drawn for purposes of clarity. At the lowest angle of incidence shown, the flow is attached everywhere except for a bubble over a small region of the leeward afterbody, that is probably due to the effects of truncating the model for a sting mount through the model base. As we increase the angle of incidence, the circumferential adverse pressure gradient just past the $\phi = 90°$ position becomes more severe, causing a progressive thickening of the flow on the leeward side of the body; until at $\alpha = 25°$, there are two regions of coalesced limiting streamlines where we interpret that 3D separations are present. (This is not a very slender ellipsoid, but a corresponding situation would exist, of course, on a more slender ellipsoid at a reduced incidence.)

Figure 16 shows the calculated and the experimental isobar patterns (as well as some circumferential pressure distributions) on a distorted surface development at $\alpha = 25°$. A favourable circumferential pressure gradient is indicated by large open arrows and unfavourable gradients by shaded arrows. At this incidence, the circumferential pressure gradients completely swamp the axial gradients. From the calculated inviscid pressure distribution, we expect separation to occur somewhere on the lee-side of the minimum pressure line and the experimental pressure distribution reflects this. The separation lines taken from the oil-dot flow visualization records are shown here as chain-dotted lines. Figure 15 displays that the turbulent boundary layer separates, along S_1, over about the rear 60 percent of the body soon after it encounters the circumferential adverse pressure gradient. The flow with separation is symmetrical, with an attachment region along the leeward meridian, $\phi = 180°$, that is especially noticeable near the rear. We also see a secondary separation line S_2, extending well forward, outboard of this attachment.

The limiting streamlines can all be traced back to emanate from the attachment region on the nose and we cannot tell from the resolution provided by the oil streaks whether or not we have a system of nodal attachment and saddle separation points as Lighthill has conjectured[39]. The separation, attachment and re-attachment lines are fed from the upstream stagnation attachment region. There is a progressive thickening of the leeward flow with axial distance from the nose, with the limiting streamlines appearing asymptotic to the 3D separation lines as they approach the lines from either side. Just

---

* The boundary-layer equations, clearly, are not valid near either separation or attachment.

where the viscous vortices start can only be determined from profile measurements through the boundary layer. There is no theory available to predict them. At $\alpha = 25°$, substantial suction peaks in the circumferential wall static pressure distributions have developed along the body from $x/L = 0.25$, indicating roll-up of the viscous vortices from the primary separation lines, S_1 [11,47]. There is fluid flow along the directions of S_1 and S_2 as well as along the (secondary) attachment line that exists between S_1 and S_2, so that the skin friction is finite everywhere. It is noteworthy that a similar ellipsoid at high incidence in Werlé's water tunnel[77], with laminar boundary layers present, exhibits similar flow features to those just discussed in turbulent flow. Calculations of the laminar boundary layer (up to the primary 3D separation line) about an ellipsoid at incidence have recently been published by Geissler[56] with good qualitative accord with the results already discussed.

In this discussion on limiting streamlines, let us now look at the case of a bluff protuberance standing normal to a wall, where the streamwise adverse pressure gradient rather than the transverse gradient dominates the flow development. Even though in supersonic flow we have a bifurcated shock structure where the foot of the detached bow shock wave contacts the viscous flow ahead of the protuberance, the qualitative details of the limiting streamlines are virtually independent of Mach number[11]. For example, Figure 17 shows the limiting streamlines about a long circular cylinder standing normal to a wall in a Mach 2.5 stream[48], where the Reynolds number based on the undisturbed boundary-layer thickness, $\delta_o = 2.5$ cm, is $R_{\delta_o} = 4.8 \times 10^5$. The flow is from left-to-right. There is a saddle-point of separation S on the axis of symmetry about two diameters ahead of the cylinder wall, from which the 3D primary separation line emerges to pass around and downstream of the cylinder. Upstream and downstream limiting streamlines converge towards the 3D separation line to feed a viscous horse-shoe vortex springing from the separation within the depth of the undisturbed boundary layer. (We note that even though the scale of the separation relative to the undisturbed boundary-layer thickness is many times less than for the slender wing or slender body flows, the consequences are still severe.) A streamline in the outer boundary layer attaches at the nodal point A in the plane of symmetry just ahead of the cylinder junction with the wall, from which an attachment line emerges along the leading-edge and divergent limiting streamlines pass around and downstream of the cylinder. One limiting streamline passes from the attachment node to the saddle point of separation. Others fan out from the attachment point in the plane of symmetry to eventually proceed towards the 3D separation line. Superimposed on the limiting streamline pattern, we observe the bow shock wave B, and the rear leg (or Mach stem, M) of the bow shock bifurcation. The lower photo on Figure 17 illustrates the flattened horse-shoe vortex made apparent by means of the vapour screen technique.

More than one separation line may be formed ahead of the cylinder, depending upon the Reynolds number of the oncoming flow and the scale of the boundary layer relative to the cylinder dimensions. The picture on Figure 18 shows a case with three such zones, for example, after Sedney and Kitchens[48].

We have seen that in all of the examples discussed, the limiting streamline that is characteristic of a 3D separation line, has one feature in common. It is a barrier across which the limiting streamlines on either side of it cannot pass. Whether we prefer to accept the subtle details of either Maskell's envelope approach[1] or Lighthill's asymptote arguments[39] on the flow conditions immediate to a separation or an attachment line, elements of both treatises would appear to exist. In general, flow visualization records do not allow us to distinguish which interpretation is absolute. More experiments are clearly necessary to diagnose the flow features adjacent to 3D separations and re-attachments.

3.0 EXAMPLES OF THREE-DIMENSIONAL SEPARATIONS ON PRACTICAL CONFIGURATIONS

3.1 Upswept Fuselages

Let us commence our illustrative examples by looking, first of all, at flows about upswept afterbodies. A typical complicated flow problem of this kind is shown on Figure 19.1. Here we can see from the tufts on the side of the upswept rear fuselage of a de Havilland of Canada Caribou aircraft that very large cross-flow angles are present, and separation is occurring along the lower rounded flanks

of the fuselage. The cross-flow is exaggerated in this illustration by the large flap angle, but even under cruising conditions for this class of rear-loading aircraft, 3D separations are sometimes present.

In the context of this review, the separations from the rounded underside are uncontrolled in that depending on the aircraft pitch and yaw angles, the separation positions will move around the body and may cause handling problems. The flow separations can be fixed in location to alleviate handling deficiencies by fitting a strake to the fuselage side, Figure 19.2, or by using a sharp edge to the fuselage underside as we seen on Figure 20, on the de Havilland of Canada Buffalo aircraft.

The next illustration, Figure 21, shows surface flow visualization on a research model tested in the NAE 5 X 5-ft. wind tunnel. The straight "beaver tail" shape, with elliptic cross-sections, is fairly typical of small aircraft of the twin-engine STOL type, but the upsweep angle, which was adjustable on this model, was set at a large upsweep angle of 20°. We note that even though primary and secondary separations are clearly present, the flow is symmetrical and well organized. We know virtually nothing, unfortunately, about turbulence fluctuation levels bordering 3D separations. Figure 22 indicates substantial increases in the amplitude of surface pressure fluctuations as the scale of the separations becomes greater.

The turbulent shear layers springing from the primary separation lines roll-up to form vortex motions, which we show on Figure 23, by pitot pressure isobars measured beneath another elliptical section afterbody. The analysis of this type of flow, which presents many difficulties, is further complicated by the presence of the wing downwash field and additional separations that may be present in the wing-root junction and from bulbous wheel housings, Figure 24. Thus, while we have a qualitative understanding of fuselage flows, we are still far from being able to predict the viscous-inviscid interactions about upswept bodies.

3.2 Pointed, Slender Missiles

On very long pointed slender bodies, we find that separation first occurs symmetrically with a pair of vortices trailing back along the body. Figure 25.1 illustrates such body separations on a blunted cone-cylinder-flare model. The symmetrical body vortices in low speed flow have been well documented by Grosche[20], an illustration from which is given on Figure 25.2 (top); when a wing is added to the body, there is a substantial change in the position of the body vortices in the flowfield due to the larger induced effects of the controlled flow separations at the wing swept edges, see Figure 25.2 (bottom). These separations have an important effect on the static and dynamic flight stability of such vehicles. At small incidences, where the separation is steady and symmetrical with respect to the incidence plane, the resulting body vortices produce a nonlinear contribution to the normal force and pitching moment. If the fin system is not symmetrically orientated with respect to the incidence plane, a cross-coupling side force, yawing moment and rolling moment can arise even at small incidences. At larger incidences, the separations and body vortices become asymmetric (but still relatively steady in space) and large side forces, yawing moments and rolling moments are developed, especially on fin-stabilized vehicles. Figure 26, which gives the primary turbulent boundary-layer separation positions on the port and starboard side of a cone-cylinder and ogive-cylinder respectively, shows that the nose shape has an important influence on the initial asymmetry of the flow. For the 18° incidence case illustrated, the conical nose is at a relative incidence of about 3.1 and has generated substantial flow asymmetry, whereas the shorter ogival nose is only at a relative incidence of about 1.3 at the nose, where the initial separation is symmetrical. A ring of grit or a ring of vortex generators downstream of a bluff-nose can reduce yawing moments by factors of two or more.[62]

We may judge the occurrence of the onset of asymmetry by, say, the side force exceeding five percent of the normal force. This is illustrated on Figure 27. At subsonic speeds, where these asymmetric effects are most pronounced, we see that (following the trend indicated on Figure 26) as the semi-apex angle at the nose is increased, the onset of flow asymmetry is delayed. A longer afterbody, as one would expect, hastens the asymmetry, by providing a larger effective normalized incidence, α/θ_c. At higher Mach numbers (at $M_\infty = 3.5$, for the tests shown on Figure 27) when shock waves are present in the cross-flow, the separation positions remain symmetrical and the side forces disappear.

3.3 Slender Wings and Slender Bodies with Strakes

The most studied example of three-dimensional separation occurs along the leading-edges of lifting slender wings, as we discussed with the aid of Figure 5. The conical, inviscid flow theories, for example, that of Mangler and Smith[10], that have accounted for the vortex sheets springing from the leading-edges and coiling-up above the wing, cannot include the effects of compressibility, nor the unloading that occurs at a subsonic trailing-edge. Polhamus[49,50] has attempted to remedy this with an overall theory, which assumes that, due to separation, the leading-edge suction force is rotated 90° into a direction normal to the wing chord plane thus given a nonlinear component to the normal force. While no theoretical proof of this method has been established, there is no doubt that it works. (In fact, Lamar has recently extended the Polhamus method to treat the vortex flow characteristics of wings with side edges[51].)

Figure 28 shows the overall normal force measured on a sharp-edged 70° delta wing under high Reynolds number conditions at Mach numbers of 0.7 and 1.6. The agreement of the subsonic measurements with the Polhamus theory is excellent up to a relative incidence of about unity. The departure from Smith's conical theory[10] is evident. We notice that there is a marked decrease in the nonlinear lift at supersonic speeds even though at Mach 1.6, the wing is still slender $\sqrt{M^2-1}\ s/L \simeq 0.43$. Other experimenters have noted that this is associated with a substantial flattening of the lee-side vortex structure[33].

More complicated, but still conical cases have been treated by Levinsky and Wei[52] using essentially the same formulation as Mangler and Smith[10], but accounting for a conical body. Some measurements that we have made using a 5° semi-apex angle cone with 75 percent strake wings are shown on the next illustration, Figure 29.1, in comparison with the Levinsky and Wei nonlinear theory. Up to relative incidences of about two, the experimental results for the subsonic and supersonic Mach numbers agree; but at higher relative incidences for the $M_\infty = 1.8$ case, conically mixed flow with internal shock waves occurs. The strakes provide a case of fixed or controlled flow separation to give a substantially different conical flow field to that on the 5° cone alone[53]. But, while the Levinsky and Wei nonlinear theory accounts for the leading-edge separations, it cannot cope with the strong body separations in the wing-body junctions[11].

The flow about an ogive-cylinder with strakes at a sweepback angle of 78° at Mach 2 were studied by Fellows and Carter[63]. If we extrapolate the trend of Figure 27, the 17° semi-apex nose angle of the ogive in Reference 63 would have precluded flow asymmetry from body vortices up to angles of attack of about 50°. Vapour screen photos on Figure 29.2 depict a progressive and massive increase in scale of the strake symmetrical vortices (in relation to body geometry) above the lee-side of the body up to α/θ_c of greater than two.

One very important use of controlled flow separation in design is the low aspect ratio strake[54,55] mounted ahead of a wing of moderate sweep and aspect ratio such as the F-16 (Fig. 4.1) and the F-17 (Fig. 30). One significant advantage offered by the strakes is the induced lift provided by strake vortices to extend the manoeuvring capabilities of the aircraft in transonic flow. With the aircraft at incidence, as we see on Figure 30, the fixed separations at the strake leading-edges form vortices that pass back over the main wing alongside the fuselage. Additional controlled separations are generated by the fuselage boundary-layer bleed diversion slots at the strake/fuselage intersection, the air from which is entrained into the strake vortices. The flow over the main wing appears to be attached, with a swept shock/turbulent boundary layer interaction proceeding to the tip. Küchemann[55] has proposed that the vortex avoids the necessity for the formation of the usual forward branch of the wing shock pattern by providing a "soft" boundary for the flow turning inboard over the leading-edge, instead of the "stiff" boundary given by the fuselage side[10].

3.4 Hypersonic Configurations

The non-slender delta wing at incidence, with supersonic leading-edges, has received considerable attention by Whitehead et al[32,33] and by Cross[57]. The lee-side flow field (Fig. 31.1) is dominated by a swept-shock boundary-layer interaction that causes a three-dimensional separation of most of the

top-wing boundary layer. The swept shock is inside the bow shock wave envelope, being positioned very close to a free stream Mach cone from the wing apex. In contrast to the subsonic leading-edge delta-wing flow that is dominated by leading-edge separation, (Fig. 31.2), the supersonic leading-edge flow is characterized by a Prandtl-Meyer expansion. Along the attachment line on the lee-side meridian, intense heating is measured[33]. If a body is attached beneath the delta wing, the flow field becomes complex in detail on the underside. Figure 32 shows flow separation and attachment lines on the under-surface of a half-cone delta wing at 15° incidence at Mach 12.6. Boundary-layer conditions are laminar. The transmitted shock from the cone produces separation on the delta wing, and there is also a junction-type separation. The high local heat transfers at the flow attachment lines on the same configuration are shown in the next graph, Figure 33, as well as the heat transfer minima at the separation lines.

As we saw on Figure 9, the contouring of the leading-edge of a planar 70° swept delta wing at Mach 6 alleviated the heating on the lee-meridian. Can the philosophy of controlled flow separation be used to reduce the peak heating on Space Shuttle shapes? Figure 34 shows surface oil flow on an Orbiter vehicle[58] at 30° incidence at a Mach number close to 20. The three-dimensional separation from the wing fillet passes back across the top surface of the wing (analogous to the strake flow discussed with reference to Fig. 30) although it is now associated with a swept shock wave. Another 3D separation, beginning about the cockpit housing, and continuing downstream is also evident, with an attachment region existing on the fuselage side and on the leeward meridian. Unfortunately, no circumferential heat transfer measurements were taken in Reference 58 to improve the identification of the attachment line regions.

The potential for altering the lee-surface geometry to achieve reduced lee-side heating[59] is shown on Figure 35 for several shuttle configurations at Mach 6 and 8. The idea was to use relatively sharp edges to fix or control the 3D separations and encourage the coiling-up of the viscous shear layers to leave the proximity of the fuselage.

On the left of Figure 35, the initial slope of the side profile was increased and then broken sharply. We see that the heating data resulting from this modification show a substantial reduction along 50 percent of the leeward meridian. Additional verification of the potential for reduced lee-side heating by controlled flow separation is discussed by Shultze and McGee[60] and by Connor[61]. The configuration of the former authors with relatively large initial slope angle and sharp break in contour generated significantly lower lee-surface heating than did the shape chosen by Connor, who used less sharp contour changes.

3.5 Swept Interactions

The three-dimensional interaction between a turbulent boundary layer, developing along a surface and a perpendicular, glancing oblique shock wave (sometimes called a "skewed" shock wave) — see Figure 37 — is a phenomenon of considerable importance in the design of swept wings, wing/body and tail/body junctions, quasi-2D and half-cone inlets. Figure 36, for example, shows a half-cone inlet of a typical fighter aircraft operating near design at Mach 1.6, with the shock from the half-cone causing a massive 3D separation of the fuselage boundary layer.

Despite several previous investigations[64-67], Green noted[68] that there was little quantitative understanding of interactions between swept shock waves and turbulent boundary layers, although Stalker[64] and Stanbrook[65] introduced some qualitative features in their early work, while later investigations by McCabe[66] and Lowrie[67] provided some insight into the crossflows developing in the interaction. Much of the existing analysis has been developed for so-called "infinite" swept flows, and so is of a quasi two-dimensional nature; while most experiments have been conducted using the nozzle boundary layers in relatively small supersonic wind tunnels. At a given mainstream Mach number, the flow deflection angle for so-called "incipient separation" has usually been determined as when the limiting streamlines become parallel to the projection of the shock wave (in the external stream) on to the wall, and Korkegi[69] has made a simple correlation of incipient separation data from References 66 and 67.

In some experiments[16,17] in the NAE 5 X 5-inch blowdown (pilot) wind tunnel, the mean flow features including wall static pressure, surface impact pressure and limiting streamline direction, and pitot and stagnation temperature profiles, were gathered through swept interactions at mainstream Mach numbers of 2 and 4, up to and beyond flow deflection angles through the shock wave that produced three-dimensional separation, see Figure 37. The Reynolds number based upon the mainstream conditions and the undisturbed boundary-layer thickness, δ_o, of 0.2-inch, was 2×10^5. The wall conditions were essentially those of zero heat transfer. (Similar boundary-layer experiments were conducted by Oskam[18] at Princeton University.)

Subsequently, for the Mach 2 flow, a small convergent/divergent tangential wall jet nozzle was installed in the test wall (Fig. 38) upstream of the interaction region, to investigate whether a strong three-dimensional shock-induced separation could be controlled or destroyed by a Mach number 3 supersonic wall jet. (The planning of the 3D experiment followed the criteria established by Peake[70] for supersonic blowing boundary-layer control in a two-dimensional shock/boundary-layer interaction.) The direction of the jet efflux could be oriented at various angles with respect to the line of separation, as we see on the diagrammatic sketch of Figure 37.

Figure 39 shows the effects of a wedge deflection angle of 16° in a Mach 4 airstream where there is a substantial 3D separation generated way ahead of the shock wave in the external flow (as we see on the wall pressure plot and the Schlieren/oil dot flow visualization picture). The pitot pressure profiles through the interaction, measured by a 3-tube yawmeter that nulled into the direction of the local velocity, are shown on the top graph of Figure 40. The profile measurement stations situated relative to the calculated shock are shown at the intersection of the pitot profiles with the abscissa. The profiles are sufficiently close together to allow a construction of the forward oblique leg of the shock bifurcation at the foot of the wedge shock. Downstream of the 3D separation line position, the presence of the shear layers with heat transfer is indicated by rapid changes and troughs on the temperature plots. From these distributions, we may postulate that the deficit troughs correspond with the core flow of a flattened vortex structure of the rolled-up shear layer from the 3D separation line, much like the corner flow model proposed by Cooper and Hankey in Reference 71 and witnessed via electron beam flow visualization by Henderson and Bertram[72]. The axis of the vortex would appear to be just ahead of the line of the calculated shock (the origin of which is the wedge apex) where the "overshoot" towards 0° on the yaw profile (that is, parallel to the mainstream at infinity) is at its maximum. The substantial swings in the total temperature distributions, Figure 41.1, that are found in distinct contrast to the expected form in unseparated flow, Figure 41.2, would appear to be a useful indicator of a 3D separated flowfield.

Can such an undesirable 3D separation be diminished or destroyed by blowing boundary-layer control, for we know that on swept wings, especially in transonic flow, the viscous vortex from a 3D separation can sometimes burst over the wing, leading to unpleasant difficulties in airplane control; while in the quasi-2D supersonic intake, once 3D separations are present on the sidewalls, they appear to promote high fluctuation and distortion levels at the compressor face further downstream. But perhaps the most significant aspect of 3D separated flows in the hypersonic régime, is the high heat transfer to the surface in the region of flow-re-attachment, which poses severe problems of skin cooling, as we have seen already. The particular losses caused by the pitot pressure deficit in the rolled-up viscous vortex, and the associated skin friction increases in re-attachment zones, have not been quantified to the author's knowledge.

On Figure 42, we demonstrate the invigoration of the 3D wedge-generated separation by a Mach 3 supersonic wall jet. This illustration provides a selection of wall static pressure distributions along and just off the tunnel centre-line for various angular settings of the jet efflux with respect to the tunnel centre-line. The positive sign of θ_j indicates a jet direction towards the wedge surface, and this angular setting yields no control, and large peaks and troughs in the static pressure distribution(s) corresponding with free vortical shear layer(s) rolling up from the three-dimensional separation line(s). On the other hand, the jet rotation angle of $-25°$ produces a relatively smooth pressure rise. The wall jet has produced a local expanding flow around the wedge leading-edge (due to the 25°-11.5° expansion angle) to alleviate the originally induced large shock pressure rise. In the present, constrained

geometrical conditions, it is not clear, unfortunately, whether the advised direction of blowing would carry over to controlling a 3D shock-induced separation on, say, a swept wing or body flow with internal shock waves[74].

4.0 CONCLUDING REMARKS

In this brief review, we have illustrated some of the diverse kinds of fixed and unfixed three-dimensional separations that can, and do, occur on aircraft and missiles. It is evident that the concept of controlled flow separation in three-dimensions provides the designer with substantial rewards in having a qualitatively non-varying flowfield at his disposal. However, we must always be aware of the consequences on flight vehicle drag, which are not readily predictable. At the outset, we have no quantitative yardstick to determine the scale of the device to "fix" separation, and to say how "sharp" should a sharp edge be? We do not understand what determines the scale of the resulting vortical flows from 3D separations, and when they will be close to the surface and when they will not? What precise influence does body shape and vehicle relative incidence have on the scale of separation? Substantial research effort is required to reveal the answers to these questions, as all practical configurations produce three-dimensional interactions and vortical flows.

A few important examples of controlled flow separation from other sharp-edge devices such as canards and notches have been omitted. However, these will be covered in the forthcoming AGARDograph (see Acknowledgment).

In closing, may we end with a plea for much greater efforts by the academic and research organizations, to resist thinking in terms of two-dimensional flows for expediency, and to work on three-dimensional interaction problems that do relate to pragmatic design.

As of now, we see that, in general, even if the inviscid interfering flowfields can be calculated, *the growth, separation and roll-up of* three-dimensional turbulent boundary layers cannot yet be adequately predicted.

5.0 ACKNOWLEDGMENTS

All of the NAE work referenced herein was promoted initially and has progressed since, in conjunction with W.J. Rainbird of Carleton University. I should like to acknowledge his continuing interest, stimulating input and motivating discussion throughout.

This review contains the framework around which an AGARDograph* is being compiled on "Three-Dimensional Interactions and Vortical Flows at High Speeds", which should be published in 1976/77. Acknowledgment is made to my editor at AGARD, Dr. R.H. Korkegi, for his permission to publish the following comments, which were given to a symposium on "Viscous Flows", held at the Lockheed — Georgia Company, Marietta, Georgia, U.S.A., on June 22/23 1976.

6.0 REFERENCES

1. Maskell, E.C. *Flow Separation in Three Dimensions.* RAE Aero. Rept. 2565, November 1955.

2. Küchemann, D. *Flow with Separations.* Unpublished RAE Tech. Memo., December 1955.

---

* Co-authored with W.J. Rainbird, Carleton University, Ottawa, Canada.

3. Maskell, E.C.
Küchemann, D.
Controlled Separation in Aerodynamic Design.
Unpublished RAE Tech. Memo., March 1956.

4. Cornish, J.J., III
High Lift Applications of Spanwise Blowing.
ICAS Paper 70-09, September 1970.

5. Bradley, R.G.
Wray, W.O.
A Conceptual Study of Leading-Edge-Vortex Enhancement by Blowing.
Jour. Aircraft, Vol. 11, No. 1, January 1974, pp. 33-38.

6. Campbell, J.F.
Augmentation of Vortex Lift by Spanwise Blowing.
AIAA 75-993, August 1975.

7. Barsby, J.E.
Calculations of the Effect of Blowing from the Leading-Edges of a Slender Delta Wing.
RAE Tech. Rept. 71077, ARC R and M 3692, 1971.

8. Spillman, J.
Goodridge, M.
Flow Characteristics about a Delta Wing at 15° Incidence with and without Leading-Edge Blowing.
Coll. of Aero., Cranfield, Rept. Aero. 9, 1972.

9. Alexander, A.J.
Experiments on a Delta Wing using Leading-Edge Blowing to Remove the Secondary Separation.
Coll. of Aero., Cranfield, Rept. 161, 1963.

10. Smith, J.H.B.
A Review of Separations in Steady, Three-Dimensional Flow.
AGARD CP-168, May 1975.

11. Peake, D.J.
Rainbird, W.J.
Atraghji, E.G.
Three-Dimensional Flow Separations on Aircraft and Missiles.
AIAA Jour., Vol. 10, No. 5, May 1972, pp. 567-580.

12. Rainbird, W.J.
Crabbe, R.S.
Peake, D.J.
Meyer, R.F.
Some Examples of Separation in Three-Dimensional Flows.
CASI Jour., Vol. 12, No. 10, December 1966, pp. 409-423.

13. Peake, D.J.
Three-Dimensional Flow Separations on Upswept Rear Fuselages.
CASI Jour., Vol. 15, NO. 10, December 1969, pp. 399-408.

14. Sedney, R.
Kitchens, C.W.
The Structure of Three-Dimensional Separated Flows in Obstacle, Boundary-Layer Interactions.
AGARD CP-168, May 1975.

15. Hsia, H.T-S.
Seifert, H.S.
Shocks Induced by Secondary Fluid Injection.
AIAA 64-111, January 1964.

16. Peake, D.J.
The Three-Dimensional Interaction of a Swept Shock Wave with a Turbulent Boundary Layer and the Effects of Air Injection on Separation.
Ph.D. Thesis, Carleton University, Ottawa, Canada, March 1975.
NRC, Aeronautical Report LR-592, National Research Council Canada, Ottawa, Ontario, July 1976.

17. Peake, D.J.
Rainbird, W.J.
The Three-Dimensional Separation of a Turbulent Boundary Layer by a Skewed Shock Wave; and its Control by the Use of Tangential Air Injecion.
AGARD CP-168, May 1975.

18. Oskam, B.
Vas, I.E.
Bogdonoff, S.M.
An Exploratory Study of a Three-Dimensional Shock Wave Boundary Layer Interaction at Mach 3.
AGARD CP-168, May 1965.

19. Korkegi, R.H.
Survey of Viscous Interactions Associated with High Mach Number Flight.
AIAA Jour., Vol. 9, No. 5, May 1971, pp. 771-784.

20. Grosche, F.R.
Wind Tunnel Investigation of the Vortex System Near an Inclined Body of Revolution with and without Wings.
AGARD CP-71, September 1970.

21. Rao, D.M.
Whitehead, A.H.
Lee-Side Vortices on Delta Wings at Hypersonic Speeds.
AIAA Jour., Vol. 10, No. 11, November 1972, pp. 1458-1465.

22. Rubesin, M.
Subgrid or Reynolds Stress Modelling for Three-Dimensional Turbulence Computations.
NASA Report in Preparation, Private Communication, July 1975.

23. Roache, P.J.
Bradshaw, P.
Letters in Response to Reference 24, Astronautics and Aeronautics, Vol. 13, No. 9, September 1975, pp. 4-6.

24. Chapman, D.R.
Mark, H.
Pirtle, M.W.
Computers Versus Wind Tunnels for Aerodynamic Flow Simulations.
Astronautics and Aeronautics, Vol. 13, No. 4, April 1975, pp. 22-29; 35.

25. Weber, J.A.
Brune, G.W.
Johnson, F.T.
Lu, P.
Rubbert, P.E.
A Three-Dimensional Solution of Flows over Wings with Leading-Edge Vortex Separation.
AIAA 75-866, June 1975.

26. Marsden, D.J.
Simpson, R.W.
Rainbird, W.J.
The Flow over Delta Wings at Low Speeds with Leading-Edge Separation.
Coll. of Aero., Cranfield, Rept. 114, February 1958.

27. McRae, D.S.
A Numerical Study of Supersonic Viscous Cone Flow at High Angle of Attack.
Private Communication, Flight Mechanics Division/FXM, Air Force Flight Dynamics Laboratory, Wright-Patterson AFB, Ohio 45433, 1975.

28. MacCormack, R.W.
The Effect of Viscosity in Hypervelocity Impact Cratering.
AIAA 66-354, 1969, pp. 1-7.

29. Tracy, R.R.
Hypersonic Flow Over a Yawed Circular Cone.
GALCIT Memo. No. 69, Graduate Aeronautical Labs., California Institute of Technology, Pasadena, California, 1963.

30. Lubard, S.C.
Rakich, J.V.
Calculation of the Flow on a Blunted Cone at High Angle of Attack.
AIAA 75-149, January 1975.

31. Cleary, J.W.
Effects of Angle of Attack and Bluntness on Laminar Heating Rate Distribution on a 15° Cone at Mach Number of 10.6.
NASA TND-5450, October 1969.

32. Whitehead, A.H.
Bertram, M.H.
Alleviation of Vortex-Induced Heating to the Lee Side of Slender Wings in Hypersonic Flow.
AIAA Jour., Vol. 9, No. 9, September 1971, pp. 1870-1872.

33. Whitehead, A.H.
Hefner, J.N.
Rao, D.M.
Lee-Surface Vortex Effects Over Configuration in Hypersonic Flow.
AIAA 72-77, January 1972.

34. Sears, W.R.
Collected Papers of W.R. Sears Through 1973.
Ed. by N.H. Kemp, March 1974, pp. 61, 94, 162, 167.

35. Maskell, E.C.
On the Principles of Aerodynamic Design.
Prog. in Aero. Sci., Vol. 1, No. 1, 1961, pp. 1-7.

36. Küchemann, D.
Aerodynamic Design.
Aero. Jour., Vol. 73, No. 698, February 1969, pp. 101-110.

37. Legendre, R.
Lignes de Courant d'un Ecoulement Continu.
Rech. Aérosp., No. 105, 1965, pp. 3-9.

38. Legendre, R.
La Condition de Joukowski en Ecoulement Tridimensionnel.
Rech. Aérosp., No. 5, 1972, pp. 241-8.

39. Lighthill, M.J.
Attachment and Separation in Three-Dimensional Flow.
Section II.2.6 of "Laminar Boundary Layers", Ed. by L. Rosenhead, Oxford Univ. Press, 1963, pp. 72-82.

40. Wild, J.M.
The Boundary Layer of Yawed Infinite Wings.
Jour. Aero. Sci., Vol. 16, No. 1, January 1949.

41. Eichelbrenner, E.A.
Oudart, A.
Observations on a Criterion of Three-Dimensional Laminar Boundary-Layer Separation.
Rech. Aéron., No. 40, July-August 1954, pp. 3-5. Also: NRC (Canada) TT-962, 1961.

42. Eichelbrenner, E.A.
Oudart, A.
Three-Dimensional Laminar Boundary-Layer Separation.
Rech. Aéron., No. 47, 1955, pp. 11-14. Also: NRC (Canada) TT-963, 1961.

43. Brown, S.
Singularities Associated with Separating Boundary Layers.
Roy. Soc. of London Phil. Trans., Series A, Vol. 257, 1965, pp. 409-444.

44. Maltby, R.L.
Flow Visualization in Wind Tunnels using Indicators.
AGARDograph 70, April 1962.

45. Eichelbrenner, E.A.
Three-Dimensional Boundary Layers.
Annual Review of Fluid Mechanics, Vol. 5, 1973, pp. 339-360.

46. Cumpsty, N.A.
Head, M.R.
The Calculation of the Three-Dimensional Turbulent Boundary Layer; Part 3, Comparison of Attachment-Line Calculations with Experiment.
Aero. Quart. Vol. XX, 1969, pp. 99-113.

47. Atraghji, E.G.
Surface Visualization, Surface Pressure and Surface Preston Tube Pitot Pressure Measurements over a 6:1 Ellipsoid at Incidence, at Mach 0.3 and 0.74.
NRC (Canada) NAE Data Report 5X5/0032, 1968.

48. Sedney, R.
Kitchens, C.W.
The Structure of Three-Dimensional Separated Flows in Obstacle, Boundary-Layer Interactions.
AGARD CP-168, May 1975.

49. Polhamus, E.C.
A Concept of the Vortex Lift of Sharp-Edge Delta Wings Based on a Leading-Edge Suction Analogy.
NASA TND-3767, December 1966.

50. Polhamus, E.C.
Applications of the Leading-Edge Suction Analogy of Vortex Lift to the Drag due to Lift of Sharp-Edge Delta Wings.
NASA TND-4739, August 1968.

51. Lamar, J.E.
Prediction of Vortex Flow Characteristics of Wings at Subsonic and Supersonic Speeds.
AIAA 75-259, January 1975.

52. Levinsky, E.S.
Wei, M.H.Y.
Non-Linear Lift and Pressure Distribution on Slender Conical Bodies with Strakes at Low Speeds.
NASA CR-1202, 1968.

53. Rainbird, W.J.
The External Flow Field about Yawed Circular Cones.
AGARD CP-30, May 1968.

54. Ray, E.J.
McKinney, L.W.
Carmichael, J.G.
Maneuver and Buffet Characteristics of Fighter Aircraft.
AGARD CP-102, 1972.

55. Küchemann, D.
On the Possibility of Designing Wings that Combine Vortex Flows with Classical Aerofoil Flows.
Unplublished RAE Tech. Memo, 1971.

56. Geissler, W.
Calculation of the Three-Dimensional Laminar Boundary Layer Around Bodies of Revolution at Incidence and with Separation.
AGARD CP-168, May 1975.

57. Cross, E.J.
Experimental and Analytical Investigation of the Expansion Flow Field over a Delta Wing at Hypersonic Speeds.
ARL 68-0027, February 1968.

58. Stone, D.R.
Mulfinger, R.
Hypersonic Stability and Control Characteristics of the Rockwell International 139-B Space Shuttle Orbiter.
NASA TMX-71968, July 1974.

59. Hefner, J.F.
Lee-Surface Heating and Flow Phenomena on Space Shuttle Orbiters at Large Angles of Attack and Hypersonic Speeds.
NASA TND-7088, November 1972.

60. Schultze, H.D.
McGee, K.W.
Heat Transfer Tests of the LMSC Delta-Body Orbiter and Stage-and-One-Half Ascent Configuration.
DMS-DR-1143, Chrysler Corporation, June 1971.

61. Conner, L.E.
Heat Transfer Tests of the Lockheed Space Shuttle Orbiter Configuration Conducted at the Langley Research Center Mach 8 Variable Density Tunnel.
TM 54/20-241, Lockheed Missiles and Space Co., December 1969.

62. Clark, W.H.
Peoples, J.R.
Briggs, M.M.
Occurrence and Inhibition of Large Yawing Moments during High Incidence Flight of Slender Missile Configurations.
AIAA 72-968, September 1972.

63. Fellows, K.A.
Carter, E.C.
Results and Analysis of Pressure Measurements on Two Isolated Slender Wings and Slender Wing-Body Combinations at Supersonic Speeds. Part 1 — Analysis.
ARC CP 1131, 1970.

64. Stalker, R.J.
Sweepback Effects in Turbulent Boundary-Layer/Shock Wave Interaction.
Jour. Aero. Sci., Vol. 27, No. 5, May 1960, pp. 348-356.

65. Stanbrook, A.
An Experimental Study of the Glancing Interaction Between a Shock Wave and a Turbulent Boundary Layer.
ARC CP 555, 1961.

66. McCabe, A.
The Three-Dimensional Interaction of a Shock Wave with a Turbulent Boundary Layer.
Ph.D. Thesis, University of Manchester, October 1963; Aero. Quart., Vol. XVII, August 1966, pp. 231-252.

67. Lowrie, B.W.
Cross-Flows Produced by the Interaction of a Swept Shock Wave with a Turbulent Boundary Layer.
Ph.D. Thesis, University of Cambridge, December 1965.

68. Green, J.E.
Interaction Between Shock Waves and Turbulent Boundary Layers.
RAE TR 69098, May 1969; Progress in Aerospace Sciences, Vol. 11, Pergamon Press at Oxford, 1970, pp. 235-340.

69. Korkegi, R.H.
A Simple Correlation of Incipient Turbulent Boundary-Layer Separation due to a Skewed Shock Wave.
AIAA Jour., Vol. 11, No. 11, November 1973, pp. 1578-1579.

70. Peake, D.J.
The Use of Air Injection to Prevent Separation of the Turbulent Boundary Layer in Supersonic Flow.
NGTE R256, November 1963; ARC CP 890, 1966; M. Sc. Thesis, University of Bristol, 1962.

71. Cooper, J.R.
Hankey, W.L.
Flowfield Measurements in an Asymmetric Axial Corner at M = 12.5.
AIAA Jour., Vol. 12, No. 10, October 1974, pp. 1353-1357.

72. Bertram, M.H.
Henderson, A.
Some Recent Research with Viscous Interacting Flow in Hypersonic Streams.
ARL 75-0212, 1969, pp. 1-30.

73. Culley, M.
Annual Report of Dept. of Supply.
Aeronautical Research Labs., Melbourne, Australia, 1966-67.

74. Rainbird, W.J.
Turbulent Boundary-Layer Growth and Separation on a Yawed Cone.
AIAA Jour., Vol. 16, No. 12, December 1968, pp. 2410-2416.

75.
Private Communication from ARA, Great Britain, 1966.

76. Küchemann, D.
The Aerodynamic Design of Aircraft — An Introduction, Part 5.
RAE Tech. Memo. Aero. 1622, February 1975.

77. Werlé, H. *Aperçu sur les Possibilités Expérimentales du Tunnel Hydrodynamique à Visualisation de l'O.N.E.R.A.* ONERA Tech. Note 48, 1958.

78. Advertisement by Northrop in *Aviation Week and Space Technology*, September 4, 1972.

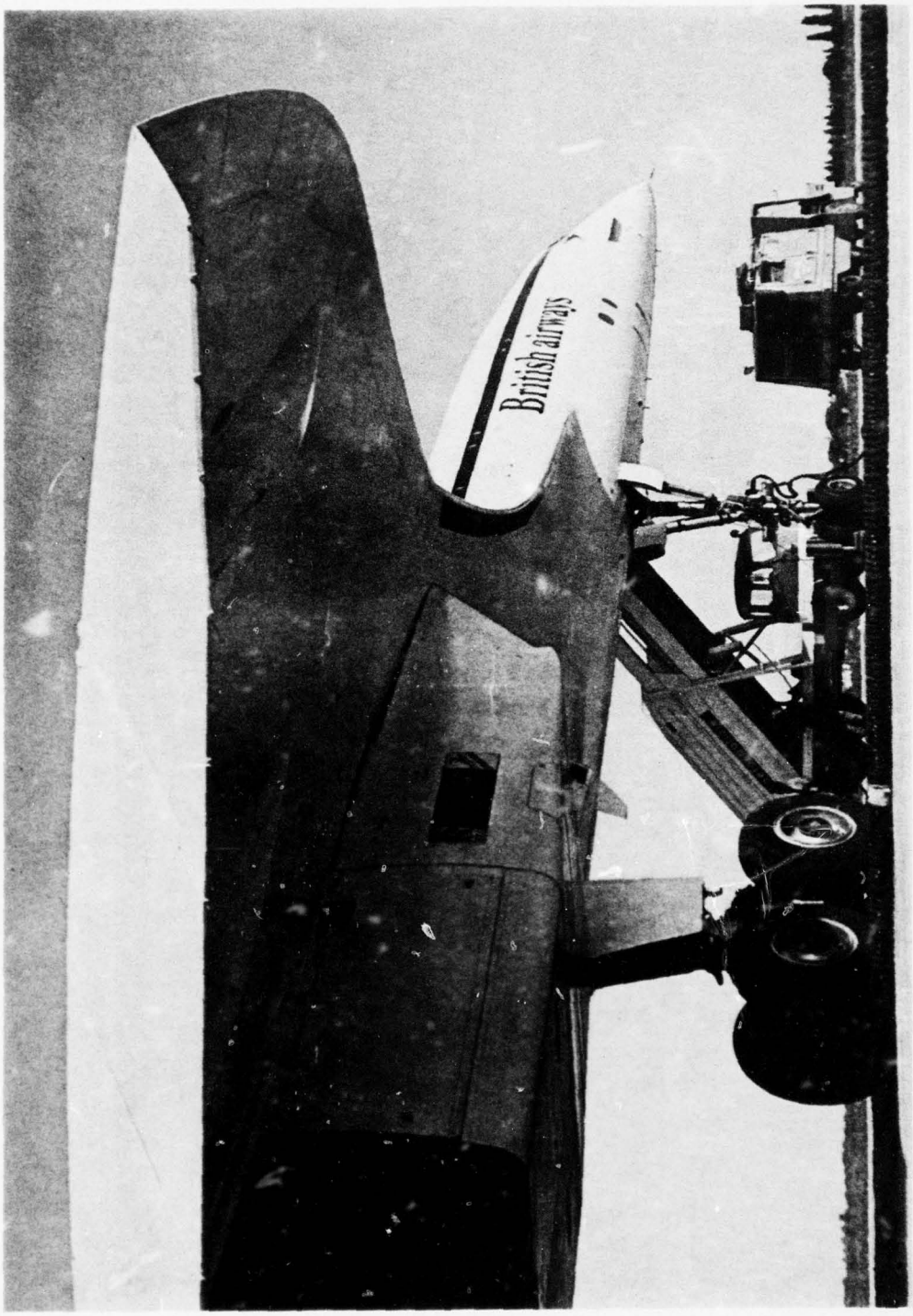

FIG. 1: SHARP SWEPT LEADING-EDGE OF "CONCORDE"

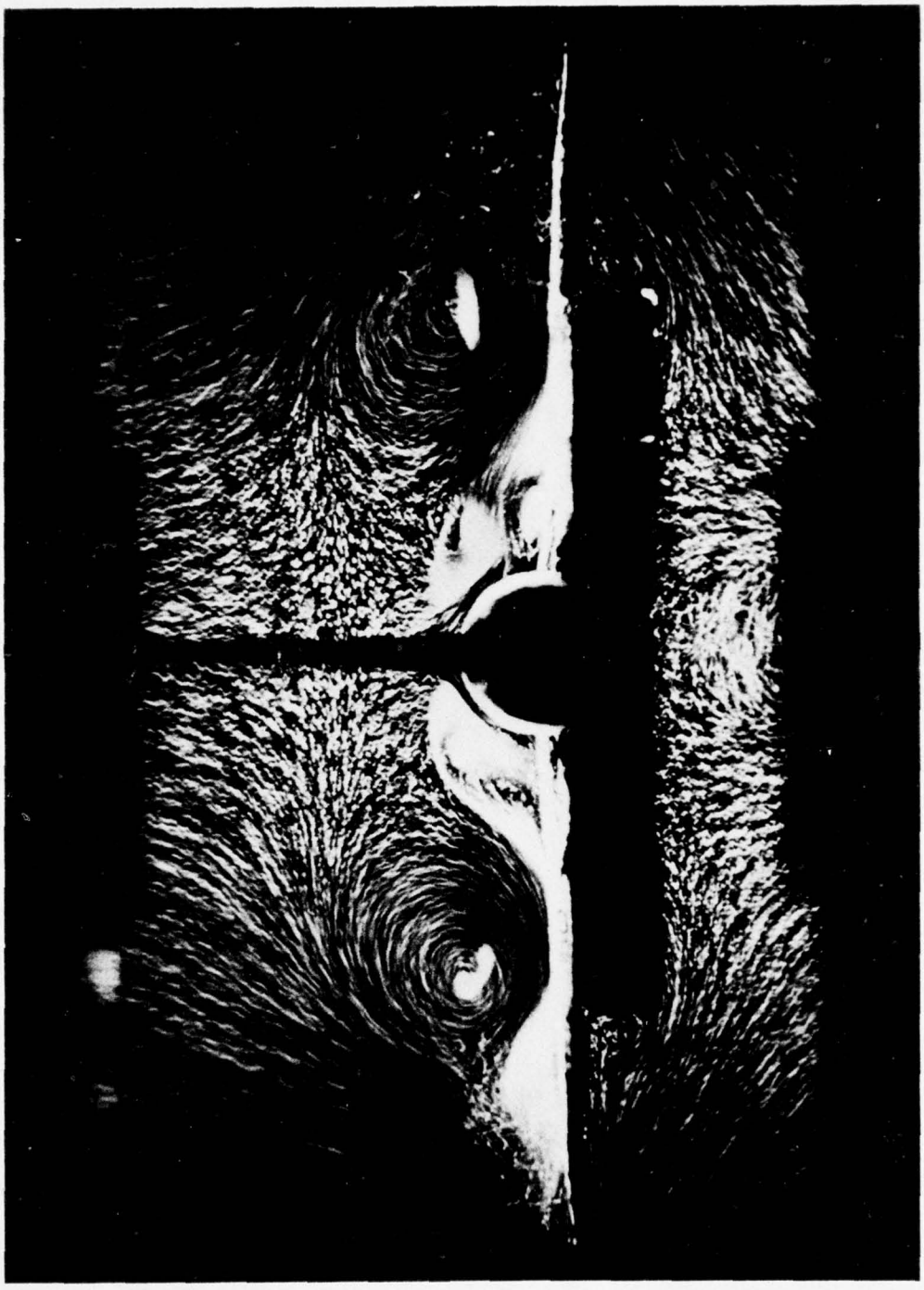

FIG. 2: VORTICES FROM SHARP SWEPT LEADING-EDGES

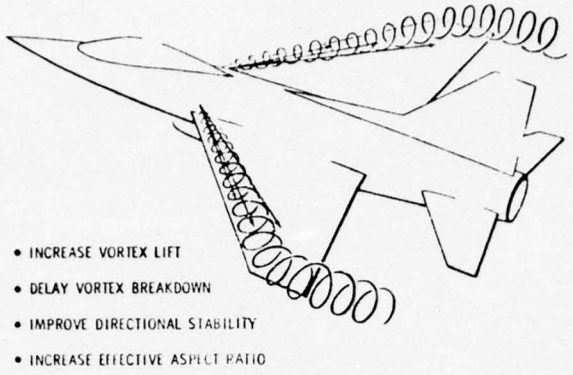

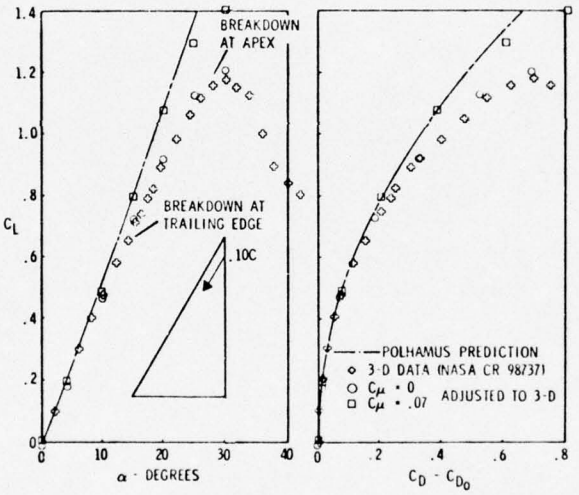

Comparison with theory—delta wing.

FIG. 3: SPANWISE BLOWING ALONG LEADING-EDGE[5]

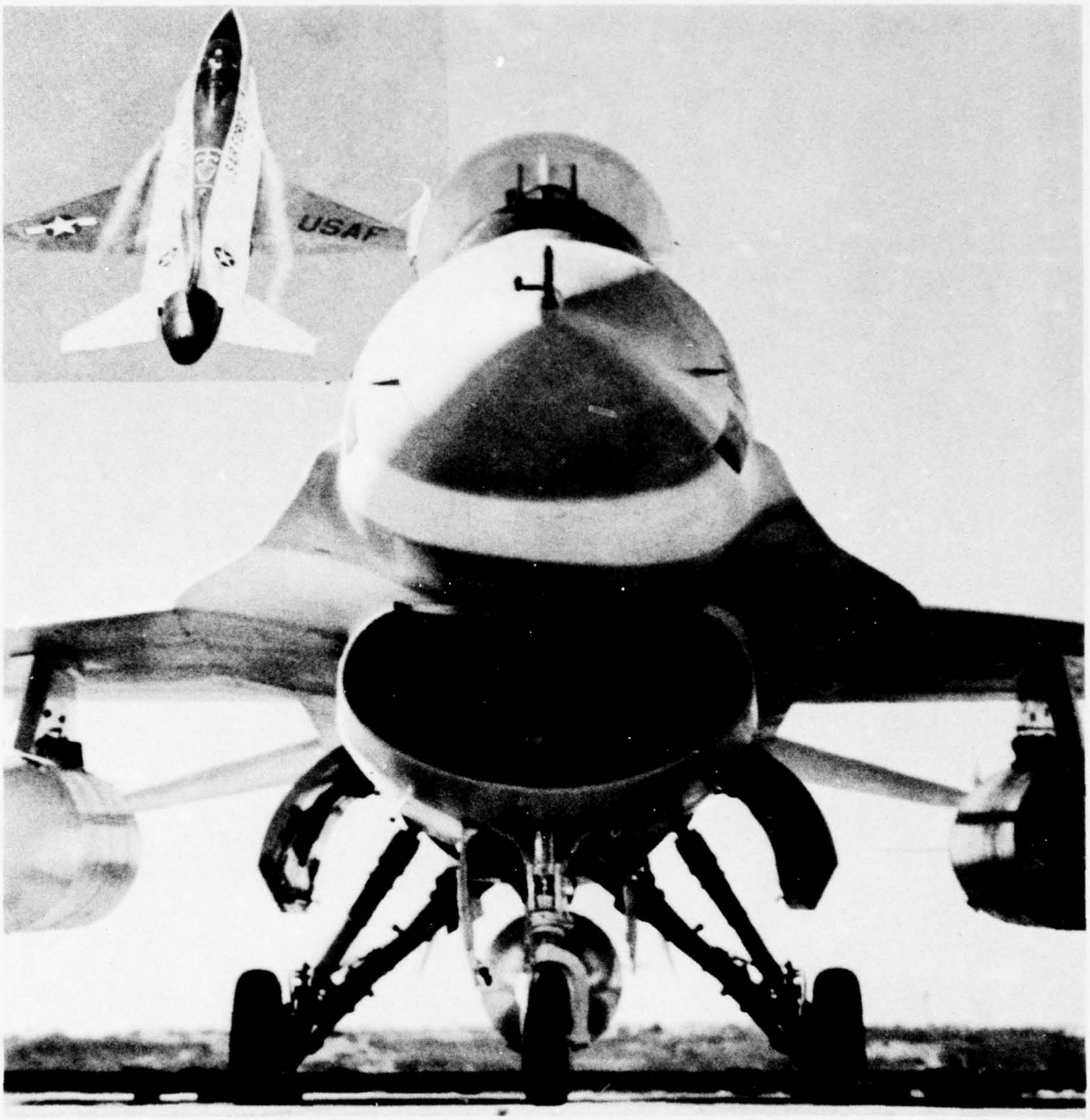

FIG. 4.1: CONTROLLED FLOW SEPARATION FROM STRAKES

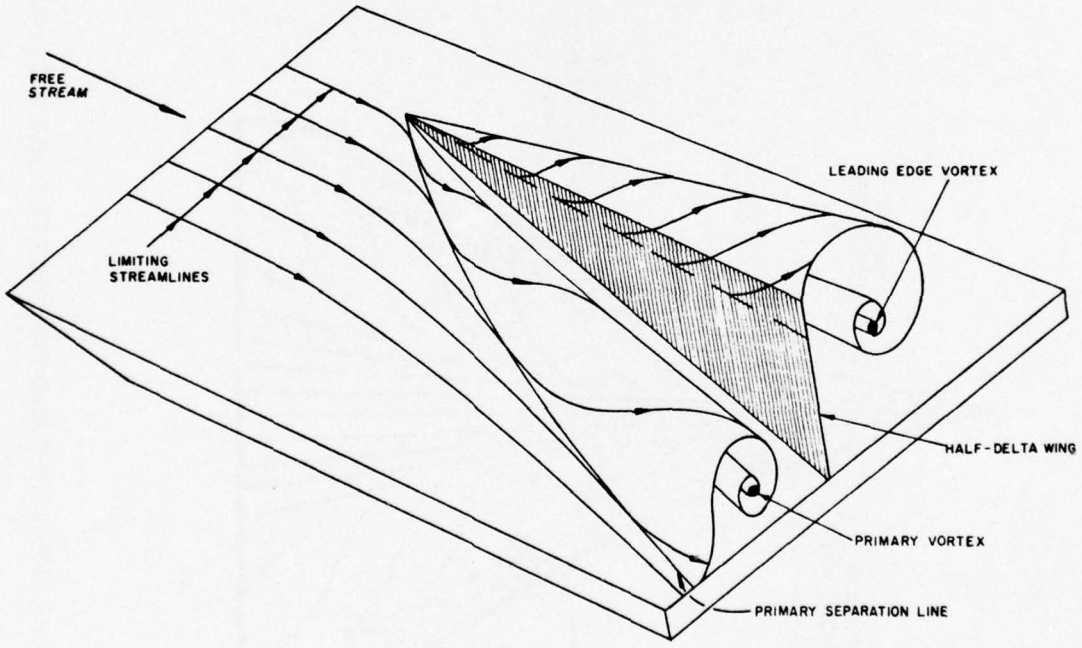

FIG. 4.2: CONTROLLED SEPARATION FROM SWEPT EDGES OF VORTEX GENERATORS ON FUSELAGE[75]

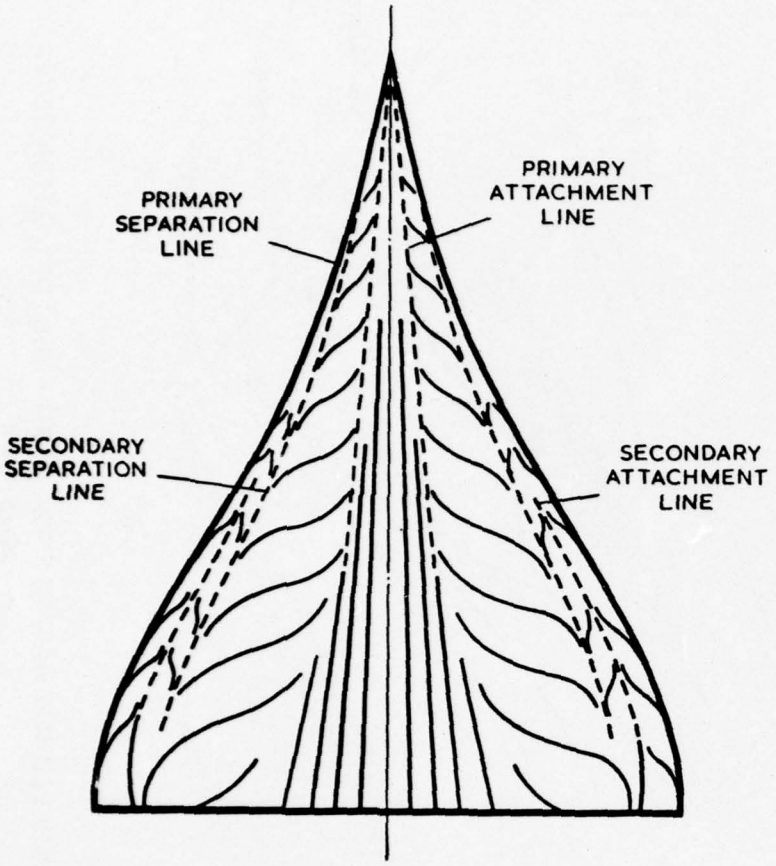

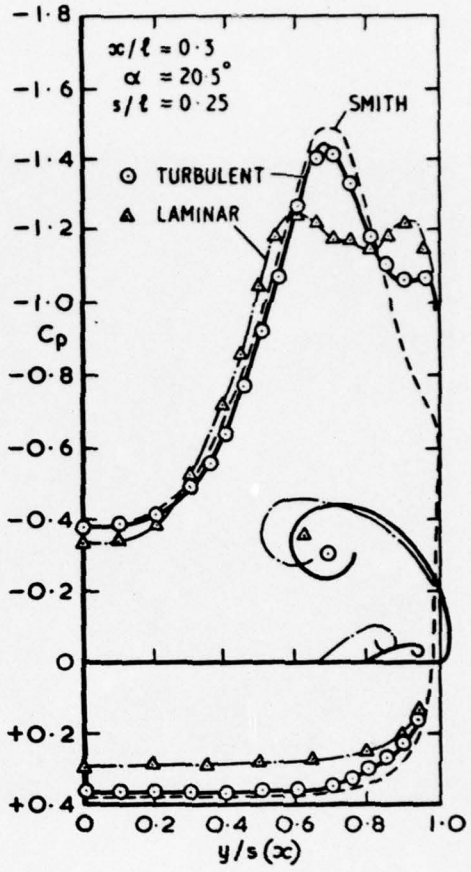

FIG. 5: SURFACE PRESSURES AND LIMITING STREAMLINES ON SLENDER WINGS WITH SUBSONIC LEADING-EDGES[76]

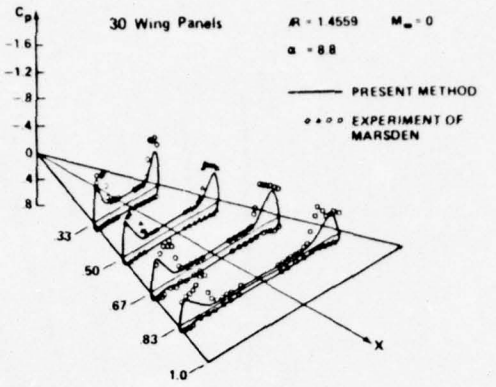

Surface Pressure Distribution of Delta Wing With 30 Wing Panels at α = 8.8°

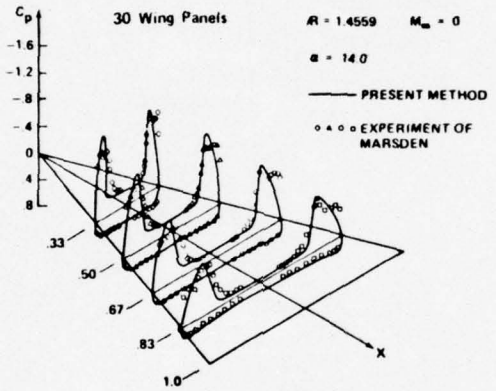

Surface Pressure Distribution of Delta Wing With 30 Wing Panels at α = 14.0°

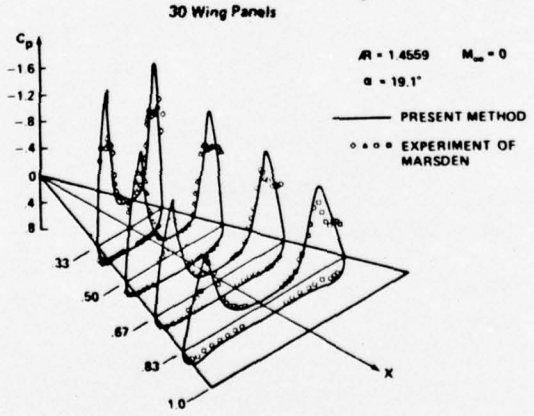

Surface Pressure Distribution of Delta Wing With 30 Wing Panels at α = 19.1°

FIG. 6: CALCULATED PRESSURES ON SLENDER WING WITH CONTROLLED[25] SEPARATION AT ALL THREE SHARP EDGES

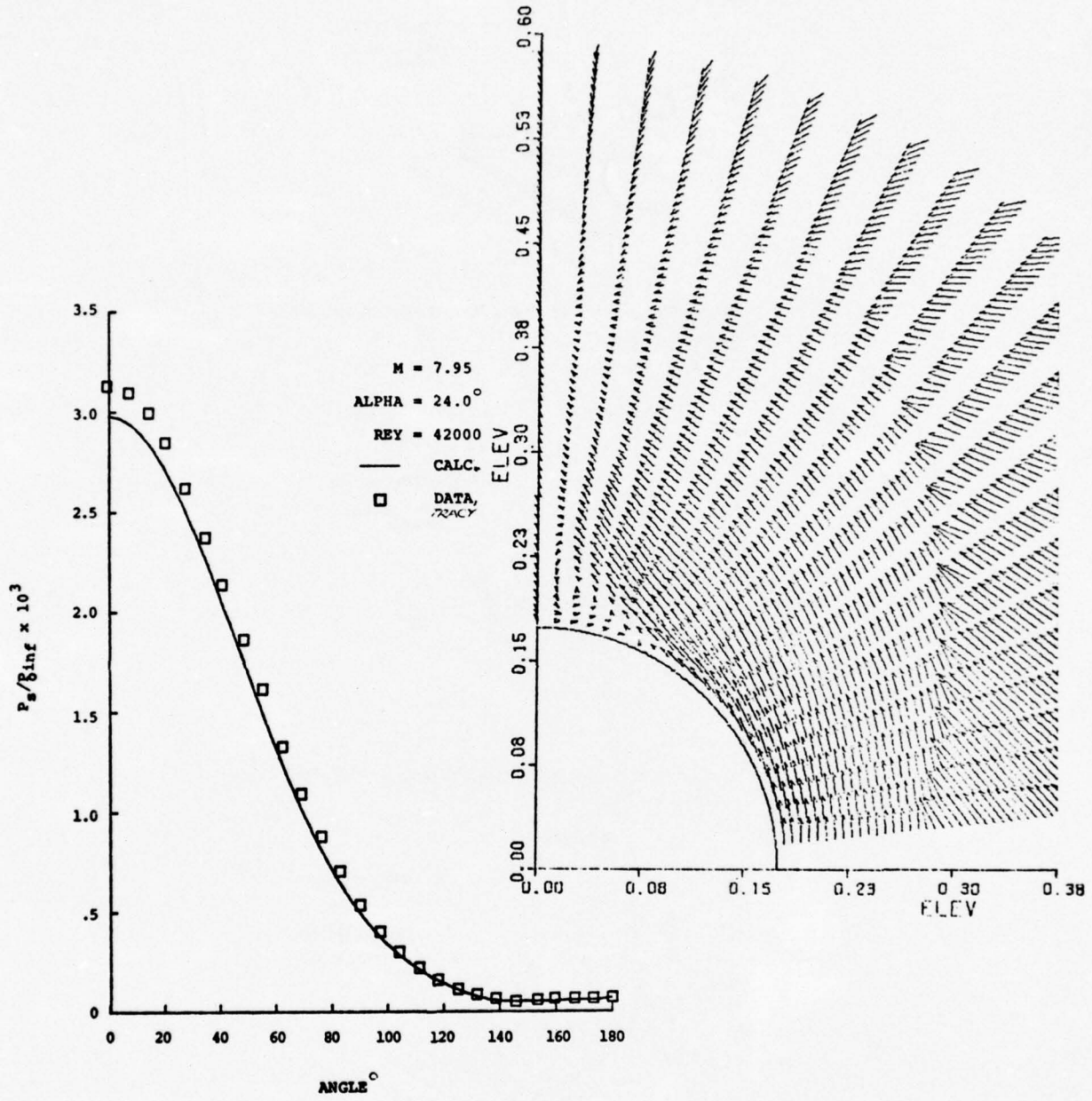

FIG. 7: SIMPLIFIED NAVIER-STOKES POINTED CONE FLOW SOLUTION[27]: θ_c = 10°, M = 8, LAMINAR

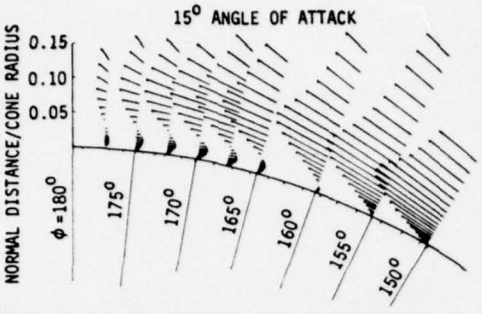

Cross Plane Vector Distribution
XN/RN = 14.8

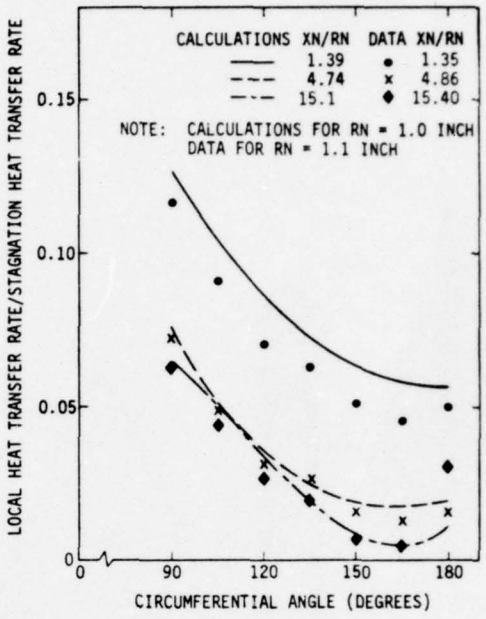

Leeward Heating Distribution

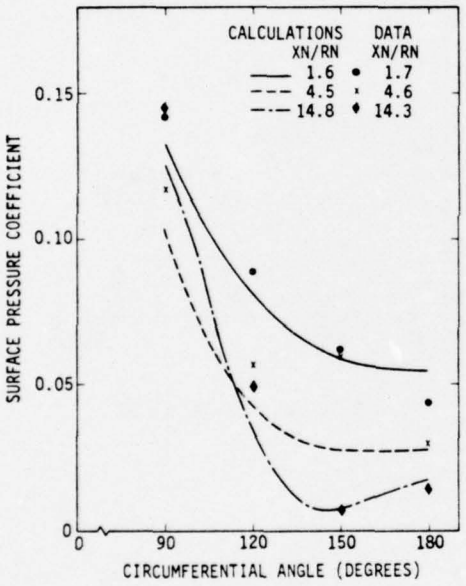

Leeward Surface Pressure Distrubution

FIG. 8: BLUNTED CONE SOLUTION USING "PARABOLIC" NAVIER-STOKES EQUATIONS[30]: θ_c = 15°, M = 10.6, LAMINAR

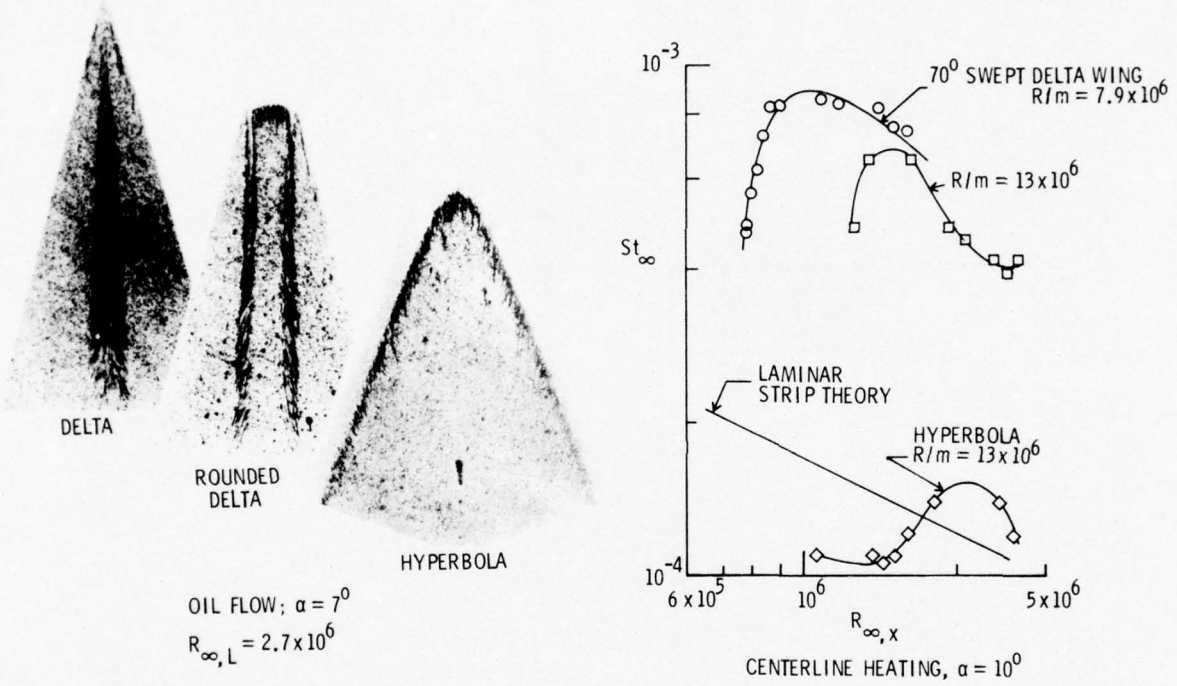

FIG. 9: LEE SURFACE FLOW OVER DELTA AND CONTOURED WINGS AT M = 6[33]

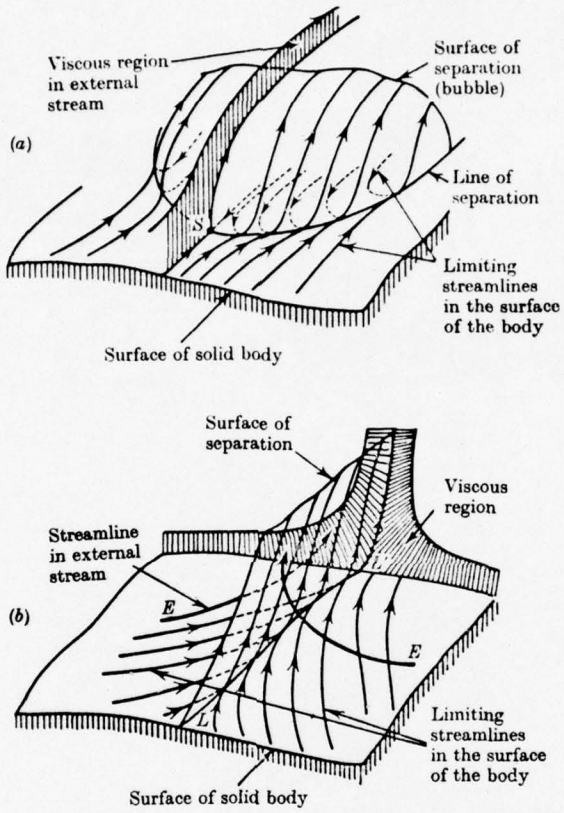

FIG. 10: 3D SEPARATIONS:[1] BUBBLE AND FREE SHEAR LAYER TYPES

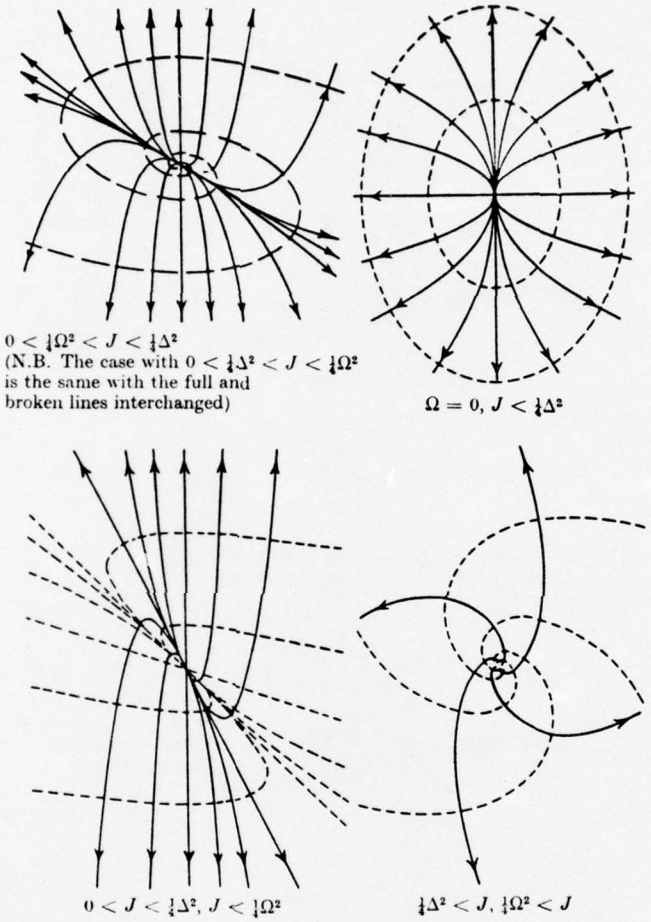

Different types of pattern of skin-friction lines (full) and vortex lines (broken) near a nodal point of attachment ($J > 0, \Delta > 0$).

FIG. 11: LIMITING STREAMLINES (FULL) ABOUT A NODAL ATTACHMENT POINT[39]

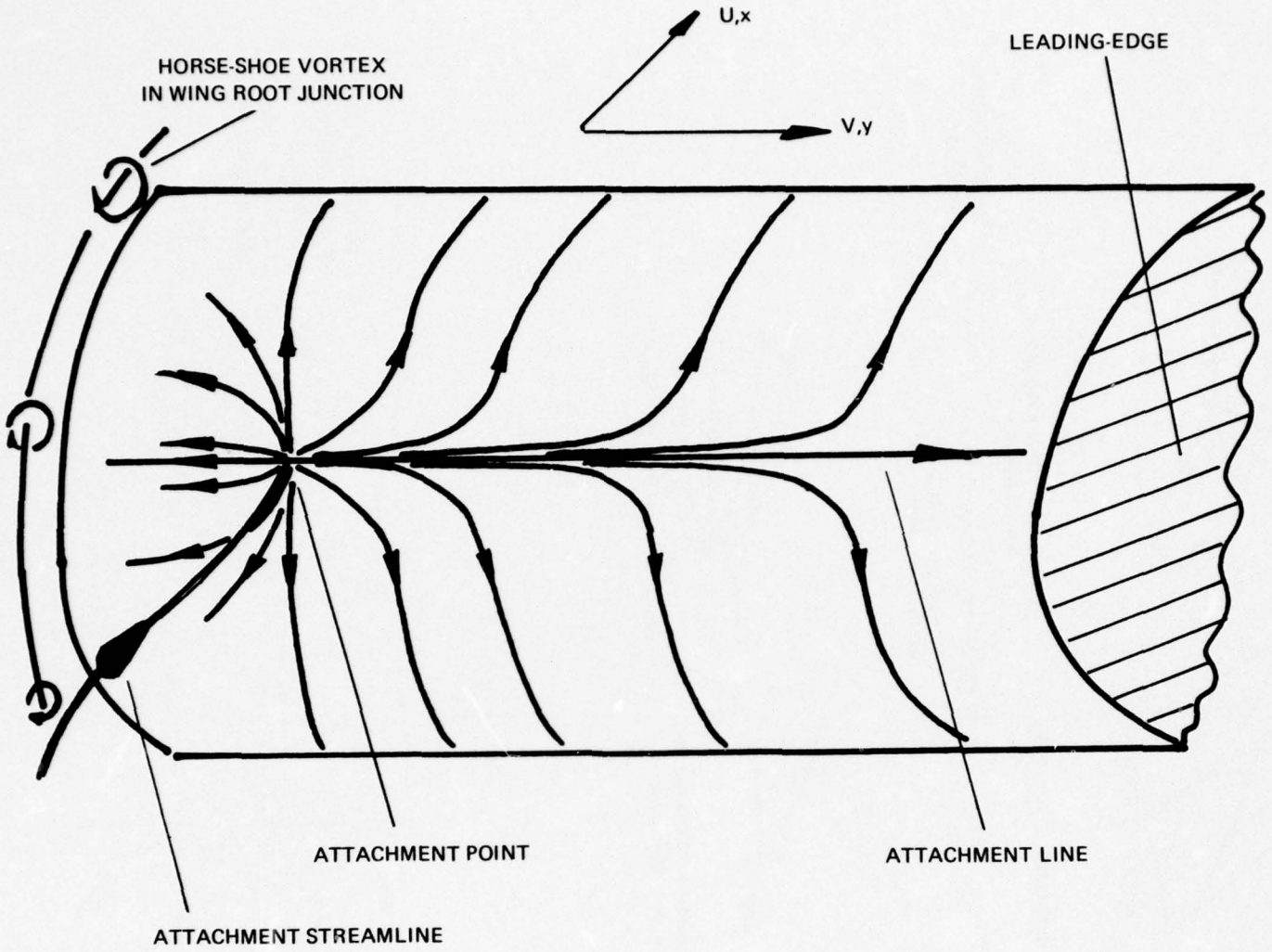

FIG. 12: POSSIBLE LIMITING STREAMLINE PATTERN ABOUT NODAL ATTACHMENT POINT ON WING LEADING-EDGE

13.1

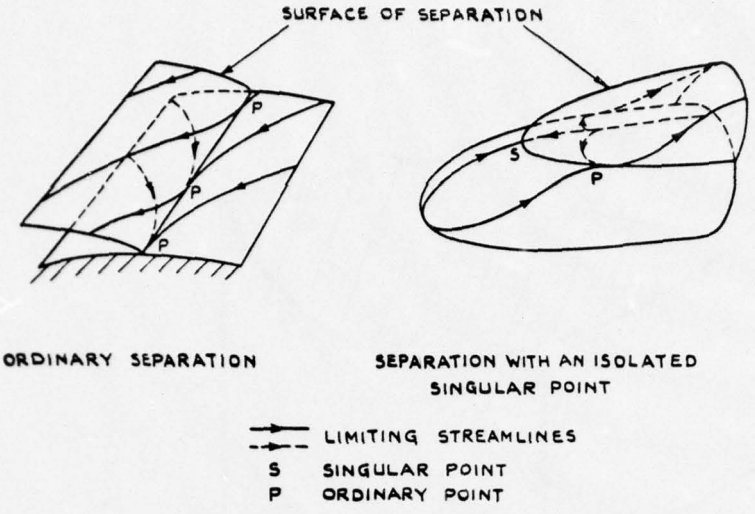

3D SEPARATION, MASKELL[1]

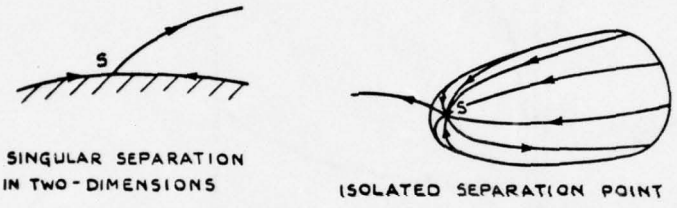

13.2

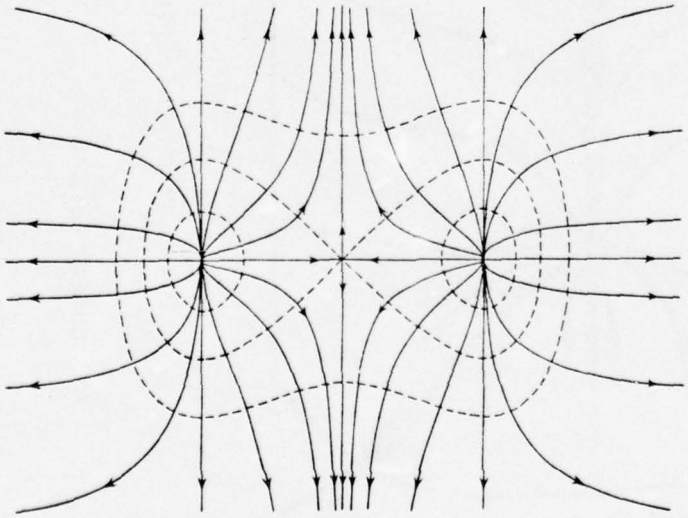

TWO NODAL POINTS OF ATTACHMENT & ONE SADDLE POINT OF SEPARATION, LIGHTHILL[39]

FIG. 13: POSTULATES OF 3D SEPARATION

14.1

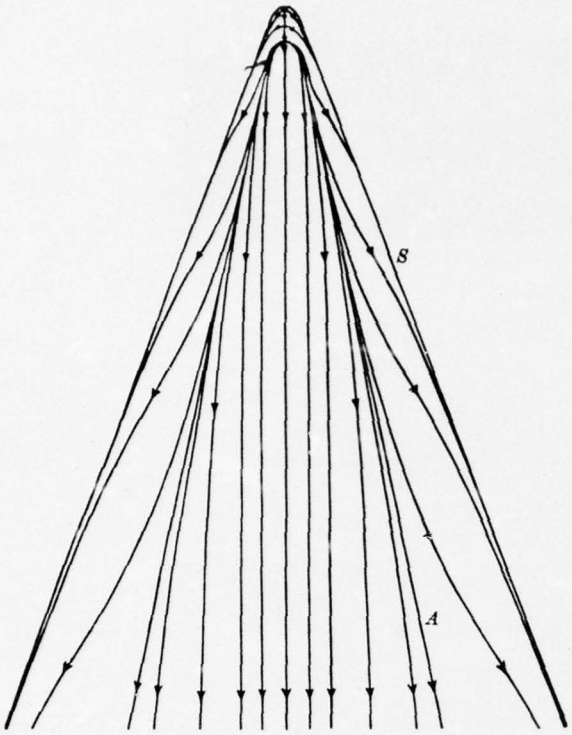

APEX ENLARGED;
SINGULARITY
THERE AS ON
FIG. 13.2,
LIGHTHILL[39]

14.2

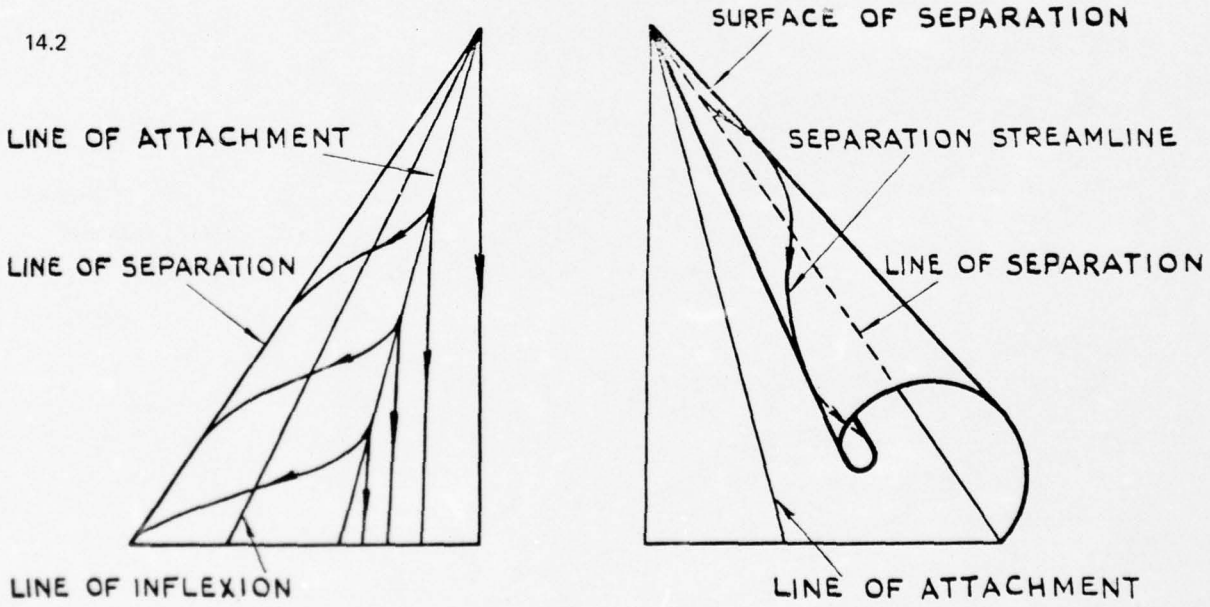

MASKELL[1]

FIG. 14: CONCEPTUAL LEE-SIDE FLOW ABOUT SLENDER WING AT INCIDENCE

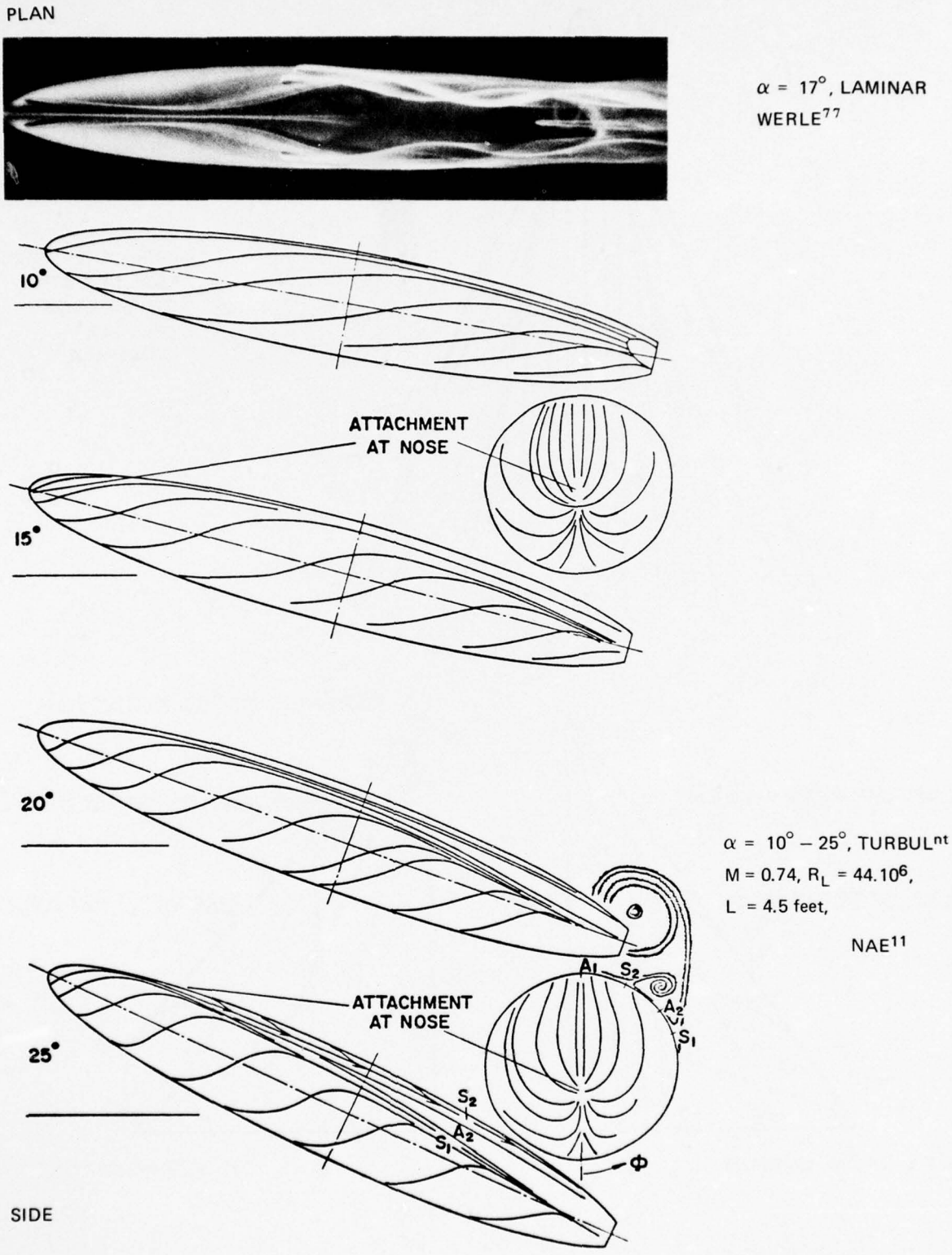

FIG. 15: LIMITING STREAMLINES AND EXTERNAL FLOW ABOUT 6:1 ELLIPSOID AT INCIDENCE

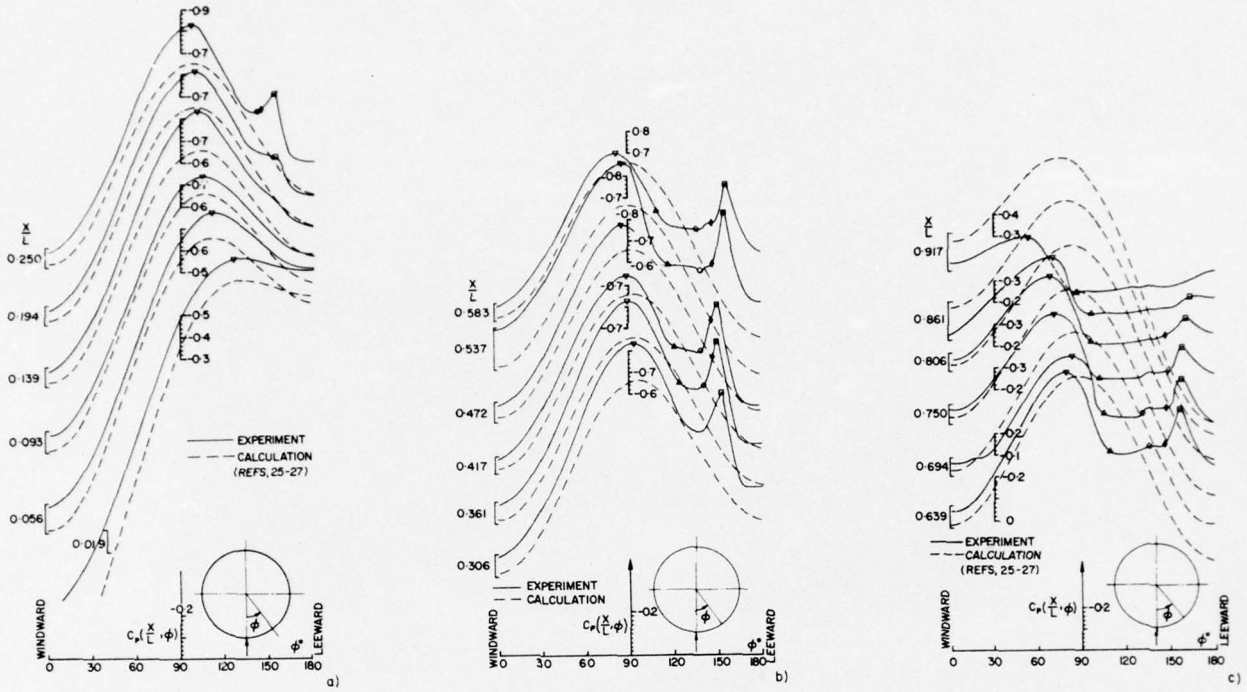

Circumferential pressures on 6:1 ellipsoid at $\alpha = 25°$, $M_\infty = 0.74$, and $R_L = 44 \times 10^6$. ∇—minimum pressure, Δ—primary separation, ○—secondary attachment, ◇—secondary separation, □—suction peak from primary vortex.

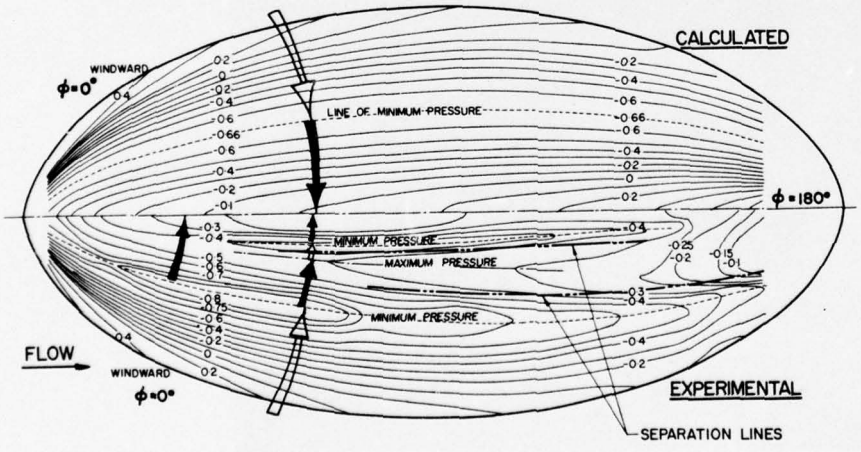

Isobars on 6:1 ellipsoid at $\alpha = 25°$, $M_\infty = 0.74$, and $R_L = 44 \times 10^6$.

FIG. 16: SURFACE PRESSURES ON 6:1 ELLIPSOID AT 25° INCIDENCE WITH TURBULENT VISCOUS FLOW

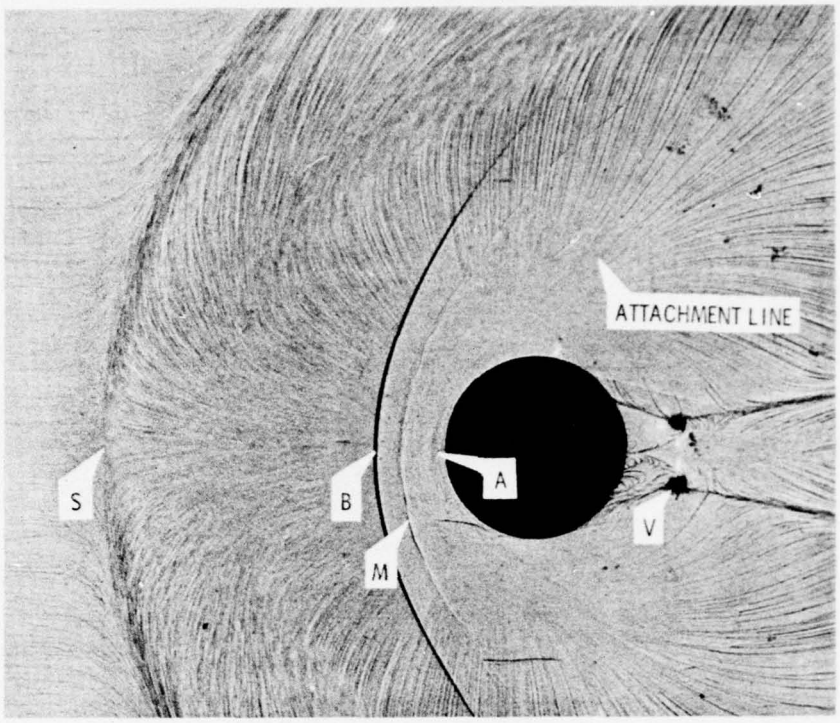

Plan-View Shadowgraph for Large Protuberance, Model 2D, M = 2.50, $R/\ell = 19.3 \times 10^6/m$. S - Primary Separation, B - Bow Shock, M - Mach Stem, A - Attachment Line, V - Vortex Core. Attachment Line Indicated Originates at Point A.

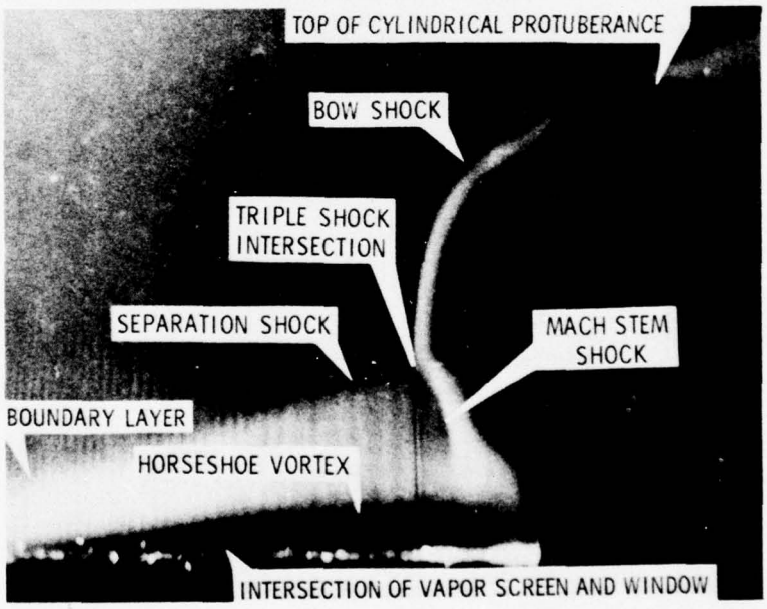

Vapor Screen Photograph for Large Protuberance, Model 2D, with Light Sheet in Symmetry Plane and Camera at 30° to Sheet, M = 2.50, $R/\ell = 9.3 \times 10^6/m$.

FIG. 17: CYLINDER PROTUBERANCE IN SUPERSONIC TURBULENT FLOW[48]

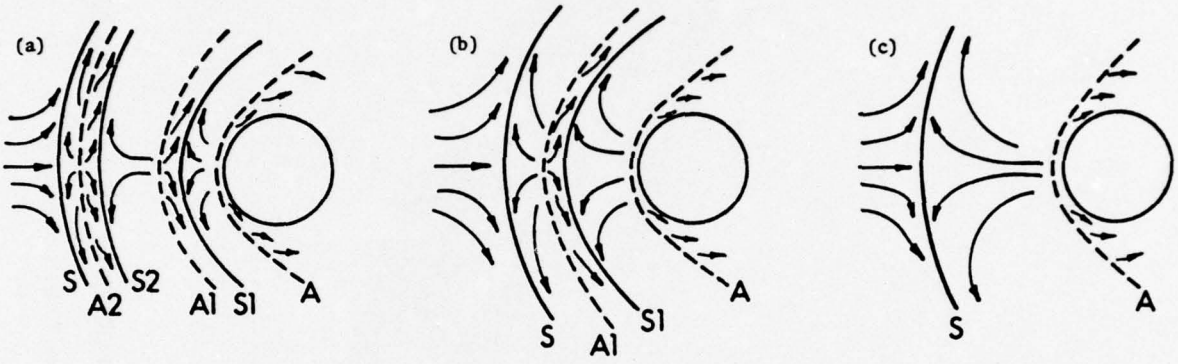

Plan-View Sketches of Separation and Attachment Upstream of Cylindrical Protuberance; (a) Six Vortices; (b) Four Vortices; (c) Two Vortices.

FIG. 18: MULTI-3D TURBULENT SEPARATIONS[48] ABOUT CYLINDER PROTUBERANCE AT M = 2.5

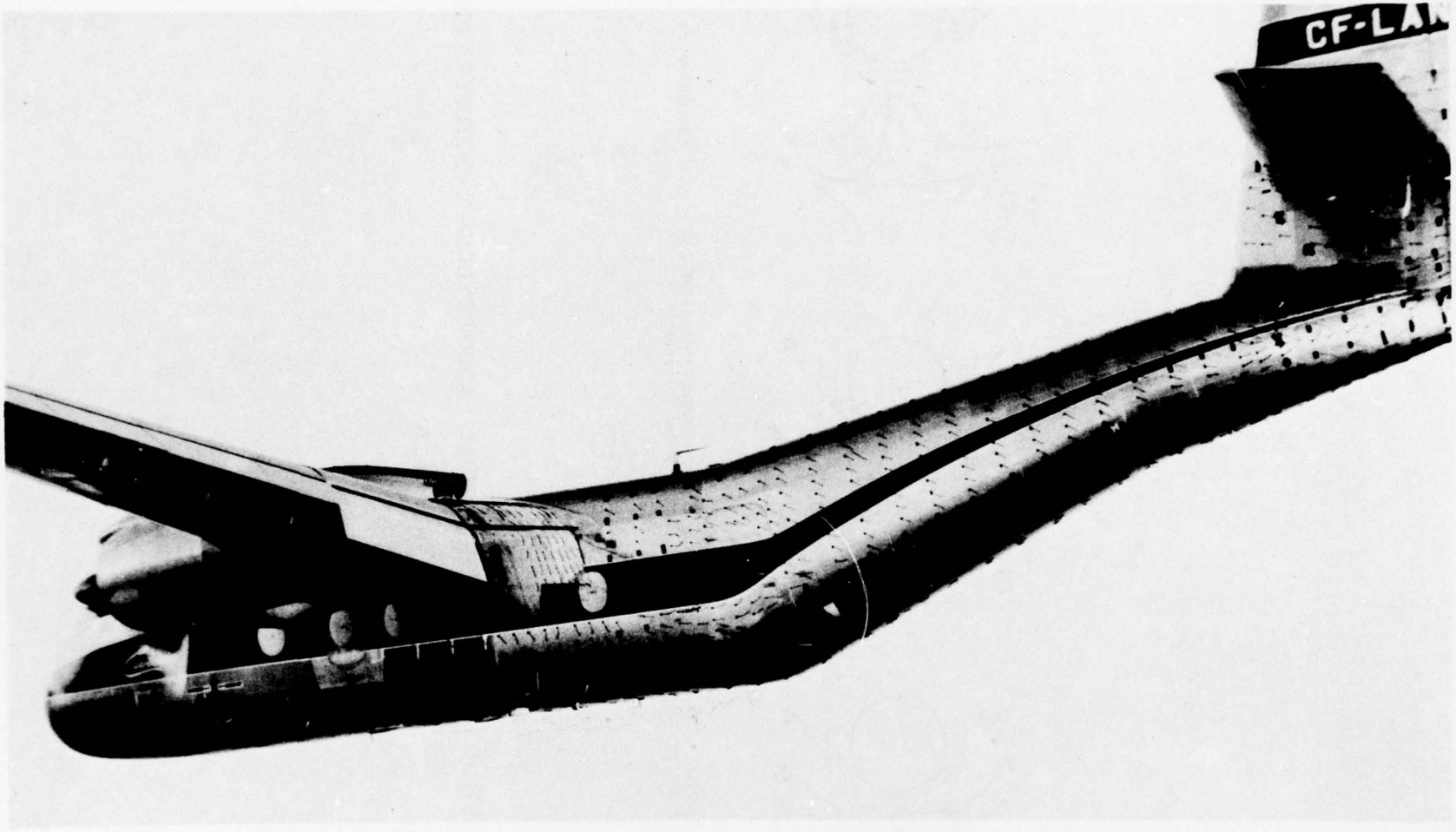

FIG. 19.1: TUFTS ON UPSWEPT FUSELAGE OF D.H. "CARIBOU"

(Courtesy of DeHavilland Aircraft of Canada)

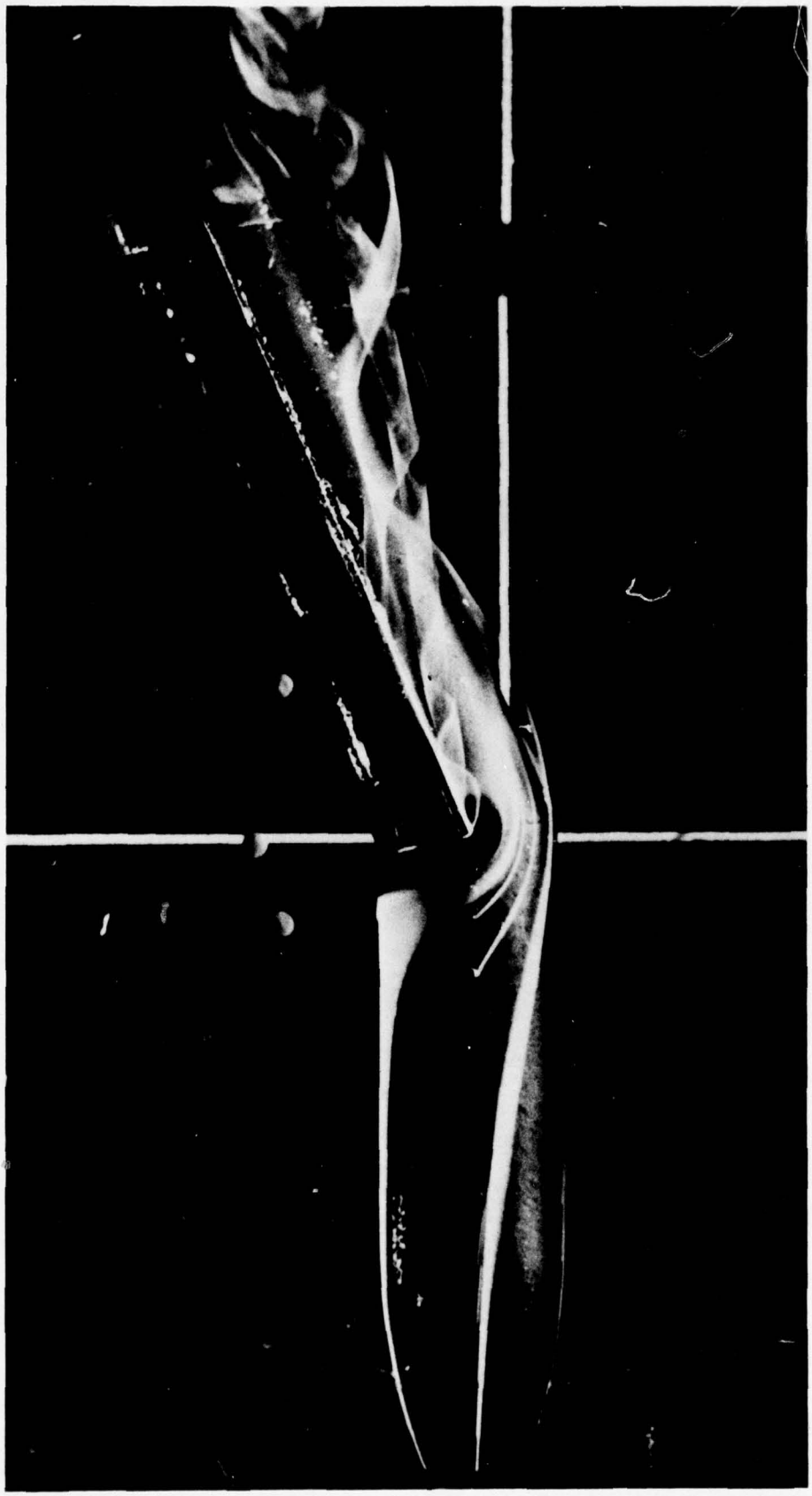

FIG. 19.2: UPSWEPT FUSELAGE WITH STRAKES

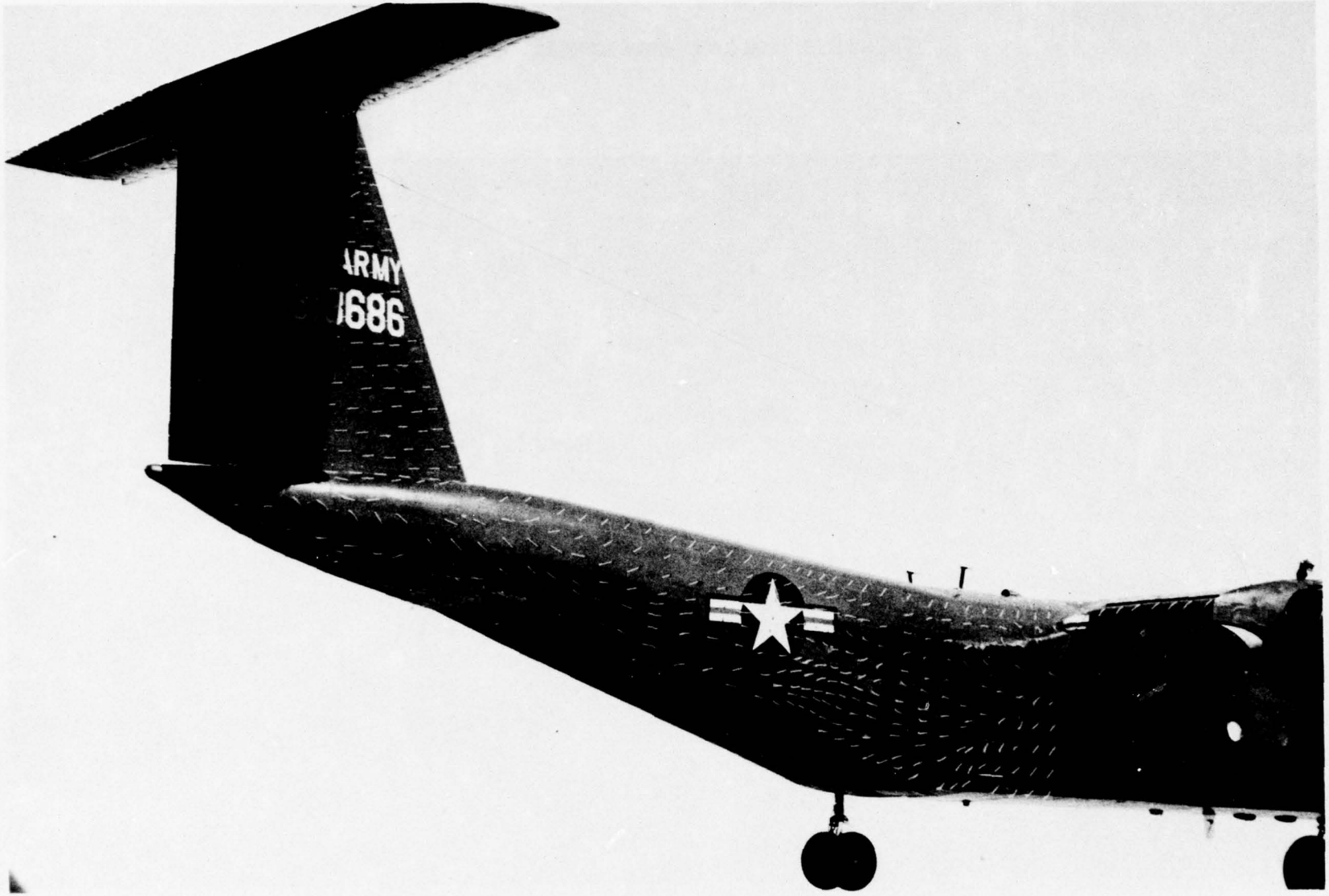

FIG. 20: SHARP EDGES ON FUSELAGE UNDERSIDE OF D.H. "BUFFALO"
(Courtesy of DeHavilland Aircraft of Canada)

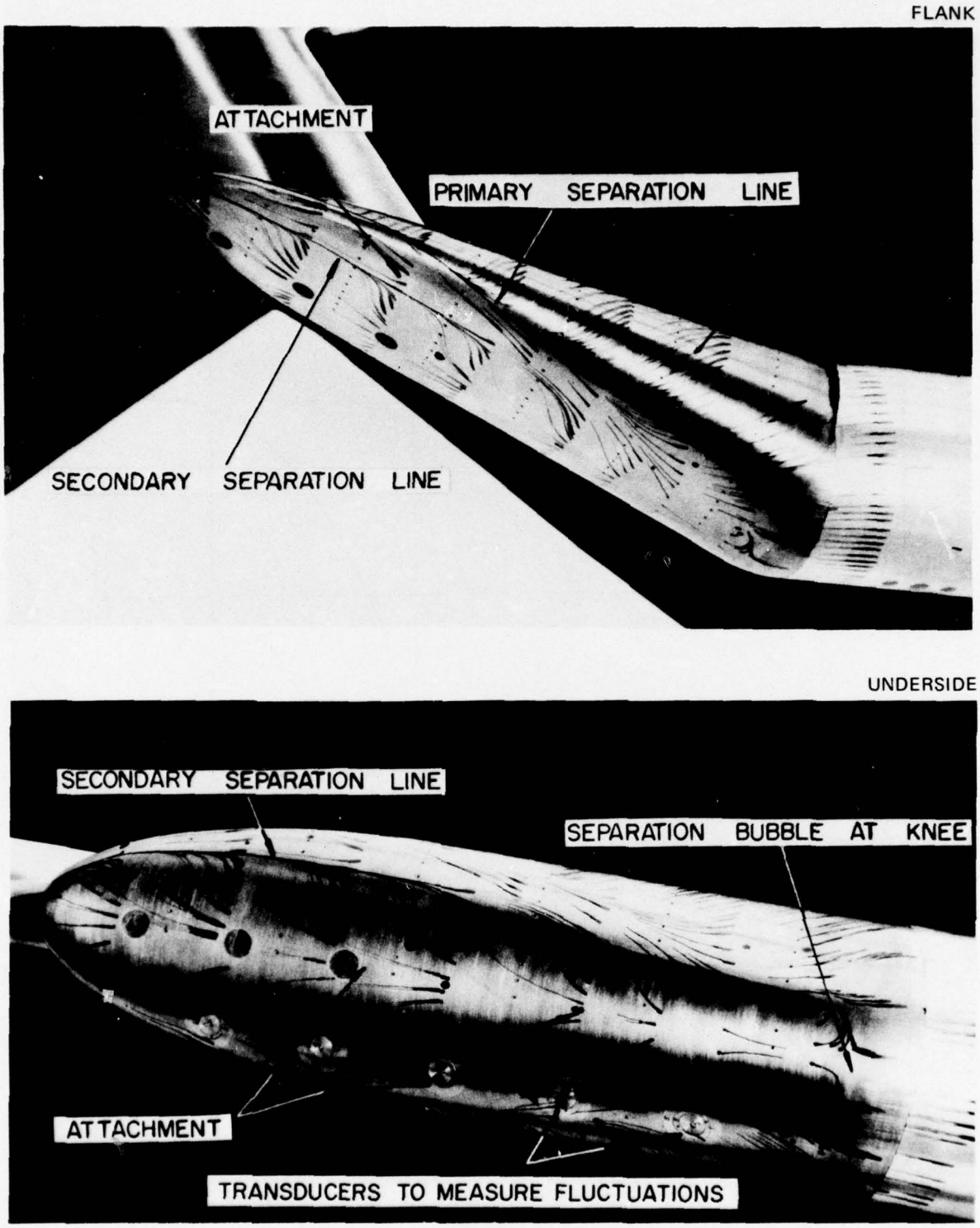

M = 0.73; R = 10×10^6 PER FT; AFTERBODY LENGTH = 17.2 IN; TURBULENT BOUNDARY LAYERS

FIG. 21: LIMITING STREAMLINES ON NAE "BEAVER TAIL" AFTERBODY AT 20° UPSWEEP

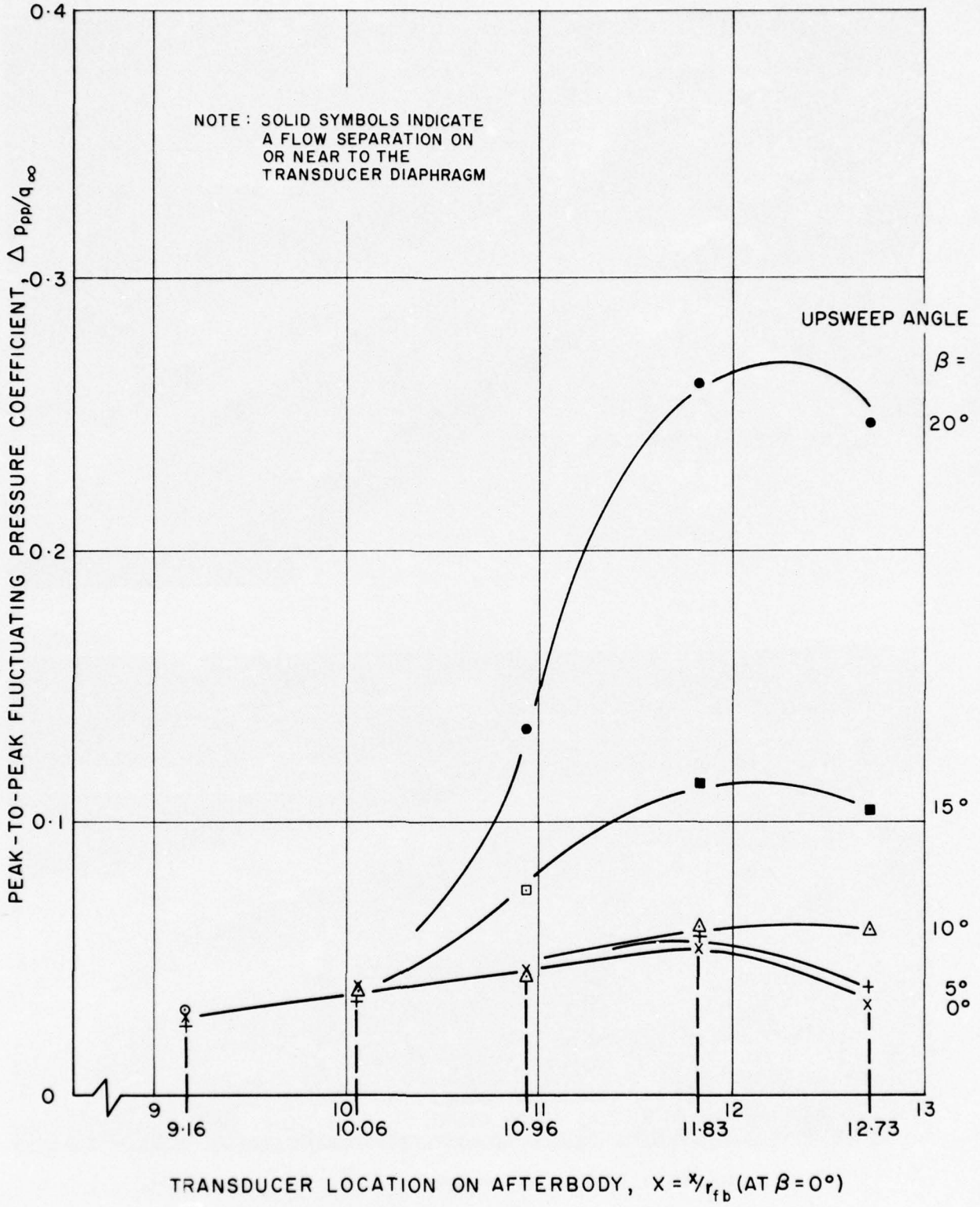

FIG. 22: PRESSURE FLUCTUATIONS ON NAE "BEAVER TAIL" AFTERBODY

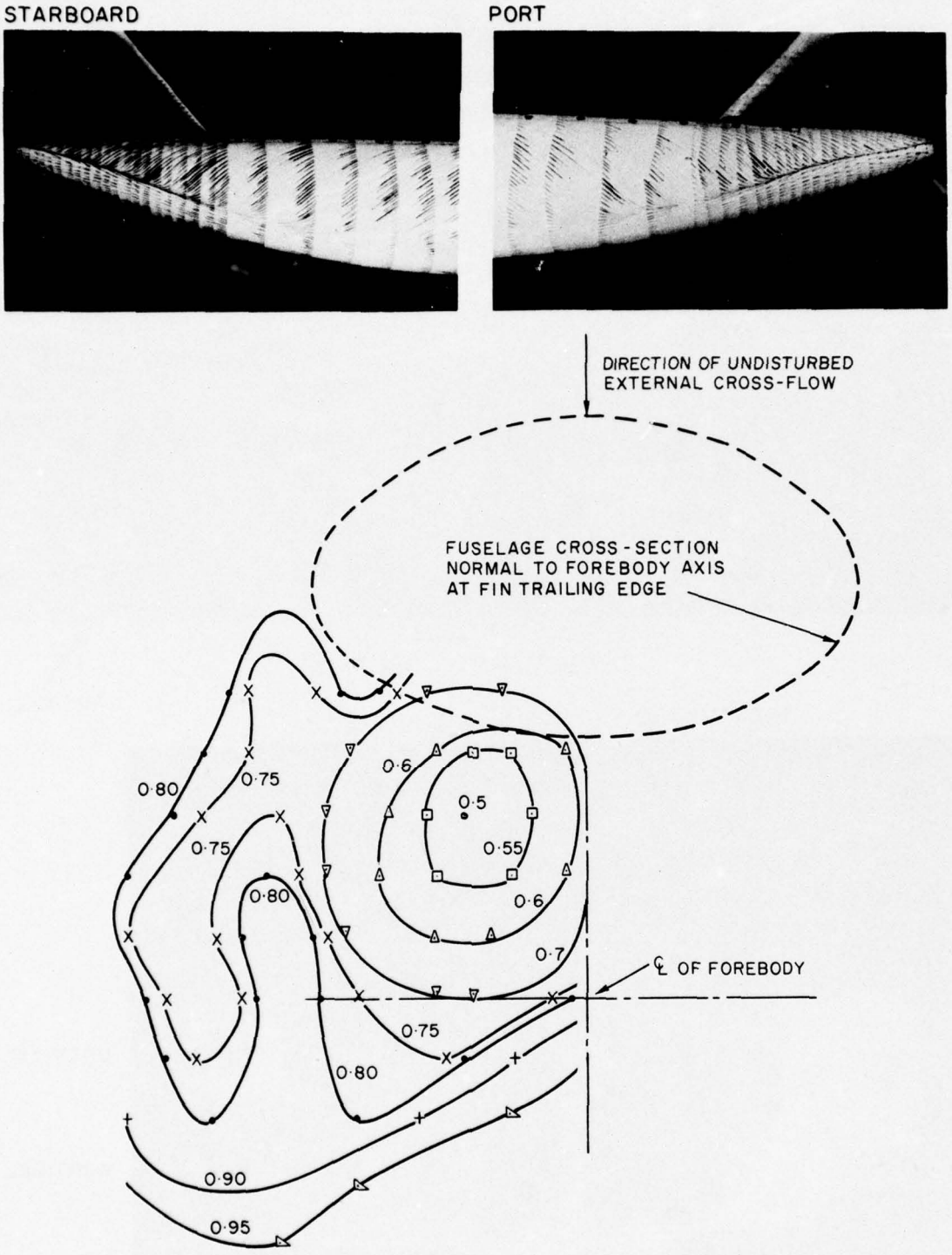

CONTOURS OF PITOT PRESSURE COEFFICIENT, C_{p_o}, JUST DOWNSTREAM OF AFTERBODY TIP (VIEW LOOKING UPSTREAM)

FIG. 23: TURBULENT VORTEX WAKE FROM 9° UPSWEPT AFTERBODY, $\alpha = -15°$, M = 0.3

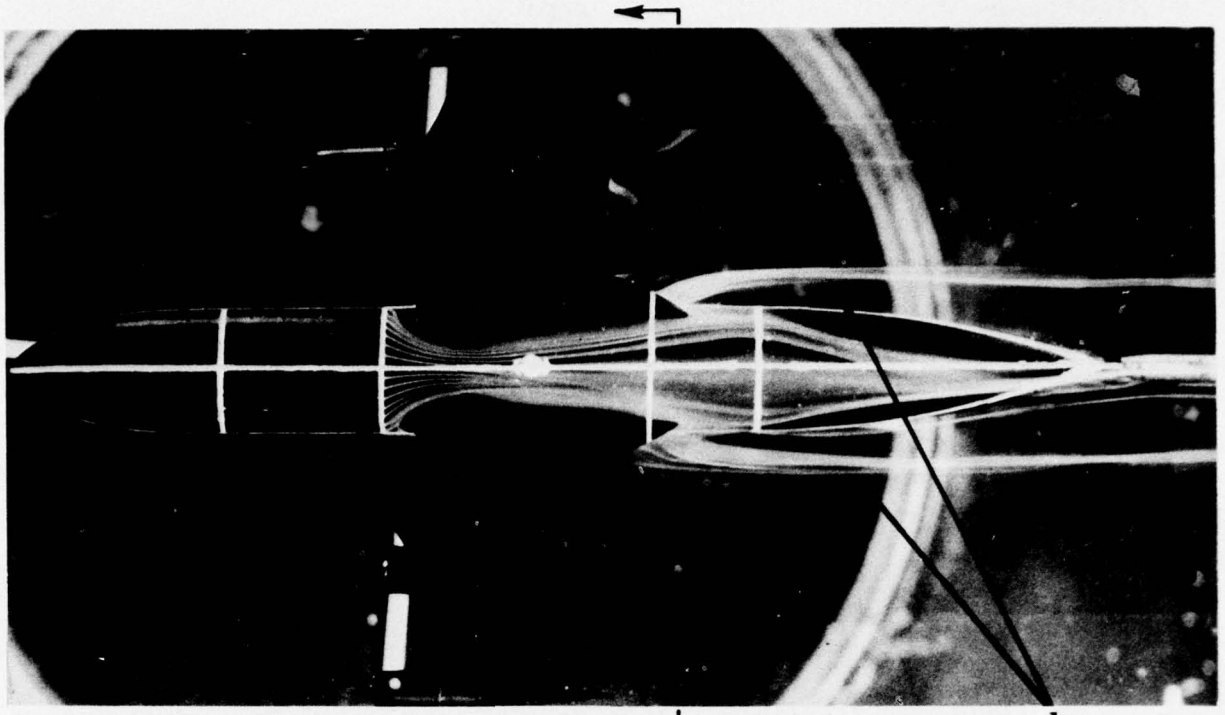

TRANSVERSE SECTION SHOWN ABOVE

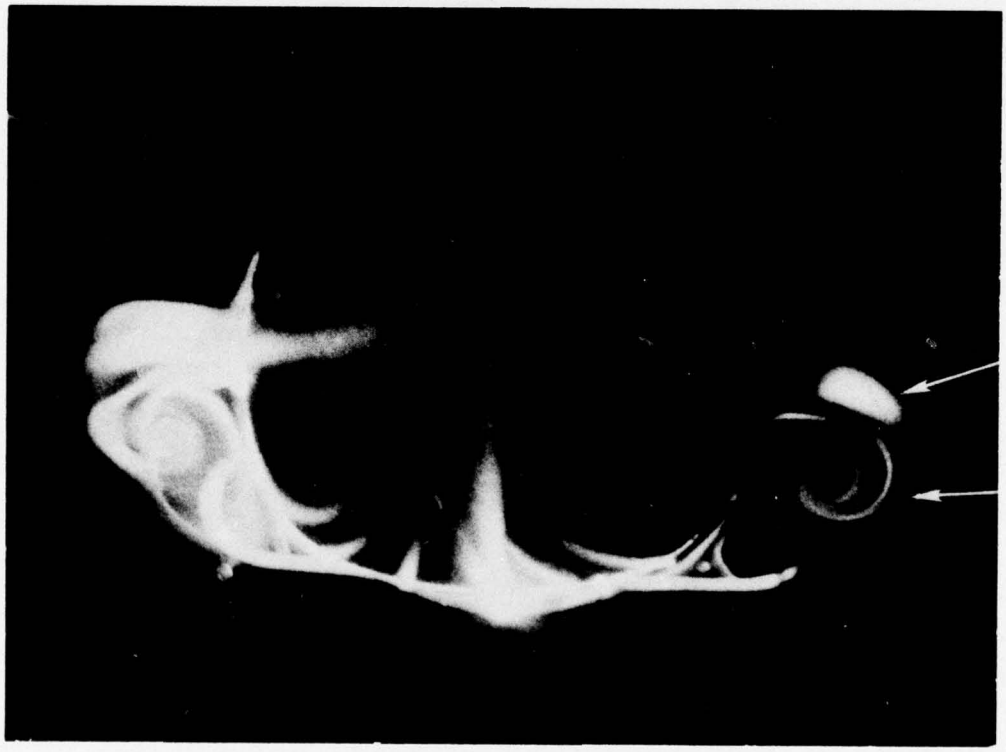

FIG. 24: WING ROOT/UNDERCARRIAGE POD INTERFERENCE: LAMINAR FLOW, L = 0.87 FOOT, $R_L = 1.7 \times 10^4$

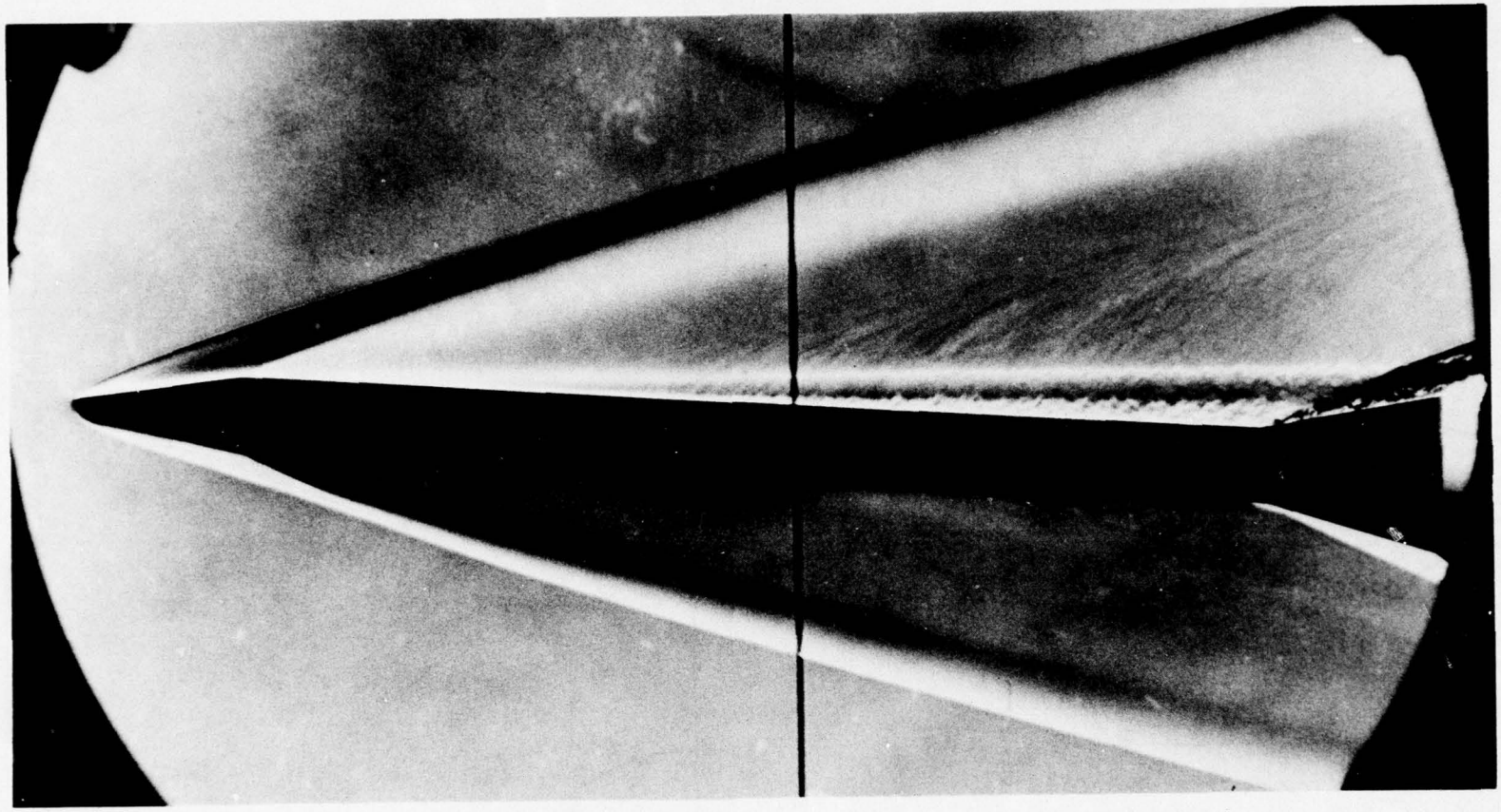

FIG. 25.1: BODY SEPARATIONS ON BLUNTED CONE-CYLINDER-FLARE AT M = 4

(Courtesy of Computing Devices of Canada)

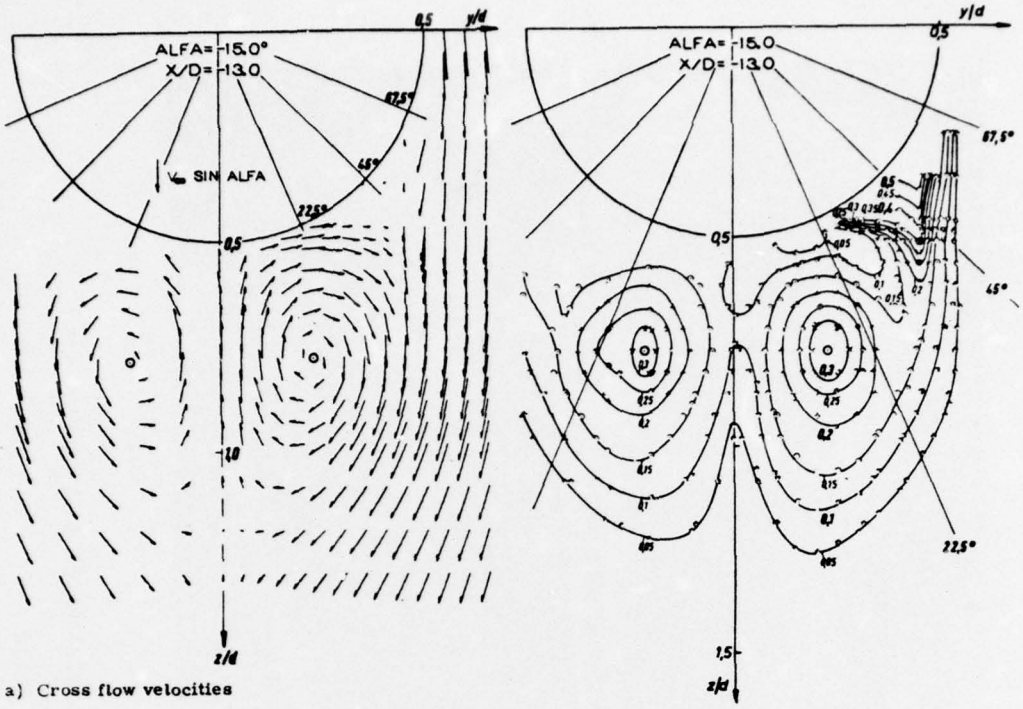

a) Cross flow velocities

b) Isobars of total pressure loss, $(p_{t\infty} - p_t)/q_\infty$ = const

Flow field at the plane x/d = - 13 ; angle of attack α = - 15° ; wingless body.

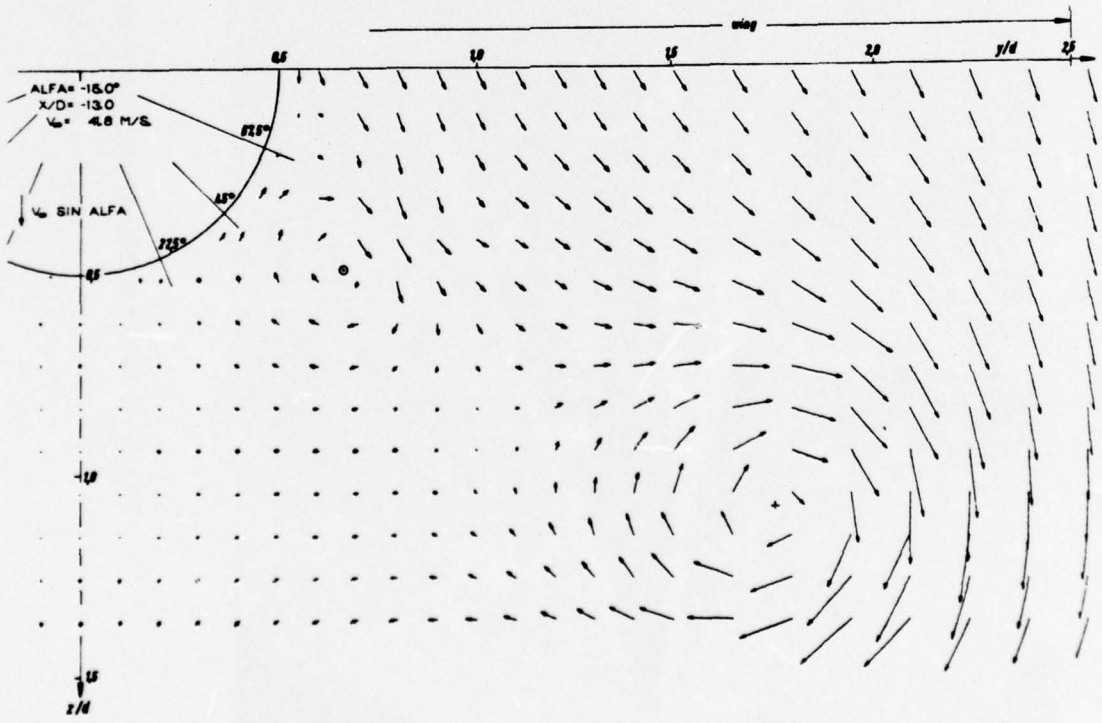

Cross flow velocities at the plane x/d = - 13 ; angle of attack α = - 15° ; with delta wing.

FIG. 25.2: BODY VORTICES IN TURBULENT, LOW SPEED FLOW[20]

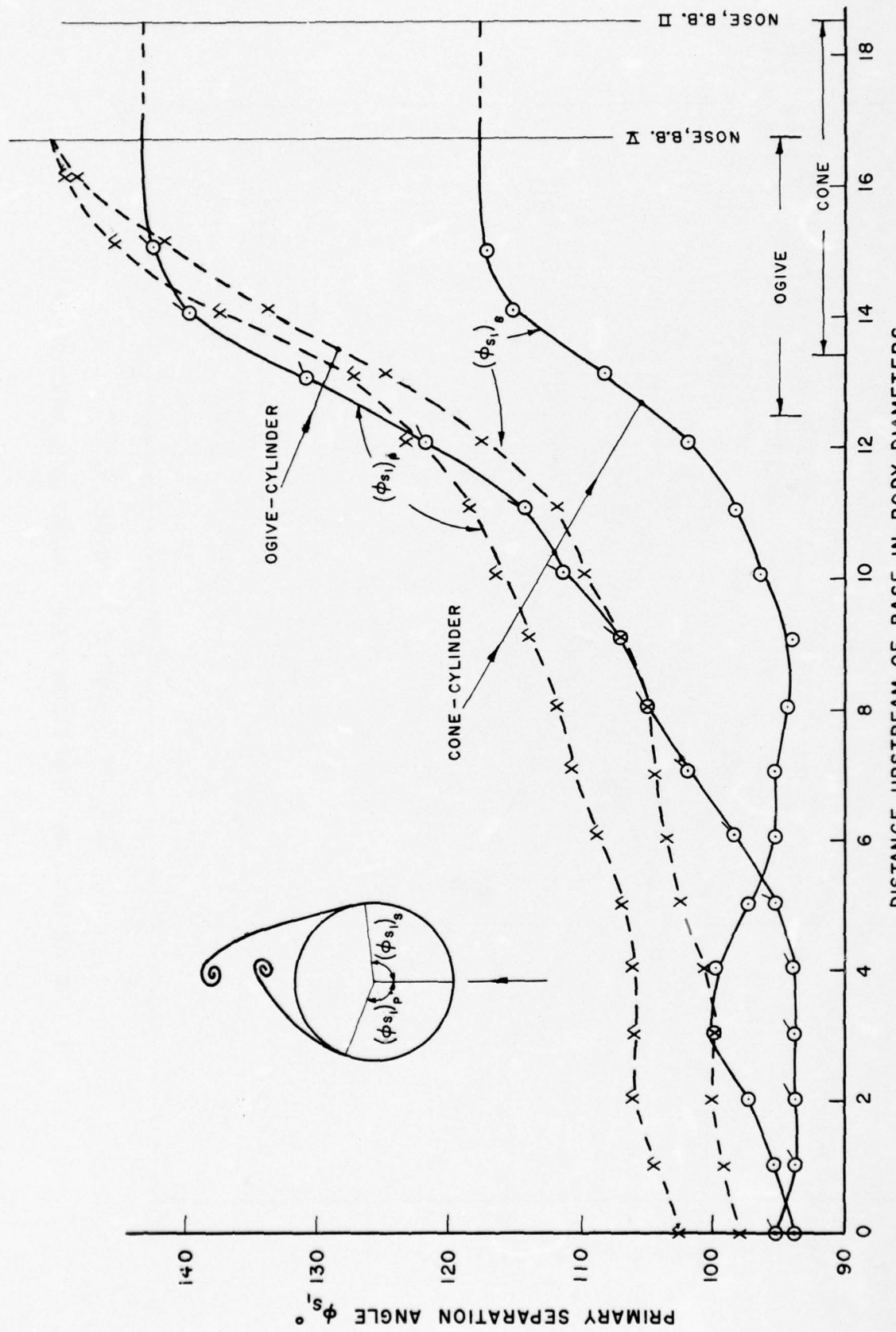

FIG. 26: ASYMMETRIC PRIMARY SEPARATION ON CONE– AND OGIVE– CYLINDERS, $\alpha = 18°$, $M \doteq 0.6$, $R_L \doteq 3.5 \times 10^7$

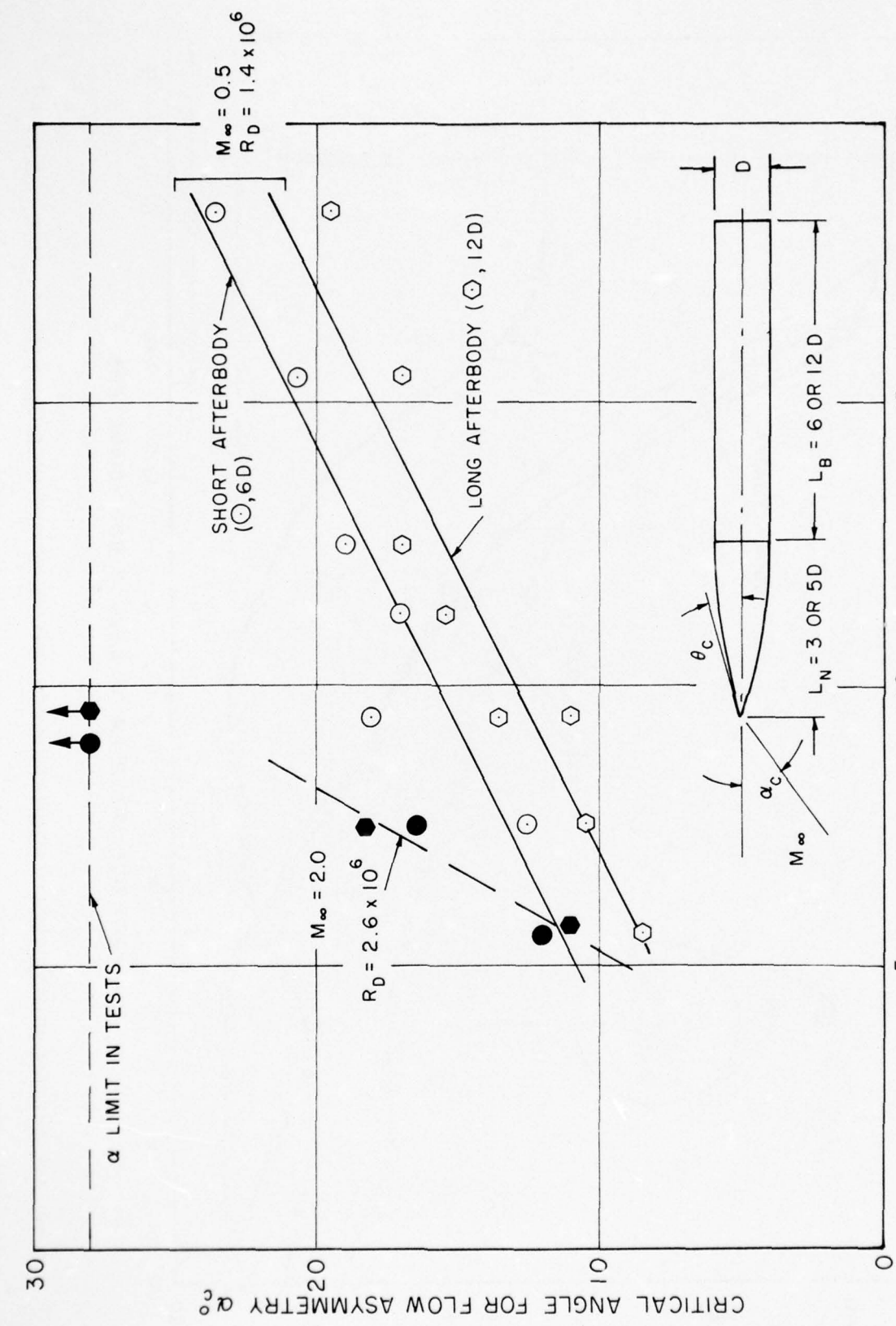

FIG. 27: CRITICAL ANGLE OF INCIDENCE FOR ONSET OF FLOW ASYMMETRY

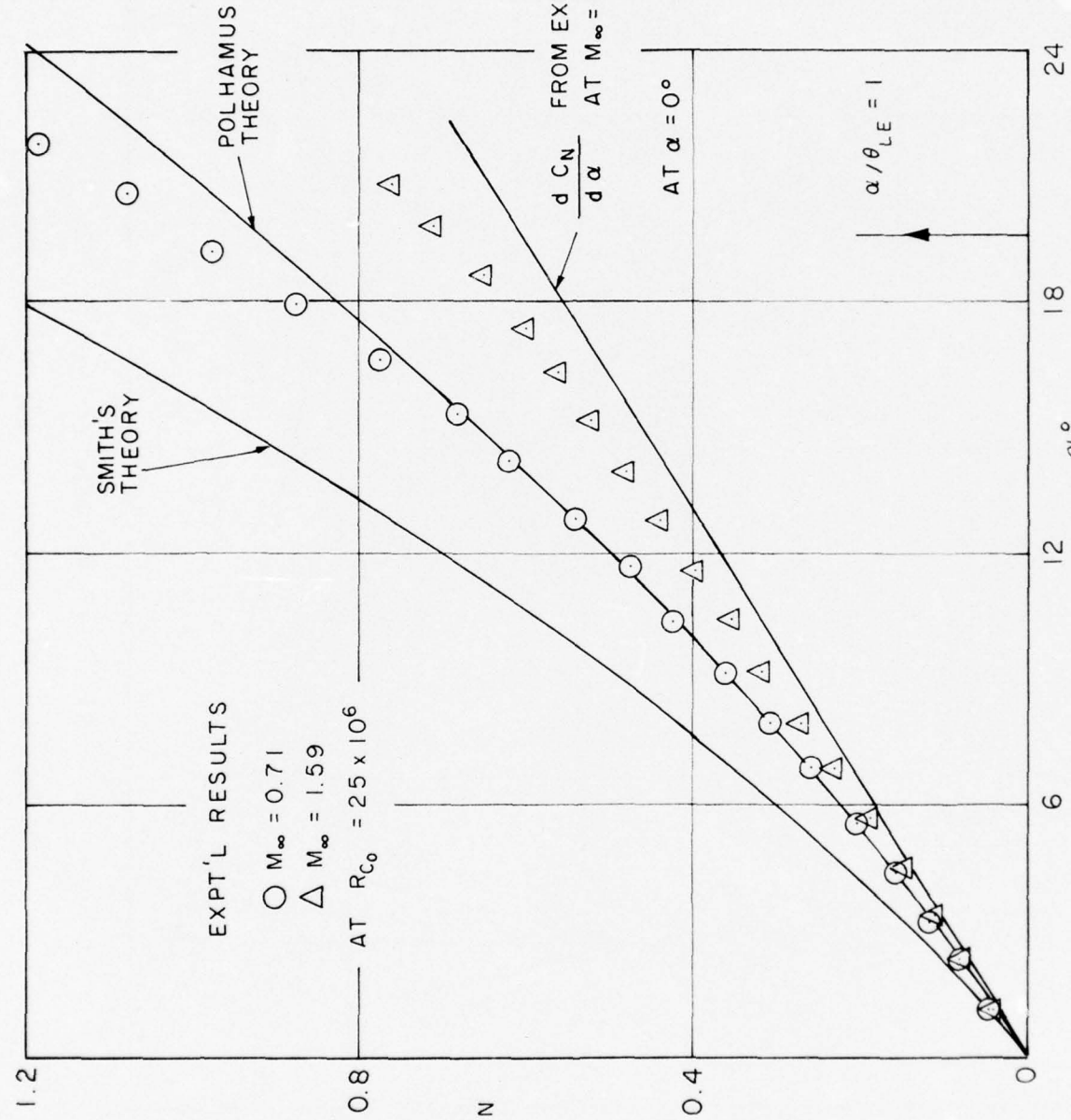

FIG. 28: OVERALL NORMAL FORCE ON 70° DELTA

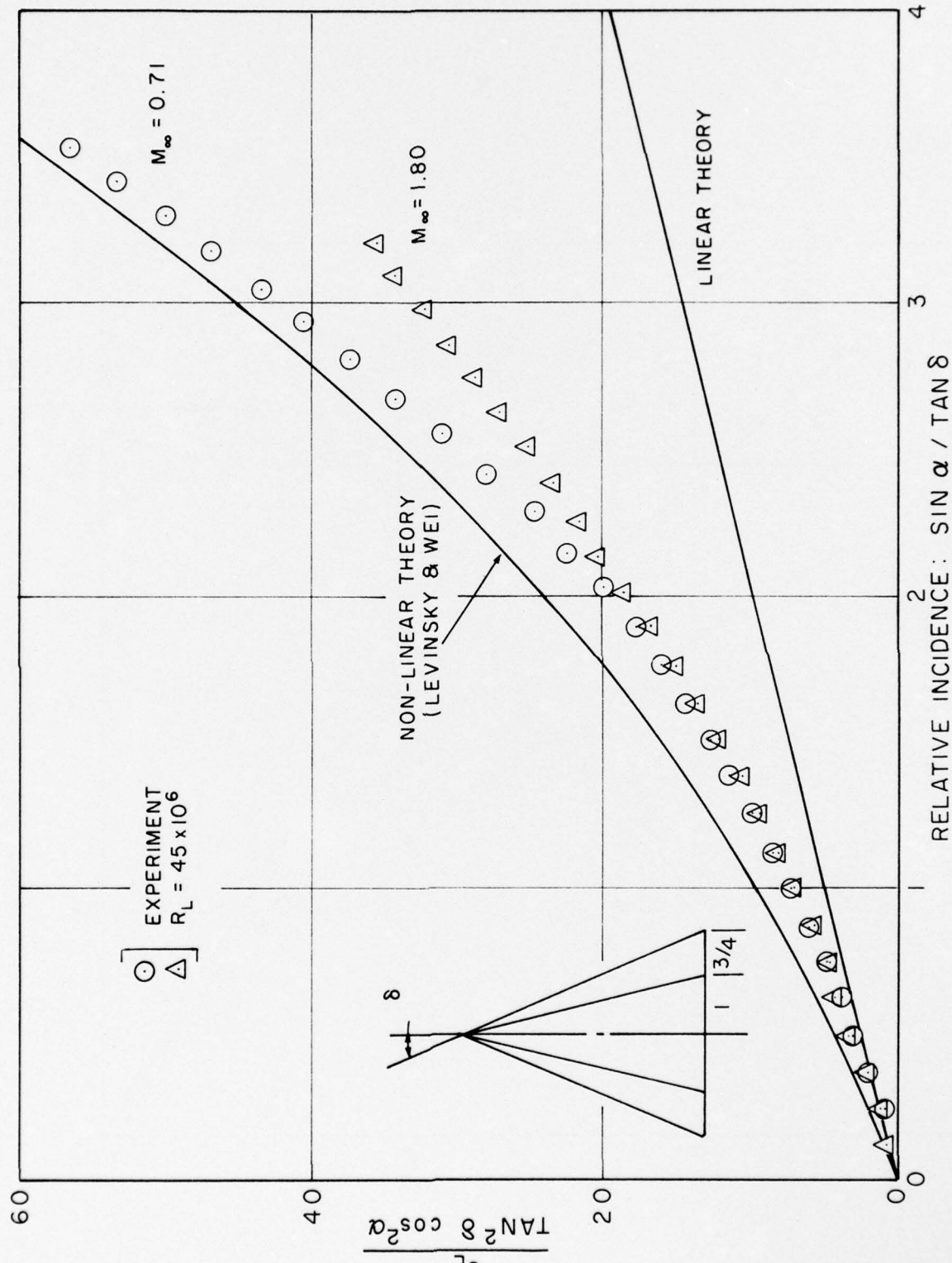

FIG. 29.1: LIFT ON 5° CIRCULAR CONE WITH 75% STRAKES

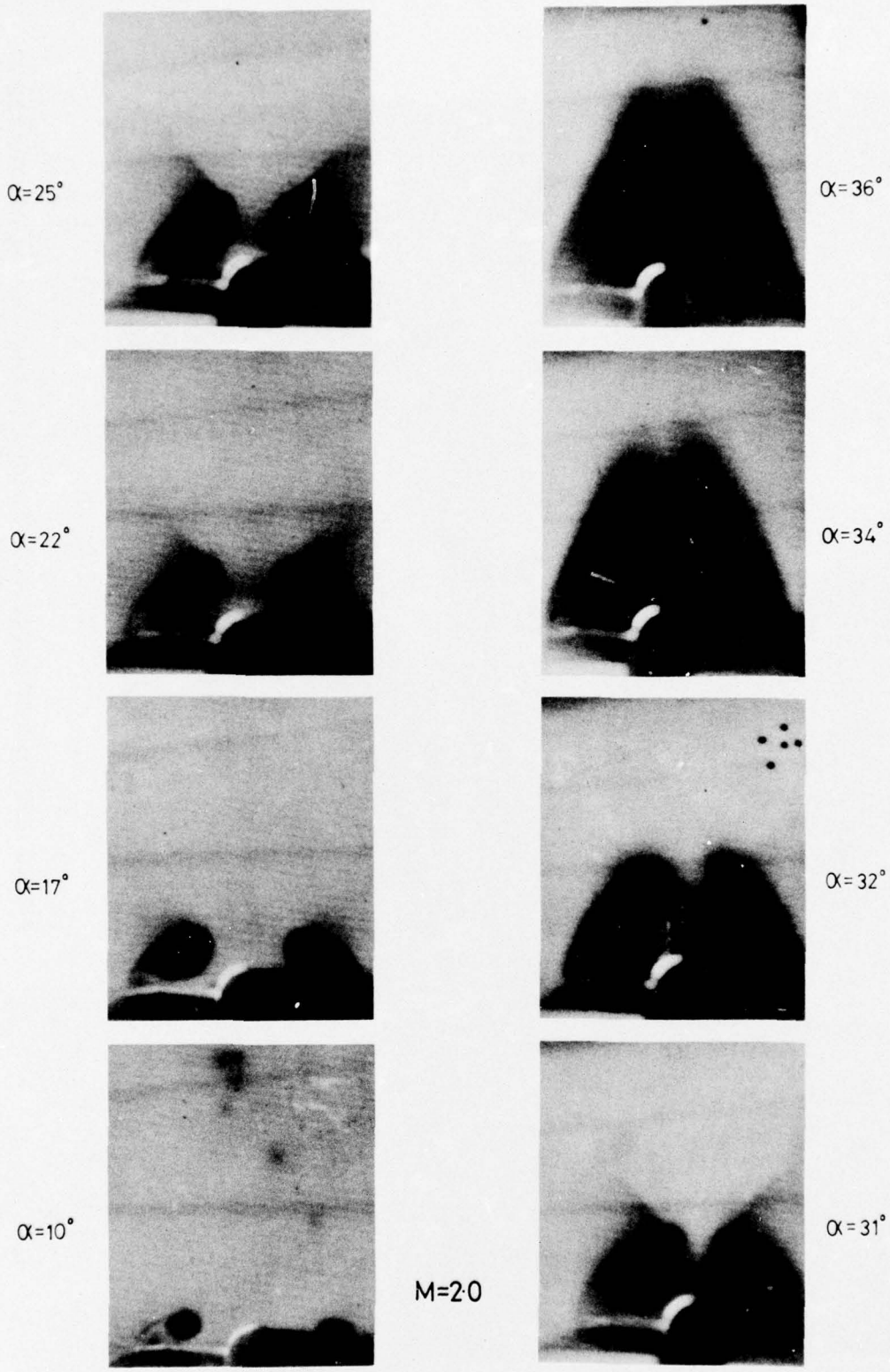

FIG. 29.2: VAPOUR SCREEN PHOTOS OF VORTICES ABOVE 78° SWEPT WINGS ATTACHED TO OGIVE-CYLINDER[63]

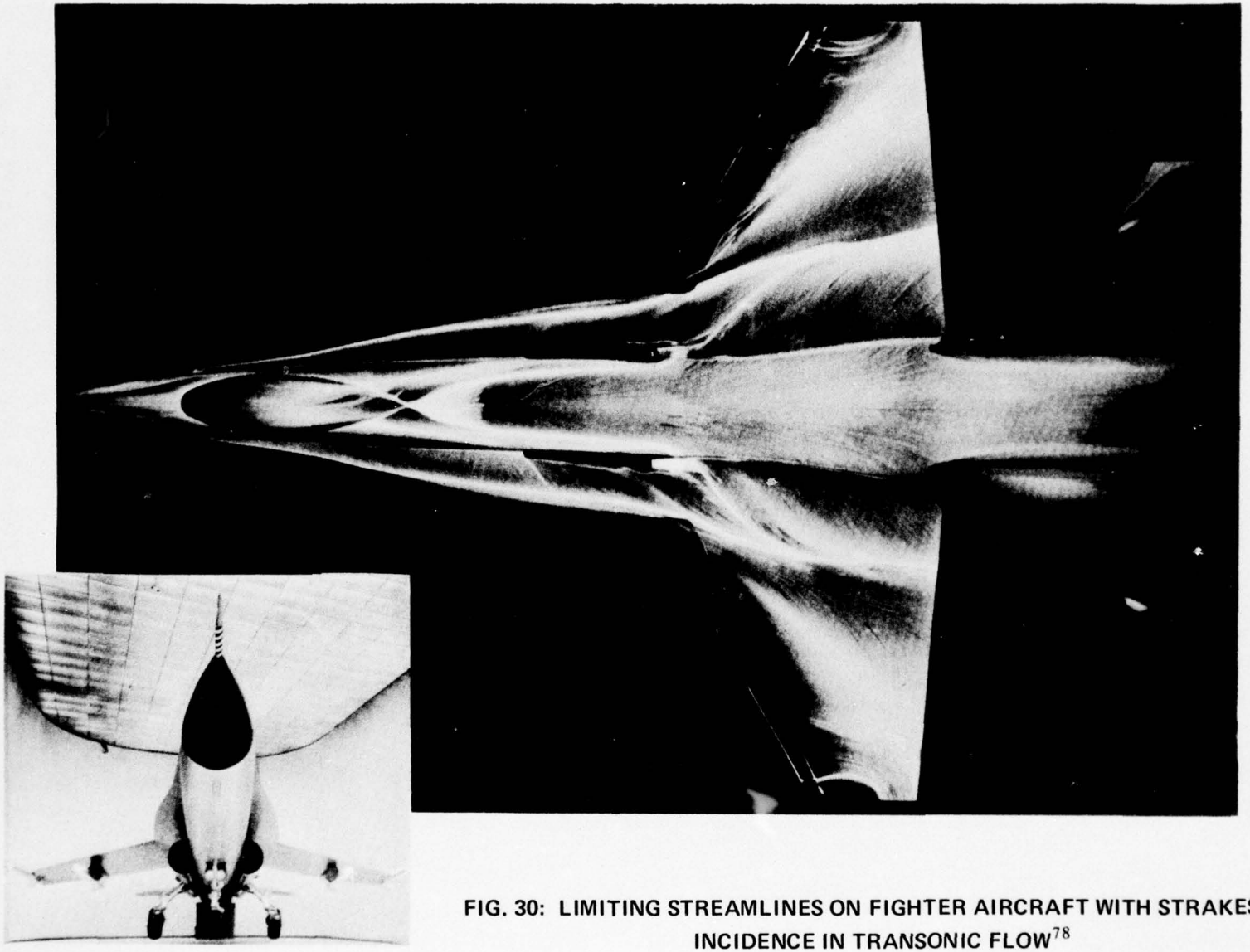

FIG. 30: LIMITING STREAMLINES ON FIGHTER AIRCRAFT WITH STRAKES AT INCIDENCE IN TRANSONIC FLOW[78]

31.1

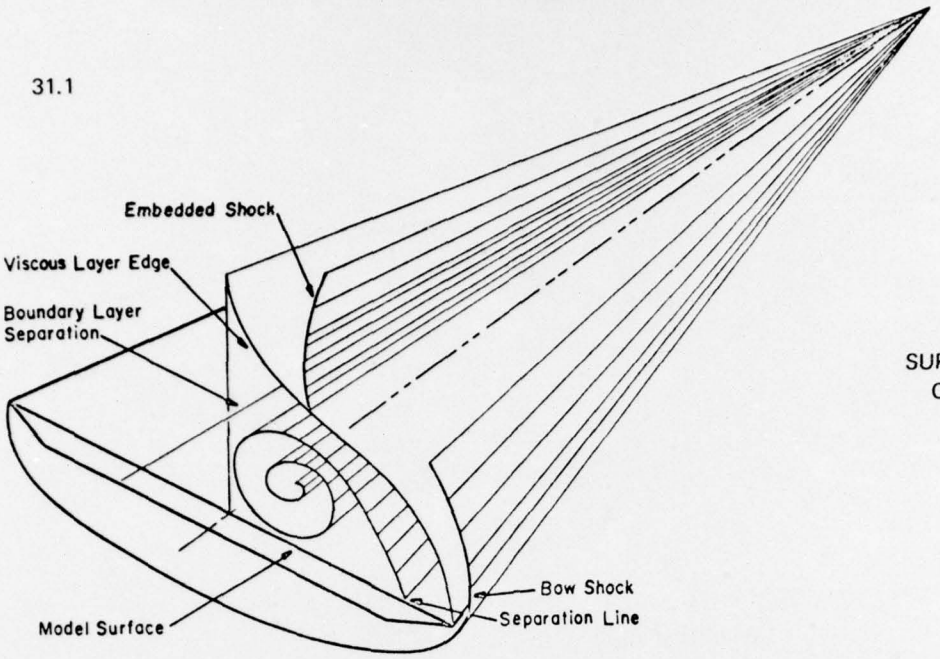

L.E.
SUPERSONIC:
CROSS[57]

DOMINANT FEATURES OF LEE SIDE FLOW FIELD/75° DELTA WING

31.2

A_1 PRIMARY ATTACHMENT LINE
S_1 PRIMARY SEPARATION LINE (LEADING EDGE)
A_2 UPPER SURFACE ATTACHMENT LINE
S_2 SECONDARY SEPARATION LINE
A_3, S_3, A_4 } OTHER SEPARATION AND ATTACHMENT LINES

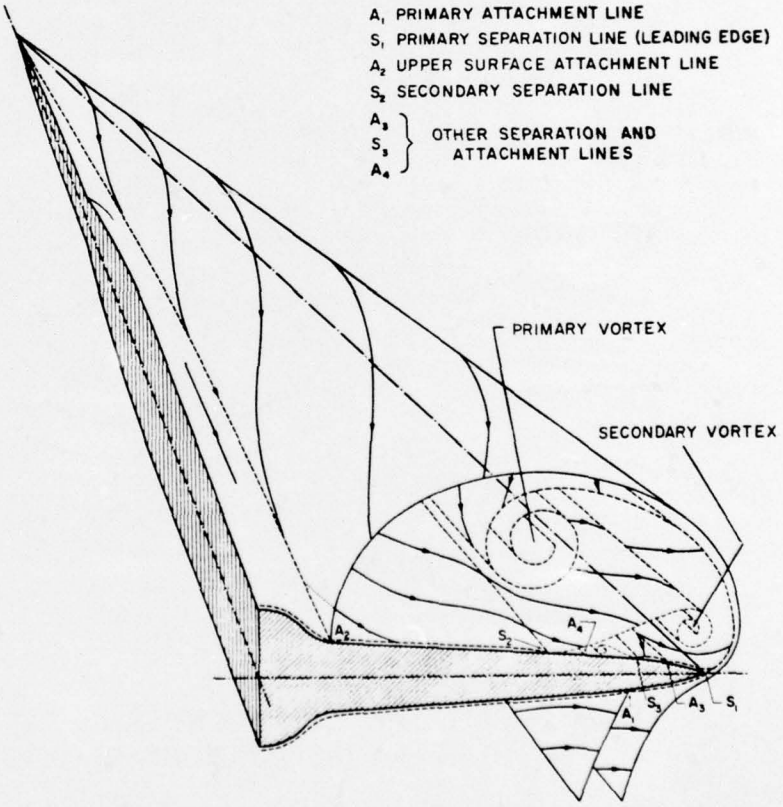

L.E.
SUBSONIC:
NAE[11]

INTERPRETATION OF FLOW ABOUT 70-DEGREE DELTA WING
AT 16.6 DEGREES INCIDENCE

FIG. 31: LEE-SIDE FLOWS OVER DELTA WINGS AT INCIDENCE

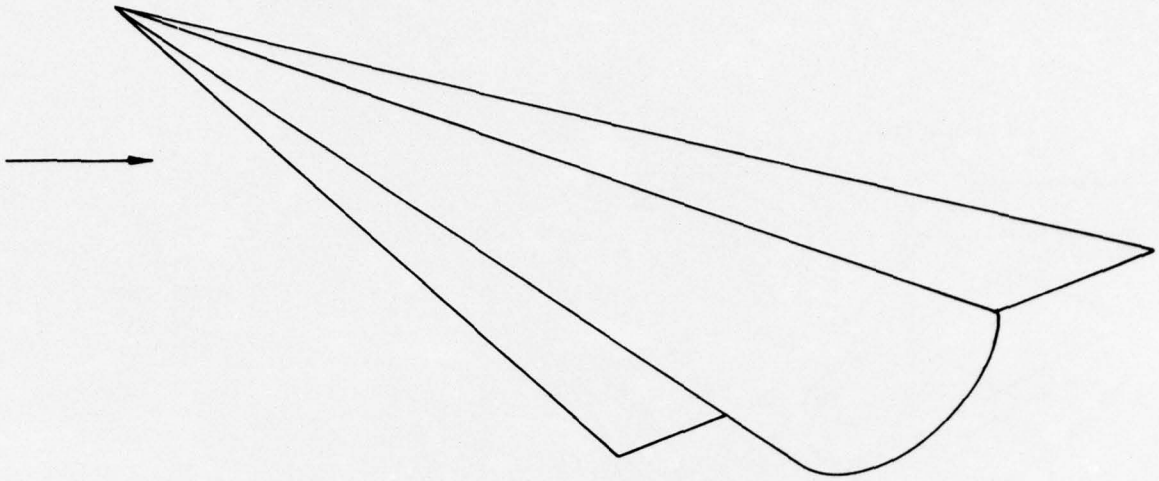

FLAT-TOPPED HALF-CONE-AND-DELTA-WING
HYPERSONIC LIFTING VEHICLE

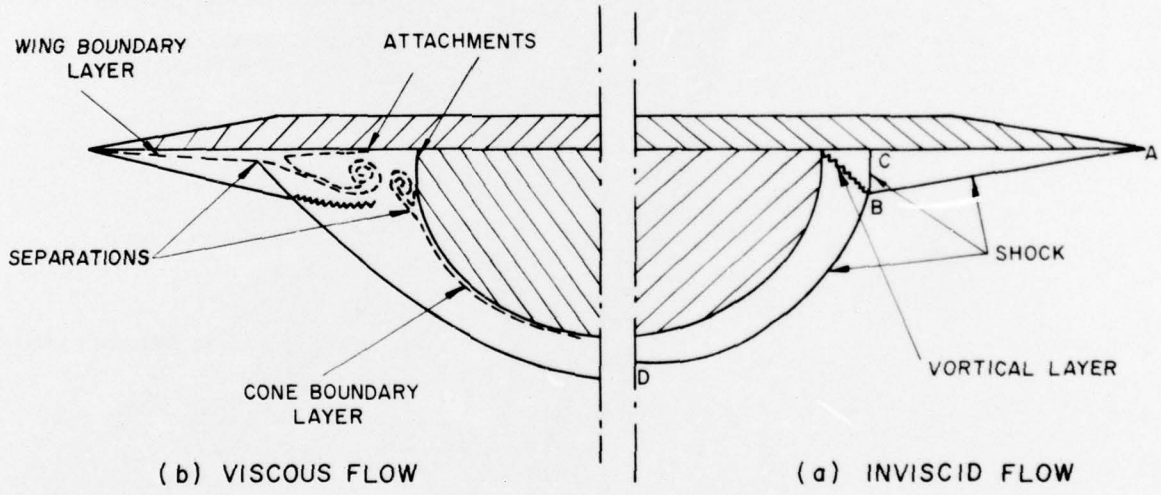

FLOW ABOUT THE HALF-CONE-AND-DELTA-WING VEHICLE
AT AN INCIDENCE OF 15 DEGREES

FIG. 32: LIFTING HYPERSONIC HALF-CONE/DELTA WING AT M = 12.6

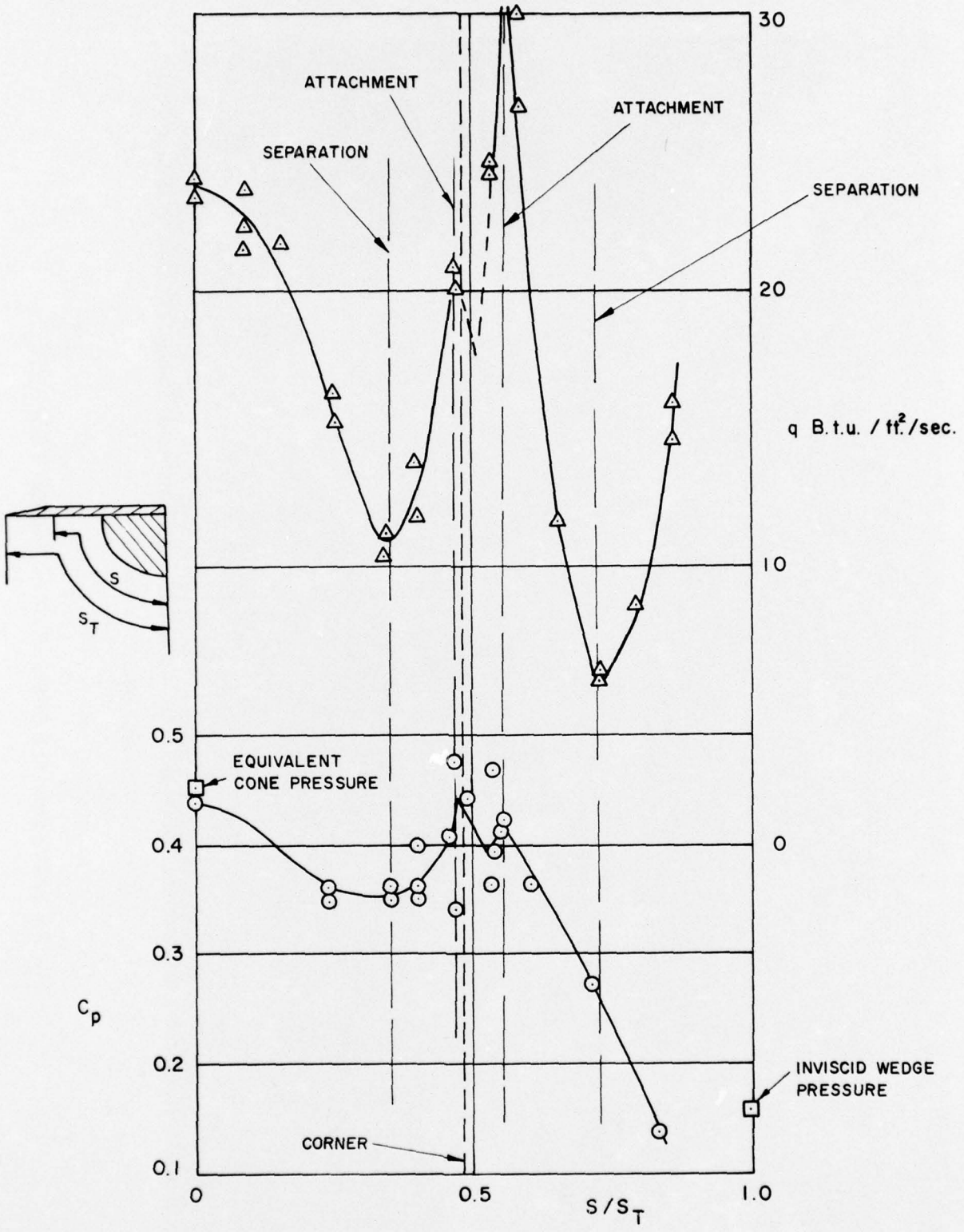

FIG. 33: HEAT TRANSFER AND SURFACE PRESSURES ON HALF-CONE/DELTA WING, $\alpha = 15°$, M = 12.6

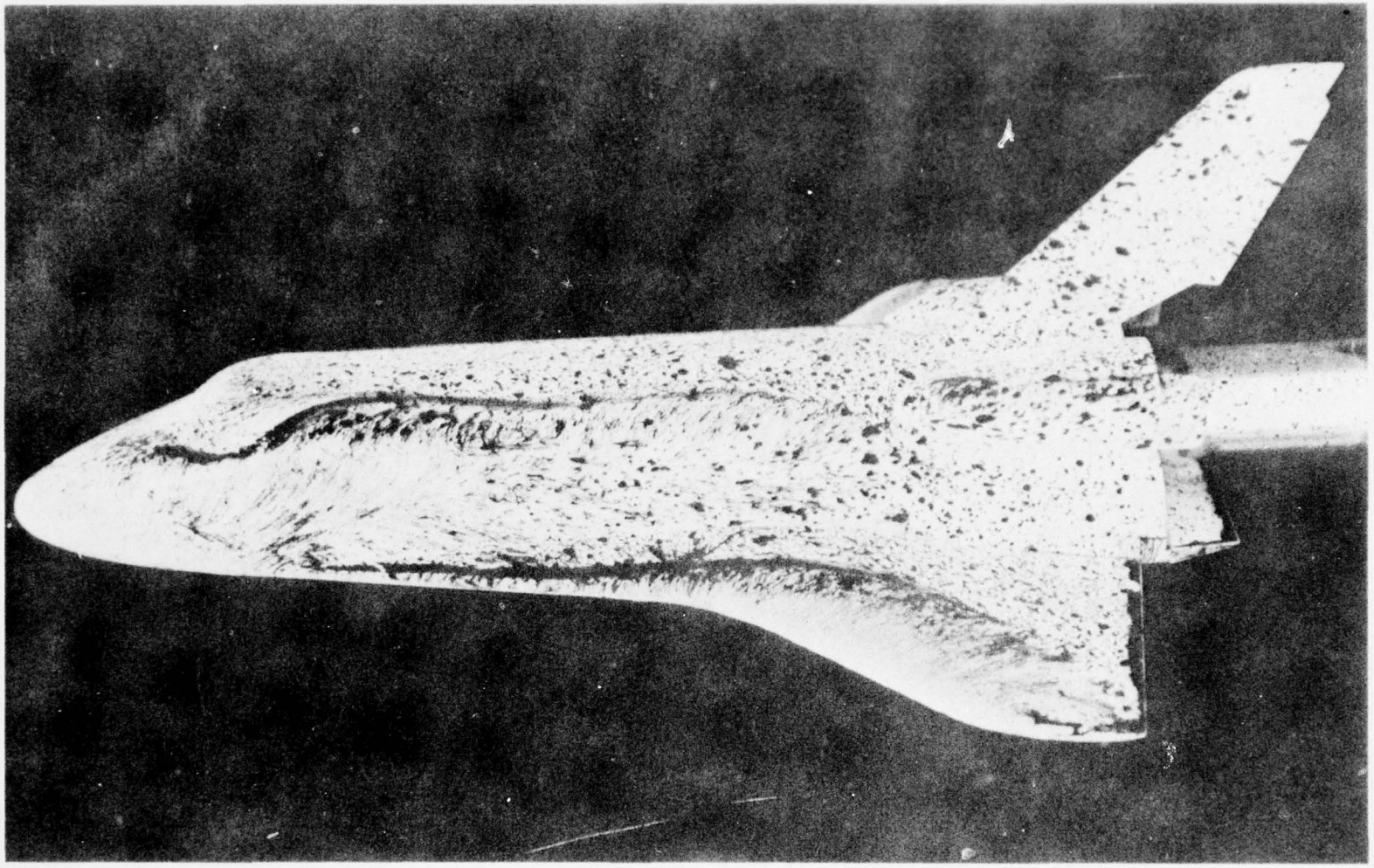

SIDE OBLIQUE VIEW

FIG. 34: SPACE SHUTTLE ORBITER AT 30° INCIDENCE, M ≐ 20[58]

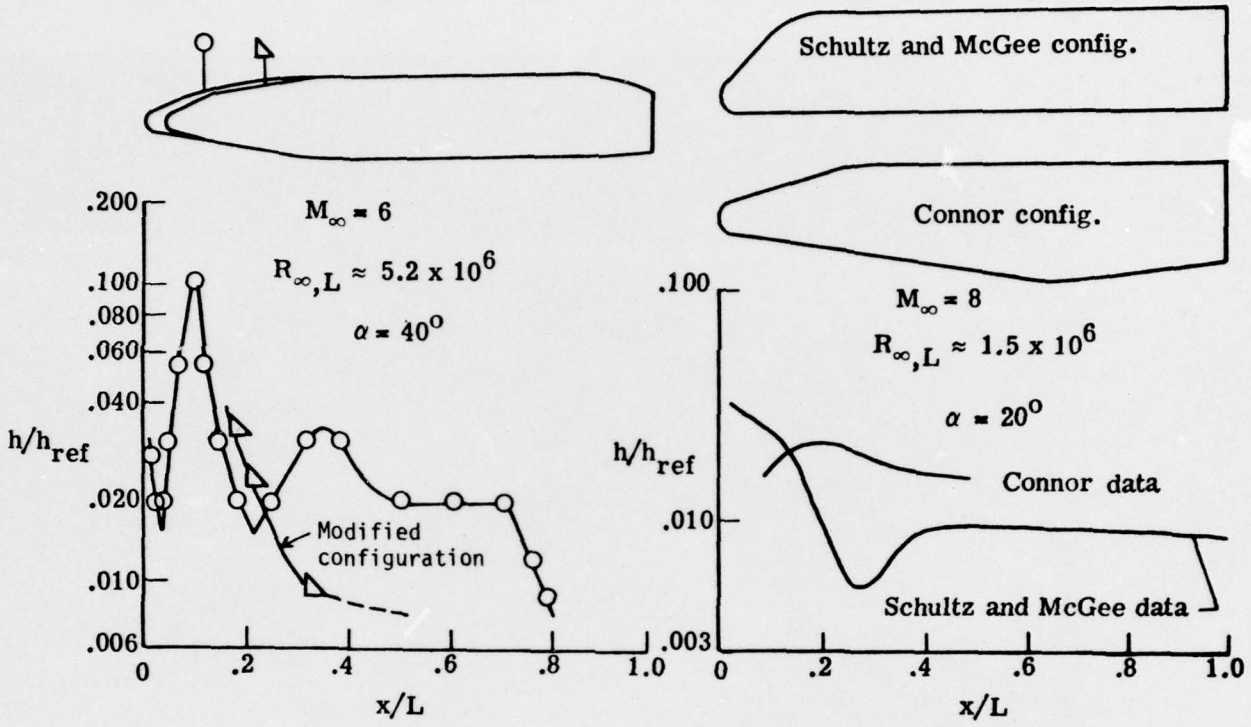

FIG. 35: EFFECT OF LEE-SURFACE GEOMETRY ON HEATING[59]

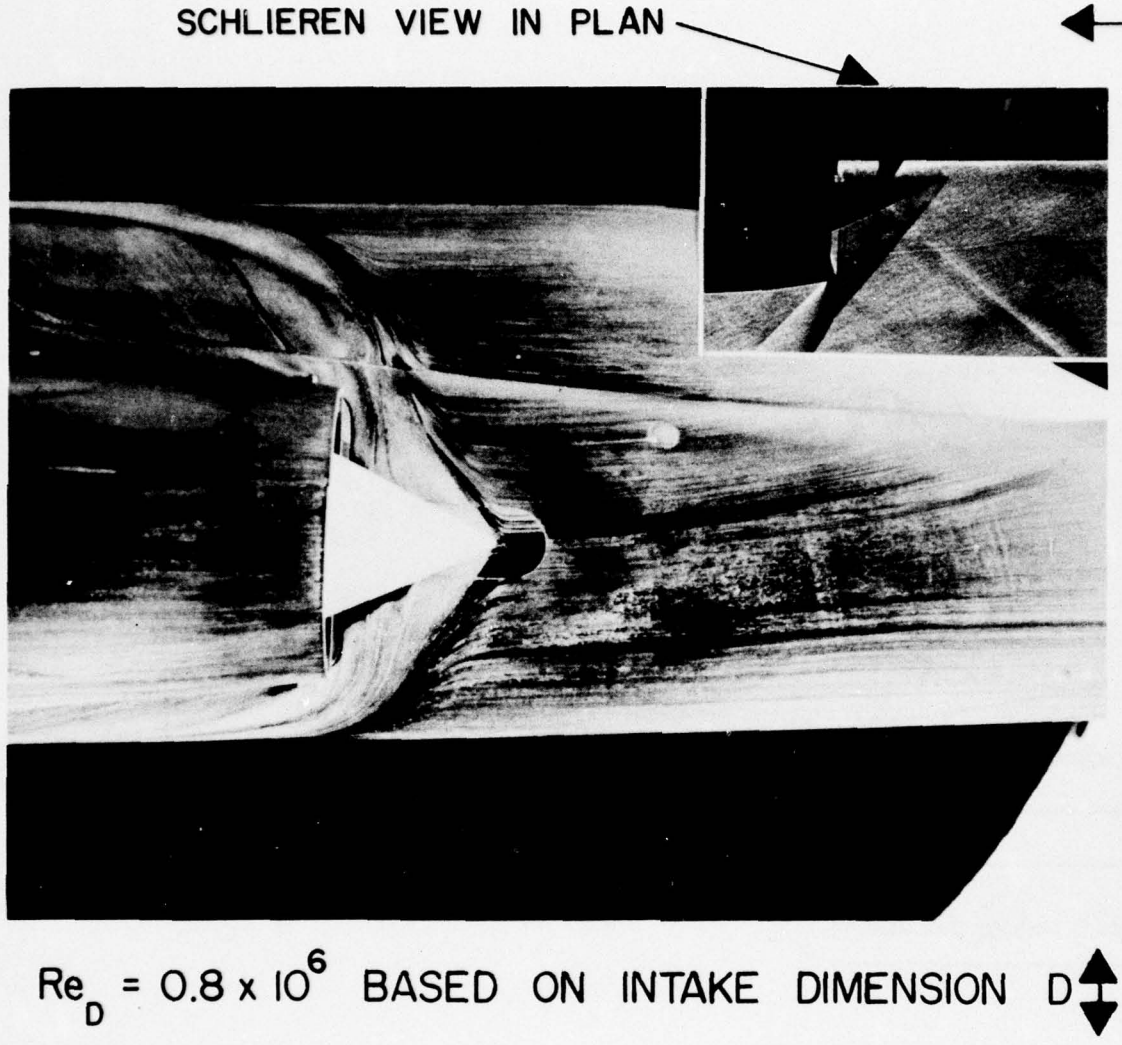

FIG. 36: SWEPT-SHOCK INDUCED 3D SEPARATION ABOUT HALF-CONE INTAKE AT M = 1.6[73]

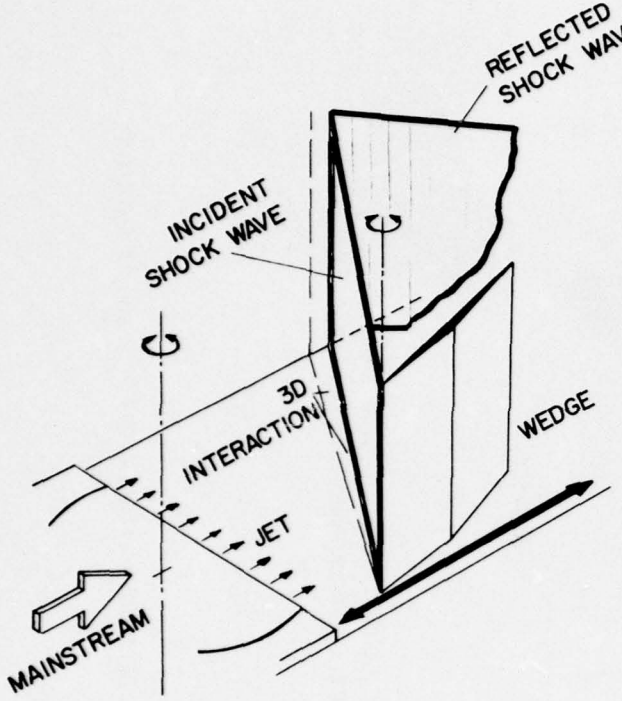

FIG. 37 FLOW CONFIGURATION

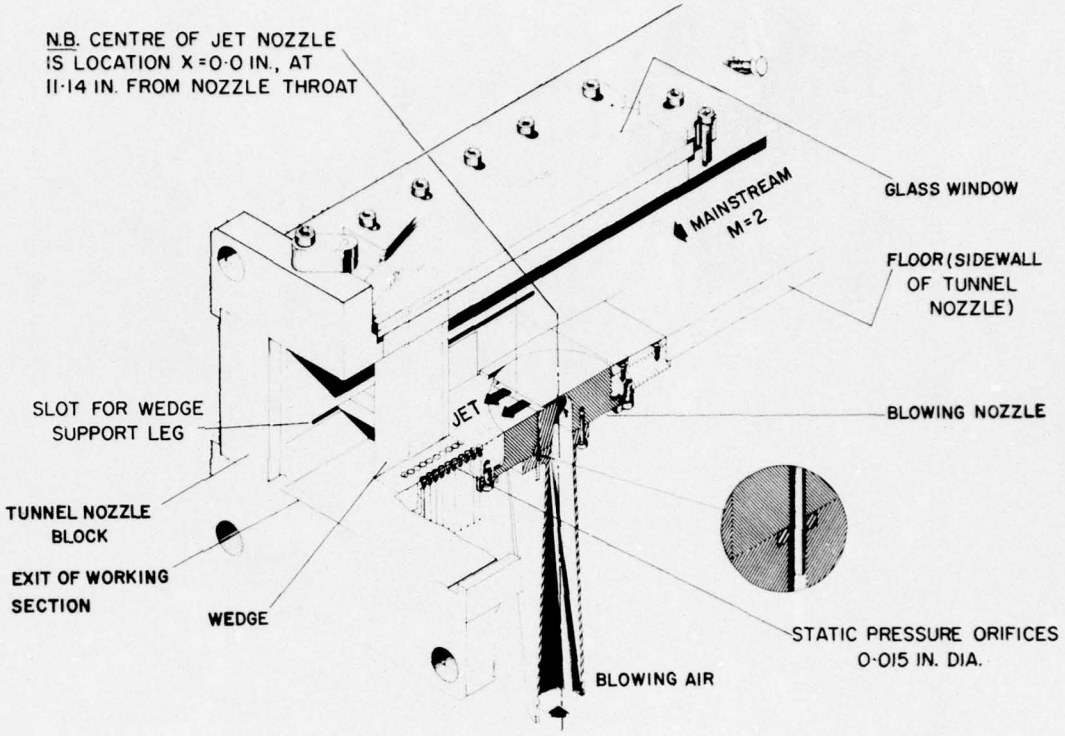

FIG. 38 TYPICAL ASSEMBLY OF WORKING SECTION OF 5 x 5 IN. WIND TUNNEL FOR BLC

FIGS 37 & 38: SWEPT SHOCK/TURBULENT BOUNDARY-LAYER INTERACTION WITH AIR INJECTION

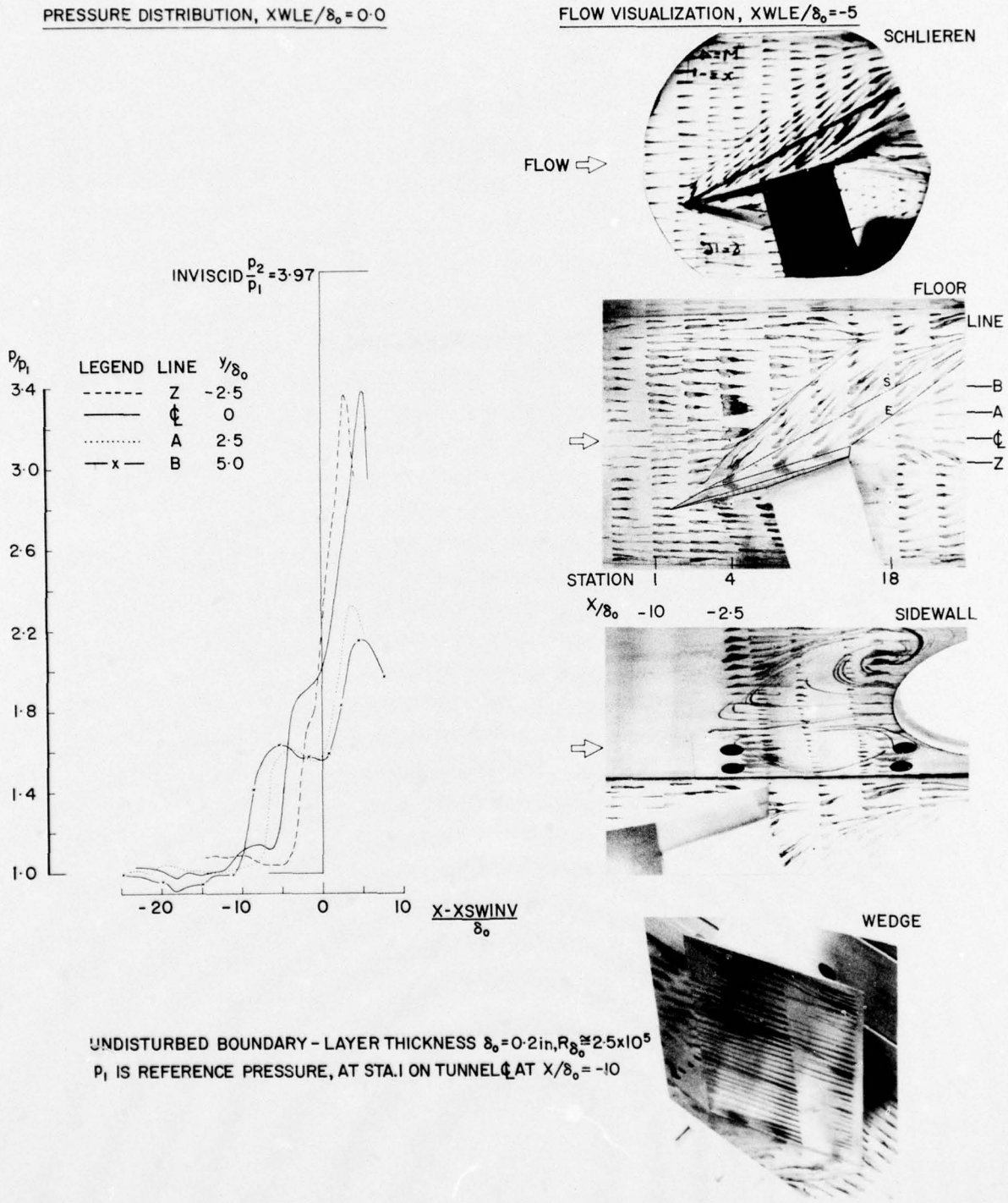

UNDISTURBED BOUNDARY - LAYER THICKNESS $\delta_0 = 0{\cdot}2$ in, $R_{\delta_0} \cong 2{\cdot}5 \times 10^5$
p_1 IS REFERENCE PRESSURE, AT STA.1 ON TUNNEL ℄ AT $X/\delta_0 = -10$

FIG. 39: 3D SEPARATION WITH $\delta_w = 16°$ AT MACH 4

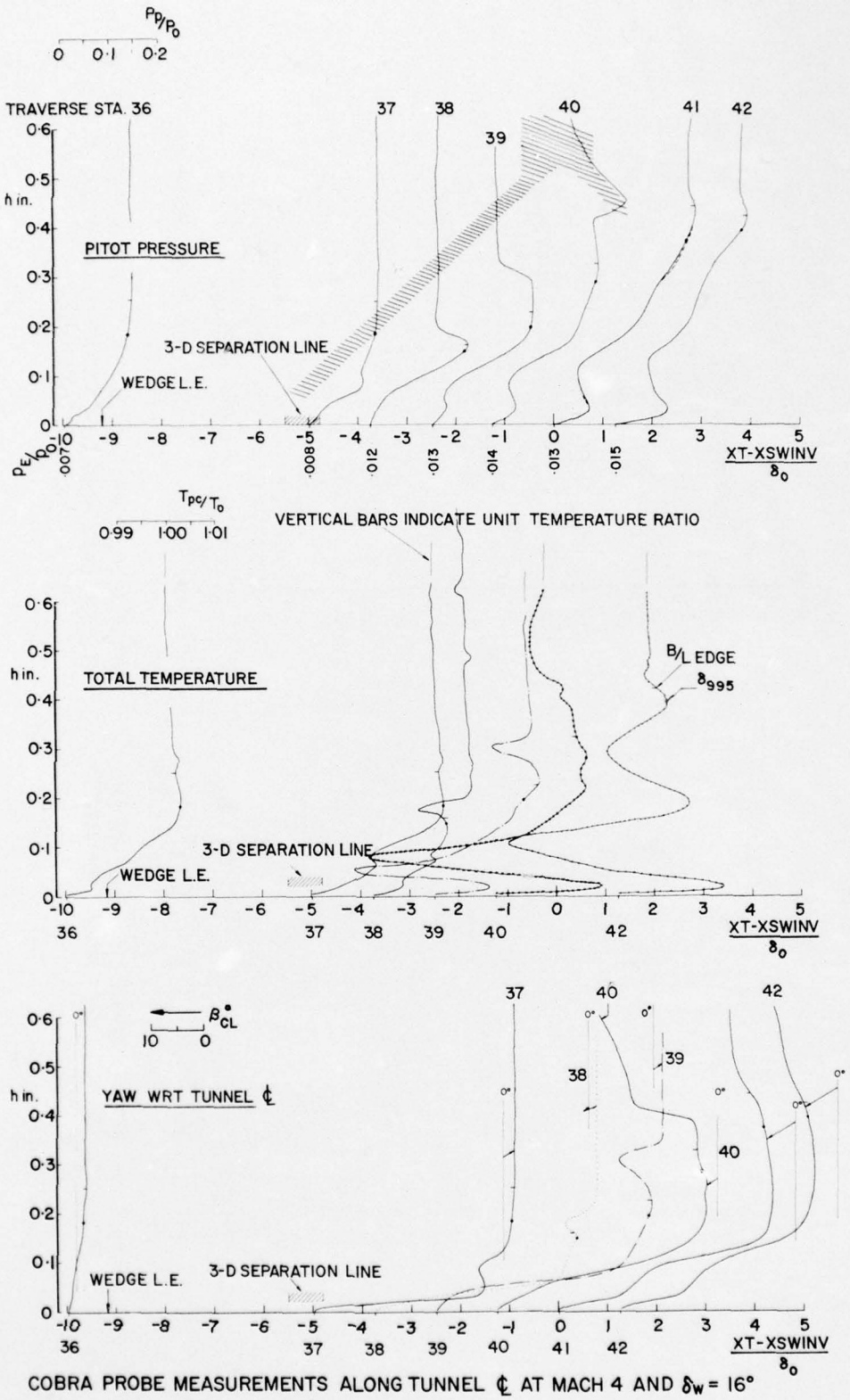

COBRA PROBE MEASUREMENTS ALONG TUNNEL ℄ AT MACH 4 AND $\delta_w = 16°$

FIG. 40: 3D BOUNDARY LAYER PROFILES ALONG ℄, M = 4, $\delta_w = 16°$

41.1

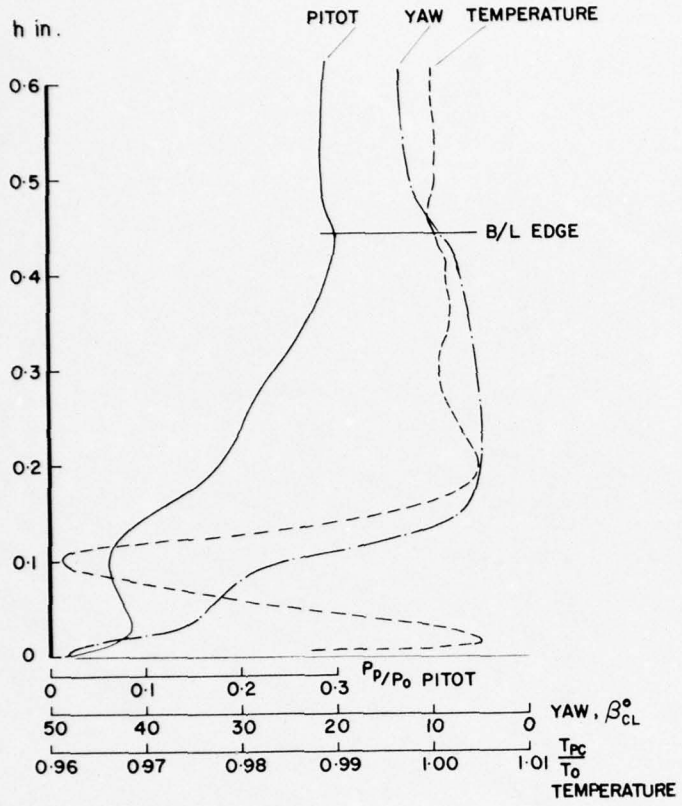

PITOT, TOTAL TEMPERATURE AND YAW ANGLE DISTRIBUTIONS FOR STATION 41 NEAR INVISCID SHOCK WAVE LOCATION; FOR $\delta_w = 16^\circ$ AT MACH 4.

41.2

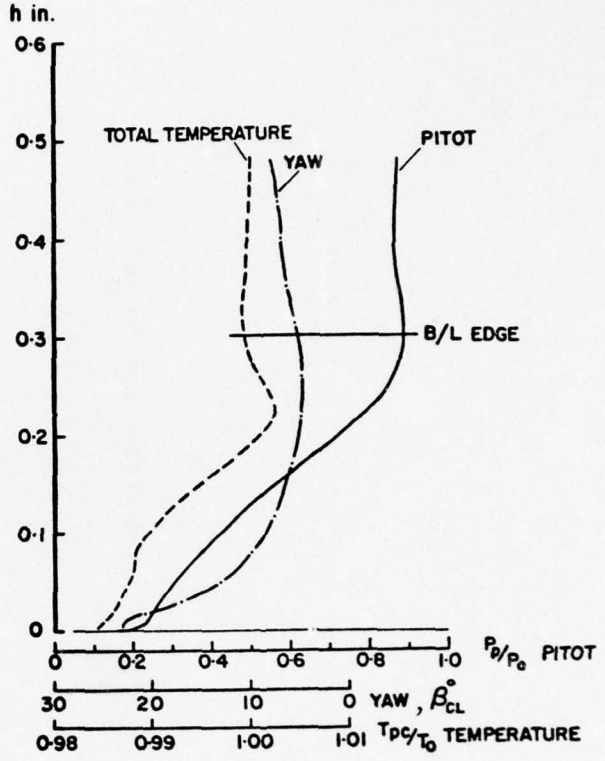

PITOT, TOTAL TEMPERATURE AND YAW ANGLE DISTRIBUTIONS FOR STATION II NEAR INVISCID SHOCK WAVE LOCATION; FOR $\delta_w = 8^\circ$ AT MACH 2

FIG. 41: STAGNATION TEMPERATURE CHANGES IN FLOW WITH 3D SEPARATION

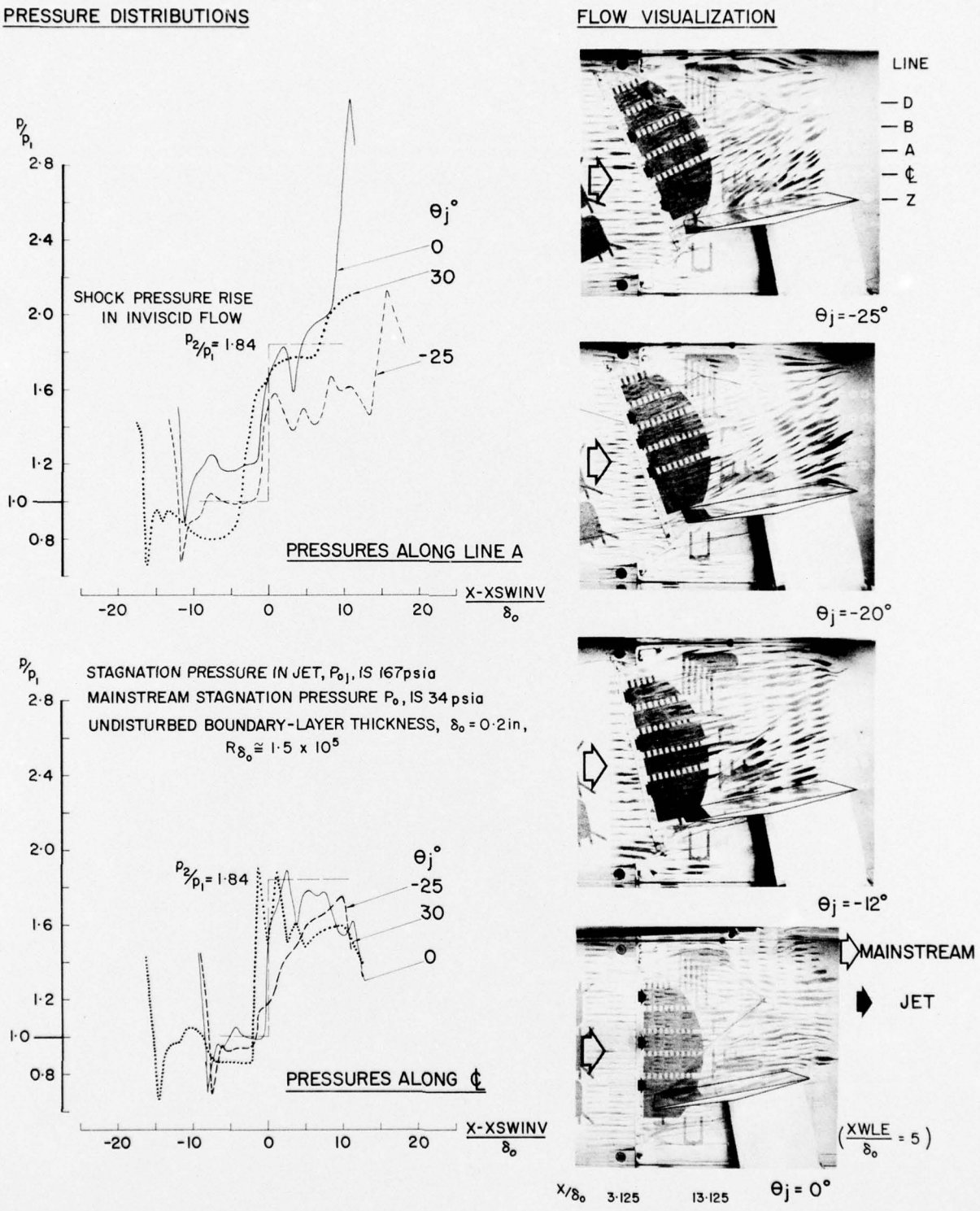

FIG. 42: EFFECT OF BLOWING DIRECTION ON SWEPT SHOCK/TURBULENT BOUNDARY-LAYER INTERACTION AT MACH 2: $\delta_w = 11.5°$, $M_j = 3$

NRC, NAE LR-591
National Research Council Canada. National Aeronautical Establishment.

CONTROLLED AND UNCONTROLLED FLOW SEPARATION IN THREE DIMENSIONS.
Peake, D.J. July 1976. 71 pp. (incl. figures).

UNCLASSIFIED

1. Separated flow.
2. Three-dimensional flow.

I. Peake, D.J.
II. NRC, NAE LR-591

The advantages of swept, sharp edges that generate controlled (or fixed) three-dimensional flow separations on a vehicle — because of the qualitatively unchanging flowfield developed throughout the range of flight conditions — are promoted in preference to allowing uncontrolled (or unfixed) separations.

The three-dimensional viscous flowfields and vortical interactions about typical components such as delta wings and bodies at incidence are discussed, in apposition to their use on selected examples of current flight vehicles.

NRC, NAE LR-591
National Research Council Canada. National Aeronautical Establishment.

CONTROLLED AND UNCONTROLLED FLOW SEPARATION IN THREE DIMENSIONS.
Peake, D.J. July 1976. 71 pp. (incl. figures).

UNCLASSIFIED

1. Separated flow.
2. Three-dimensional flow.

I. Peake, D.J.
II. NRC, NAE LR-591

The advantages of swept, sharp edges that generate controlled (or fixed) three-dimensional flow separations on a vehicle — because of the qualitatively unchanging flowfield developed throughout the range of flight conditions — are promoted in preference to allowing uncontrolled (or unfixed) separations.

The three-dimensional viscous flowfields and vortical interactions about typical components such as delta wings and bodies at incidence are discussed, in apposition to their use on selected examples of current flight vehicles.

NRC, NAE LR-591
National Research Council Canada. National Aeronautical Establishment.

CONTROLLED AND UNCONTROLLED FLOW SEPARATION IN THREE DIMENSIONS.
Peake, D.J. July 1976. 71 pp. (incl. figures).

UNCLASSIFIED

1. Separated flow.
2. Three-dimensional flow.

I. Peake, D.J.
II. NRC, NAE LR-591

The advantages of swept, sharp edges that generate controlled (or fixed) three-dimensional flow separations on a vehicle — because of the qualitatively unchanging flowfield developed throughout the range of flight conditions — are promoted in preference to allowing uncontrolled (or unfixed) separations.

The three-dimensional viscous flowfields and vortical interactions about typical components such as delta wings and bodies at incidence are discussed, in apposition to their use on selected examples of current flight vehicles.

NRC, NAE LR-591
National Research Council Canada. National Aeronautical Establishment.

CONTROLLED AND UNCONTROLLED FLOW SEPARATION IN THREE DIMENSIONS.
Peake, D.J. July 1976. 71 pp. (incl. figures).

UNCLASSIFIED

1. Separated flow.
2. Three-dimensional flow.

I. Peake, D.J.
II. NRC, NAE LR-591

The advantages of swept, sharp edges that generate controlled (or fixed) three-dimensional flow separations on a vehicle — because of the qualitatively unchanging flowfield developed throughout the range of flight conditions — are promoted in preference to allowing uncontrolled (or unfixed) separations.

The three-dimensional viscous flowfields and vortical interactions about typical components such as delta wings and bodies at incidence are discussed, in apposition to their use on selected examples of current flight vehicles.